Role of the EHF Transcription Factor in Tissue Homeostasis and Intestinal Disease

Camilla Marstrander Reehorst

MBiotech

A thesis submitted in total fulfilment

of the requirements for the degree of

Doctor of Philosophy

School of Cancer Medicine

Olivia Newton-John Cancer Research Institute

College of Science, Health and Engineering

La Trobe University

Victoria, Australia

June 2021

Table of contents

List of Figures

Chapter 1

Chapter 2

Chapter 3

Chapter 4

Chapter 5

List of Tables

Chapter 2

List of Abbreviations

5-FU	5-Fluorouracil
AOM	Azoxymethane
Apc	Adenomatous polyposis coli
BMP	Bone morphogenesis pathway
BrdU	5-bromo-2'-deoxyuridine
BRF	Bio-Resource Facility
CBC	Crypt-base columnar
CD	Crohn's disease
ChIP	Chromatin immunoprecipitation
CIMP	CpG island methylator phenotype
CIN	Chromosomal instability
CRC	Colorectal cancer
D	Ducts
DAB	3, 3-diaminobenzidine
DCS	Deep crypt secretory
DNA	Deoxyribonucleic acid
dP	day of pregnancy
DPX	Dibutylphthalate Polystyrene Xylene
DSS	Dextran sodium sulphate
EDTA	Ethylenediaminetetraacetic acid
EECs	Enteroendocrine cells
EGF	Epidermal growth factor
EHF	Ets homologous factor
EMT	Epithelial-to-mesenchymal transition
ER	Oestrogen receptor

ES	Embryonic stem
ESCC	Oesophageal squamous cell carcinoma
ESE	Epithelial-specific-ETS
FAE	Follicle-associated epithelium
FDR	False discovery rate
FdU	5-fluoro-2'-deoxyuridine
GALT	Gut associated lymphoid tissue
GSEA	Gene set enrichment analysis
HGD	High-grade dysplasia
HPs	Hyperplastic polyps
IBD	Inflammatory bowel disease
IHC	Immunohistochemistry
ISC	Intestinal stem cell
LOH	Loss of heterozygosity
M	Mucous acini
M cells	Microfold cells
MaSCs	Mammary stem cells
MECs	Mammary epithelial cells
Min	Multiple intestinal neoplasia
MMR	Mismatch repair
MSI	Microsatellite instability
MSigDB	Molecular Signatures Database
MSS	Microsatellite stability
N	Adjacent normal tissue
ONJCRI	Olivia Newton-John Cancer Research Institute
OSCC	Oral squamous cell carcinoma

PBS	Phosphate-buffered saline
PBST	PBS with 0.1% Tween20
PCR	Polymerase chain reaction
PDAC	Pancreatic ductal adenocarcinoma
PNT	Pointed domain
PR	Progesterone
Prl	Prolactin
PTC	Papillary thyroid cancer
q-RT-PCR	Quantitative real time polymerase chain reaction
RO	Reverse osmosis
SC	Secretory cells
SI	Small intestine
SNP	Single nucleotide polymorphism
SSA	Sessile serrated adenoma
T	Tumour
TAE buffer	Tris-Borate-EDTA buffer
TBST	Tris-buffered saline with Tween20
TCGA	The cancer genome atlas
TEBs	Terminal end buds
TJs	Tight junctions
TNBS	Trinitrobenzene sulfonic acid
TSA	Traditional serrated adenoma
UC	Ulcerative colitis

Abstract

Ets homologous factor (EHF) is a member of the epithelial-specific ETS (ESE) family of transcription factors. It is highly expressed in epithelial tissues including the skin, colon, prostate and mammary gland, however its role in normal development and homeostasis of these tissues is largely unknown. Studies in cancer cell lines have also suggested a role for EHF in either tumour suppression or promotion depending on the tumour type, however these effects have not been investigated in a genetic mouse model in vivo.

The aims of this thesis were therefore to investigate the role of EHF in normal mouse development and epithelial tissue homeostasis. We further sought to investigate its role in protecting against inflammation and tumorigenesis in the colonic epithelium.

To achieve this, we generated a series of novel mouse strains in which the ETS DNA-binding domain of *Ehf* was deleted in all tissues (*Ehf* $^{-/-}$) or specifically in the small intestinal or colonic epithelium. *Ehf* $^{-/-}$ mice were born at the expected Mendelian ratio, but showed reduced body weight gain, and developed a series of pathologies during their lifetime. These included papillomas in the skin, abscesses in the preputial glands (males) or vulvae (females), and corneal ulcers. We also identified an impaired ability of *Ehf* $^{-/-}$ female mice to lactate, due to a failure of the mammary gland to undergo differentiation during pregnancy.

Ehf deletion also increased epithelial cell proliferation and impaired goblet cell differentiation in the intestinal epithelium, and increased susceptibility to experimentally induced colitis. Furthermore, *Ehf* deletion induced extensive transcriptional reprogramming in the colonic epithelium and enhanced growth of *Apc*-initiated colonic adenomas.

EHF is therefore essential for postnatal homeostasis of the epidermis, mammary gland and colonic epithelium, and its loss increases sensitivity to colitis and promotes colonic tumour growth.

Statement of Authorship

Except where reference is made in the text of the thesis, this thesis contains no material published elsewhere or extracted in whole or in part from a thesis accepted for the award of any other degree or diploma. No other person's work has been used without due acknowledgement in the main text of the thesis. This thesis has not been submitted for the award of any degree or diploma in any other tertiary institution.

In accordance with the regulations of the La Trobe University, I acknowledge that some of the work presented in this thesis was undertaken collaboratively. Specifically:

Chapter 3 – Figure 3.1, Confirmation of *Ehf* deletion by q-RT-PCR was performed by Kael Schoffer.

Chapter 3 – Figure 3.7, Immunofluorescence staining and image scanning of K14, K6 and Loricrin performed by Kael Schoffer.

Chapter 3 – Figure 3.8, Genotyping of dead pups was performed by Rebecca Nightingale.

Chapter 3 – Figure 3.10, 3.11, 3.12, Management of timed pregnancies and collection of mammary glands was performed by myself and Rebecca Nightingale (30%-70%).

Chapter 4 – Figure 4.4, 4.5, 4.7, 4.8, Collection of colonic tissue and colonic epithelial cells performed with the assistance of Rebecca Nightingale.

Chapter 4 – Figure 4.6, Organoid growth performed with the assistance of Cameron Scott.

Chapter 4 – Figure 4.8, The KRT20 stain was performed by Rebecca Nightingale, and the DCLK1 stain was performed by Dr Michael Buchert.

Chapter 4 – Figure 4.10, 4.11, Principal component analysis and identification of differentially expressed genes performed by Dr Dimitri Mouradov.

Chapter 4 – Figure 4.11, 'Hallmark gene sets' analysis performed by Laura Jenkins.

Chapter 5 – Figure 5.1, 5.2, 5.5, 5.8, 5.15, Collection of colonic tissue and adenomas performed with the assistance of Rebecca Nightingale.

Camilla Marstrander Reehorst Date: 30 June 2021

Preface

This work was supported by a La Trobe University Postgraduate Research Scholarship (LTUPRS).

This work was supported by a La Trobe University Full Fee Research Scholarship (LTUFFRS).

All research procedures reported in the thesis were approved by the Austin Health Animal Ethics Committee and conformed to the Australian Code of Practice for the Care and Use of Animals for Scientific Purposes.

Chapter 3, 4 and 5 consists of research published in Development:

Reehorst CM, Nightingale R, Luk IY, Jenkins L, Koentgen F, Williams DS, Darido C, Tan F, Anderton H, Chopin M, Schoffer K, Eissmann MF, Buchert M, Mouradov D, Sieber OM, Ernst M, Dhillon AS, Mariadason JM. EHF is essential for epidermal and colonic epithelial homeostasis, and suppresses Apc-initiated colonic tumorigenesis. Development. 2021 Jun 15;148(12):dev199542. doi: 10.1242/dev.199542. Epub 2021 Jun 28. PMID: 34180969.

Chapter 1 consists of sections from a review article published in Molecules:

Luk IY*, **Reehorst CM***, Mariadason JM. ELF3, ELF5, EHF and SPDEF Transcription Factors in Tissue Homeostasis and Cancer. Molecules. 2018 Aug 30;23(9):2191. doi: 10.3390/molecules23092191. PMID: 30200227;

*Denotes co-first author

Publications

In addition to those listed above, here is a list of publications I have co-authorship on during my PhD:

Dávalos-Salas M, Montgomery MK, **Reehorst CM**, Nightingale R, Ng I, Anderton H, Al-Obaidi S, Lesmana A, Scott CM, Ioannidis P, Kalra H, Keerthikumar S, Tögel L, Rigopoulos A, Gong SJ, Williams DS, Yoganantharaja P, Bell-Anderson K, Mathivanan S, Gibert Y, Hiebert S, Scott AM, Watt MJ, Mariadason JM. Deletion of intestinal Hdac3 remodels the lipidome of enterocytes and protects mice from diet-induced obesity. Nat Commun. 2019 Nov 22;10(1):5291. doi: 10.1038/s41467-019-13180-8. PMID: 31757939;

Lau DK, Mouradov D, Wasenang W, Luk IY, Scott CM, Williams DS, Yeung YH, Limpaiboon T, Iatropoulos GF, Jenkins LJ, **Reehorst CM**, Chionh F, Nikfarjam M, Croagh D, Dhillon AS, Weickhardt AJ, Muramatsu T, Saito Y, Tebbutt NC, Sieber OM, Mariadason JM. Genomic Profiling of Biliary Tract Cancer Cell Lines Reveals Molecular Subtypes and Actionable Drug Targets. iScience. 2019 Nov 22;21:624-637. doi: 10.1016/j.isci.2019.10.044. Epub 2019 Oct 31. PMID: 31731200;

Acknowledgements

I would like to thank my primary supervisor Professor John M. Mariadason for his guidance and encouragement throughout this PhD. I am thankful for having been given the opportunity to work in his supportive and professional environment that has allowed me to grow as a researcher. Many of the skills I have acquired since commencing my PhD can be attributed to his mentorship. He has provided me with the framework needed to complete a thesis I can be proud of, and for that I am eternally grateful. I would also like to thank my co-supervisor, Associate Professor Amardeep S. Dhillon, and my mentor Dr Michael Buchert for their intellectual support and suggestions.

Next, I would like to extend a very special thank you to Rebecca Nightingale who taught me everything I needed to know in the lab when I started my PhD, and throughout this whole process she has supported me professionally, mentally and socially. I would also like to thank the rest of the Oncogenic Transcription Laboratory members who I have thoroughly enjoyed working alongside with: Dr Jennifer Mooi, Laura Jenkins, Dr Ian Luk, Dr David Lau, Irvin Ng, Dr Fiona Chionh, Zakia Alam and Stan Kaczmarczyk.

I would also like to thank my personal support team, my friends and my family. I am positive I could not have completed this undertaking without the support of my husband, Nicholas. He has been my rock and my voice of calm, always prioritising my needs. I appreciate everything he and his family have done for me. Lastly, I wish to extend gratitude to my mother, Iselin, who has given me the strength and determination to accomplish what I set my mind to, and my father, Per, who taught me critical thinking and who has been a source of motivation throughout this process.

Chapter 1: Literature Review

1.1 Ets homologous factor (EHF)

The Ets homologous factor (EHF) is a member of the ETS family of transcription factors which comprises 28 members in humans and 27 members in mice [1]. *EHF* was first cloned from mouse pituitary somatotroph tumour tissue [2] and there are currently three predicted isoforms: *ESE-3a*, *ESE-3b* and *ESE-3j* [3]. However, only transcripts of *ESE-3a* and *ESE-3b* have been isolated from cells and *ESE-3b* is the dominant isoform [3-5]. The *EHF* gene consists of a pointed domain (PNT) with potential for homodimerization, co-operative binding with other transcription factors and gene transactivation, and an evolutionarily conserved winged helix-turn-helix ETS DNA-binding domain which binds DNA sequences with consensus A(T/C)(C/G)AGGAAGT [6]. Members of the ETS family of transcription factors are subdivided based on homology of their ETS DNA-binding domain and tissue-restricted expression profile. Based on these criteria, EHF is a member of the epithelial-specific-ETS (ESE) subfamily which also contains ELF3, ELF5 and SPDEF. EHF shares 84% and 65% homology of the ETS DNA-binding domain with ELF3 and ELF5 respectively and all members of this subfamily share significant overlap in their expression profiles which is predominantly restricted to epithelial tissues [4]. Notably, *EHF* and *ELF5* are located ~110kB apart on chromosome 11p13 likely as a result of a gene duplication event [7]. Nevertheless, *EHF* and *ELF5* are transcribed in opposite directions and are therefore unlikely to be co-regulated. The ESE transcription factors play key roles in normal development, differentiation and homeostasis of specific epithelial tissues, and have been implicated in the pathogenesis of a wide range of cancers.

The mouse and human EHF transcription factor share 88% nucleotide and 93% amino acid identity [8]. Highest expression of EHF is found in secretory organs including salivary gland, prostate and mammary gland, but it is also highly expressed in colon, lung, stomach and trachea. The following sections will describe the roles of EHF in tissue homeostasis and cancer which have been described to-date.

1.1.1 Role of EHF in epithelial tissues

Airway epithelium: EHF has been extensively studied as a potential modifier gene of the severity of the cystic fibrosis phenotype. These studies stem from genome-wide association studies which identified a single nucleotide polymorphism (SNP) associated with the severity of lung disease in cystic fibrosis patients (rs12793173) located at chromosome 11p13 within or close to potential

EHF cis-regulatory elements [9, 10]. Several subsequent studies sought to determine the role of EHF in bronchial epithelial cells where EHF is basally expressed and is induced in response to inflammatory mediators [11, 12]. Direct EHF targets in primary human bronchial epithelial cells are enriched for genes involved in lung pathology including epithelial-to-mesenchymal transition (EMT) and wound response, and knockdown of *EHF* reduced wound closure in bronchial epithelial cells derived from both healthy and cystic fibrosis patients [13]. Recently, a direct role for EHF in repressing CFTR expression was demonstrated in bronchial epithelial cells, and EHF binding to a regulatory region 35 kb upstream of the CFTR promoter was demonstrated by chromatin immunoprecipitation (ChIP) [14].

Intestinal epithelium: EHF mRNA and protein is highly expressed in the normal colon with maximal expression in the proliferative stem-cell compartment of the crypt base [7]. EHF was also among the ~500 genes found to be highly expressed in LGR5+ intestinal stem cells compared to their immediate progeny [15].

During the course of this PhD a study was published which implicated a major role for EHF in the maintenance of stem cell numbers. Specifically, the authors demonstrated that mice in which *EHF* was deleted by CRISPR-Cas9-mediated genome editing, had decreased LGR5+ intestinal stem cell (ISC) numbers inferred by OLFM4 and ASCL2 staining, and impaired organoid formation when intestinal epithelial cells were cultured *ex vivo* [16]. Furthermore, the small intestinal epithelium of these mice displayed an impaired ability to self-renew following irradiation-induced injury. Mechanistically, EHF was found to be a direct transcriptional activator of LGR4 and LGR5 as well as other Wnt- and ISC-related genes.

EHF has also been shown to be highly expressed in specialised microfold (M) cells located in the follicle-associated epithelium (FAE) which overlies Payer's patches in the intestine. Here, M cells contribute to immune surveillance by mediating transcytosis of potential antigens from the intestinal lumen into the underlying immune cells [17]. *EHF* promoter activity was induced in the Caco-2 cell line model of FAE, and ectopic expression of *EHF* in this model induced expression of transcytosis associated genes. Notably however, *EHF* overexpression was not sufficient to induce M cell differentiation in this model, suggesting EHF may promote functional maturation of the FAE rather than establishing the M cell lineage [18].

Corneal epithelium: Ehf mRNA is highly expressed in the mouse corneal epithelium during adult corneal development (P14-P28) [19]. ChIP-sequencing analysis of genome-wide EHF binding revealed that EHF binds to a number of promoters of genes involved in cell signalling, migration and epithelial morphogenesis. Knockdown of *EHF* in human corneocytes caused significant transcriptional changes including down-regulation of SPRR proteins involved in barrier function,

up-regulation of SERPIN genes involved in corneal transparency, and up-regulation of TNF superfamily members which are regulators of inflammation and apoptosis.

Epidermis: EHF mRNA and protein is highly expressed in epidermal keratinocytes [20]. Genome-wide profiling of enhancer regions in keratinocytes identified the GGAA ETS motif as the most enriched transcription factor binding site. As EHF was the ESE factor found to have the highest lineage-specific expression in stratified epithelia, its role in keratinocyte differentiation was directly investigated by knockdown in organotypic human epidermal tissue, revealing that EHF regulates ~400 genes in this tissue including several associated with keratinocyte differentiation [21].

1.1.2 Role of EHF in non-epithelial tissues

Innate immune cells: While the expression of EHF is predominantly restricted to epithelial cells, its expression has been reported in different components of the innate immune system. Specifically, EHF plays an important role in the development and antigen-presenting function of immunogenic monocyte-derived dendritic cells [3, 20]. Furthermore, EHF has been shown to be expressed in Langerhans cells which are tissue-resident macrophages of the skin [20], although the role of EHF in this cell population is unknown.

EHF also plays a role in suppressing activation of mast cells, the major effector of IgE-driven hypersensitivity. TGFβ suppresses mast cell activation, inducing EHF mRNA and protein expression during this process. Overexpression of *EHF* in mast cells mimicked several of the TGFβ-induced transcriptional changes and inhibited mast cell degranulation, suggesting a direct role in TGFβ-mediated suppression of mast cell activity [22], although knockdown or knockout studies are still needed to confirm these findings.

Liver: Although EHF mRNA is not normally expressed in liver cells (hepatocytes) [23], its up-regulation has been implicated in the development of cirrhosis in patients with chronic hepatitis B [24], and advanced fibrosis in patients with chronic liver disease [25]. As the studies cited are mainly correlative, further studies are needed to directly establish its role in these conditions.

1.1.3 Role of EHF in cancer

Mutations in *EHF* are relatively rare in human cancers and those which do arise are predominantly non-recurring missense mutations (Figure 1.1). However, occasional truncating mutations occur in gastric, uterine and cervical cancers, suggestive of a potential tumour suppressive role. Conversely, EHF amplifications occur in a subset of oesophageal, ovarian, stomach, bladder, and

head and neck cancers, however, as discussed above, EHF is located within close proximity to ELF5 and has an amplification and deletion profile which is very similar to ELF5 [26], making it difficult to determine whether overexpression of one, or perhaps both transcription factors provide a selective advantage for these tumours.

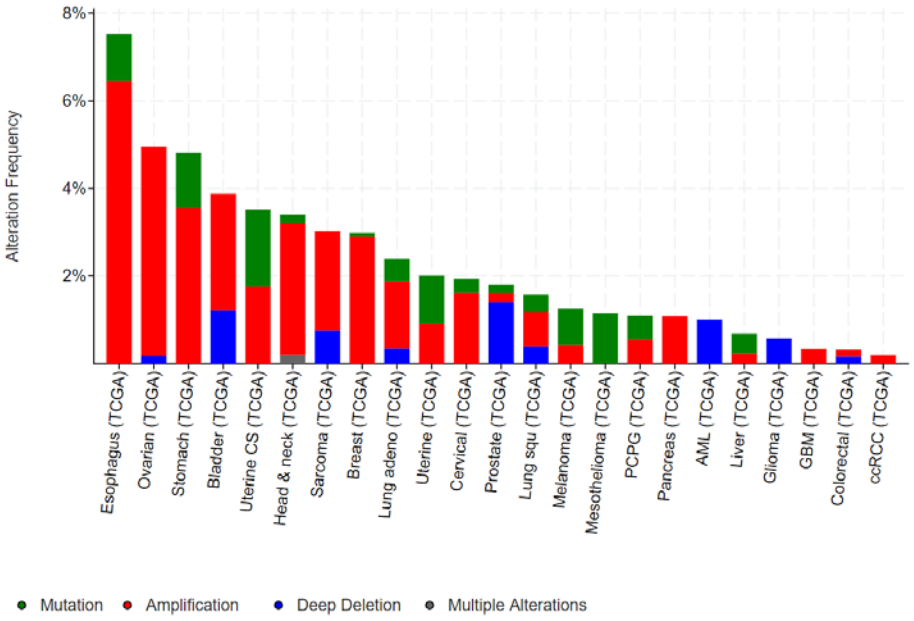

Figure 1.1. Genomic alterations in EHF in human cancers. Data from cancer bioportal. Only showing cancers in which >50 cases were analysed [26].

1.1.3.1 EHF as a tumour suppressor gene

Prostate cancer: There is evidence that EHF may act as either a tumour suppressor gene or an oncogene in prostate cancer. An initial study of the role of EHF in prostate cancer demonstrated that knockdown of *EHF* in prostate cancer cell lines resulted in cellular senescence mediated by induced expression of p16 and p27, which significantly reduced tumour growth *in vivo* [27]. However, the majority of evidence generated to-date suggests EHF functions as a tumour suppressor gene in prostate cancer where EHF mRNA and protein expression is reduced, which was linked to methylation of a conserved CpG residue within the *EHF* promoter [28, 29]. Loss of EHF expression is more pronounced in tumours with higher expression of cancer stem cell markers and is associated with poorer patient outcome. Re-expression of *EHF* in prostate cancer cells inhibited clonogenic survival and induced apoptosis by directly driving caspase-3 expression [28]. Subsequent studies demonstrated that *EHF* re-expression in prostate cancer cells inhibited stem like properties and promoted epithelial differentiation by repressing EMT drivers, such as TWIST1, ZEB2, NANOG and POU5F1 [30]. This effect was mechanistically linked to EHF-mediated repression of the Lin28a and Lin28b RNA binding proteins, and re-expression of members of the let-7 family

of miRNAs [31]. EHF also represses IL-6 in prostate epithelial cells by directly binding to the IL-6 promoter, and EHF loss drives tumour progression by de-repression of IL-6, and subsequent stimulation of STAT3 signalling [32]. Finally, Kunderfranco et al. demonstrated that EHF contributes to tumour suppression of prostate cancer cells by repressing expression of the epigenetic regulator EZH2 [29, 33] and promoting expression of the tumour suppressor Nkx3.1 [29].

Colorectal cancer: As with prostate cancer, the role of EHF in colorectal cancer (CRC) is contradictory. EHF mRNA expression and protein has been reported to be increased in colorectal cancers compared to adjacent normal tissue [8, 34]. Specifically, a study by Wang et al. found that *EHF* overexpression correlated positively with poor differentiation, advanced T stage, and shorter overall survival of CRC patients [34]. Furthermore, the authors found that over-expression of *EHF* in CRC cell lines promoted cell proliferation, migration and invasion *in vitro* and *in vivo*. Mechanistically, this was shown to occur through upregulation of TGFβ1 expression, and subsequent activation of the TGFβ signalling pathway [34]. Supportive of such a role for EHF in CRC, Taniue et al. demonstrated that *EHF* knockdown increased apoptosis in p53 wildtype colon cancer cells through reduced expression of RUVBL, suggesting that EHF is required for survival of colon cancer cells [35]. Conversely, work from my own laboratory has demonstrated that knockdown of *EHF* increased migration and invasion of colon cancer cells, indicative of a tumour suppressor role. Furthermore, members of my laboratory have also observed that EHF co-operates with the CDX1 transcription factor to maintain differentiation of colorectal cancer cell lines (submitted - unpublished).

Pancreatic cancer: EHF mRNA and protein expression are reduced in pancreatic ductal adenocarcinoma (PDAC) compared to normal pancreatic tissue and low EHF mRNA correlates with poorer patient survival [36]. Furthermore, EHF expression is inversely correlated with PDAC histological grade. *EHF* re-expression in PDAC cell lines inhibited proliferation, as well as migration and invasion. This was at least partly mediated through loss of expression of CDH1, which was shown to be directly regulated by EHF. Furthermore, the authors demonstrated that re-expression of *EHF* could inhibit proliferation and metastasis in two *in vivo* models of pancreatic cancer (orthotopic and intrasplenic). Consistent with a tumour suppressive role of EHF in pancreatic cancer, a recent study by Zhou et al. demonstrated that silencing of EHF in PDAC cell lines increased cancer stemness evidenced by increased sphere forming capacity and upregulation of the stemness-related genes SOX9, SOX2, OCT4 and NANOG [37]. Furthermore, it was shown that EHF inhibits the crosstalk between pancreatic cancer cells and the adjacent cancer stem cell niche by transcriptionally suppressing the CXCL12 receptor CXCR4 involved in this process. Interestingly, the authors performed a screen of 190 compounds from a drug library that revealed that EHF

could be re-expressed in PDAC cells by treatment with Rosiglitazone which was found to be due to transcriptional activation mediated by PPARγ. Finally, a study investigating the efficacy of immune checkpoint blockade therapy (anti-PD1 therapy) of PDAC cells grown *in vivo* found that tumours where EHF is depleted accumulate regulatory T cells and myeloid-derived suppressor cells which led to lower response to anti-PD1 therapy [38]. These studies highlight the potential use of re-expression of EHF as a therapeutic strategy in PDACs.

Oesophageal cancer: In oesophageal squamous cell carcinoma (ESCC), the primary mechanism of EHF protein dysregulation is altered subcellular localization, where in contrast to its predominantly nuclear expression in the normal oesophageal epithelium, EHF is localized to the cytoplasm [39]. While the mechanisms driving the cytoplasmic mis-localization of EHF are yet to be defined, re-expression of *EHF* in ESCC cell lines which restored its nuclear expression, inhibited cell proliferation, colony formation, migration, and invasion.

1.1.3.2 EHF as an oncogene

Breast cancer: Ehf mRNA is upregulated in murine breast cancer cell lines and in tumours from mouse models of breast cancer compared to normal mammary epithelial cell lines [40]. Similarly, EHF mRNA and protein are highly expressed in many human breast cancer cell lines and patient-derived breast cancer biopsies compared with normal epithelial cell lines and tissue [41]. It is important to note however, that single cell sequencing from various stages of mammary gland development show that EHF mRNA is mainly expressed in alveolar progenitor cells and mature alveolar cells during pregnancy which may skew these comparisons (data mined from mammary gland developmental portal, Maroni lab, Cambridge, UK [42]). Furthermore, EHF has been postulated to play a role in cisplatin resistance in MCF7 cells [43].

Ovarian cancer: EHF mRNA is highly expressed in ovarian cancer cells compared with normal tissue and is associated with poorer overall survival. Knockdown of *EHF* in ovarian cancer cell lines inhibited cell proliferation, which was associated with reduced expression of Cyclin B1 and Cyclin D1, and upregulation of the cyclin-dependent kinase inhibitor, p21. *EHF* knockdown also inhibited migration and invasion of ovarian cancer cell lines, and reduced expression of the matrix metalloprotease MMP9, which is involved in extracellular matrix degradation [44].

Gastric cancer: The rate of *EHF* amplification in gastric cancer identified in large genomic studies is ~4%, however, Shi et al. reported *EHF* amplification in ~40% of cases, which was associated with worse patient outcome [45]. Similarly, *EHF* was identified to be highly upregulated in gastric tumours in a study that compared differentially expressed genes between gastric tumours and normal gastric tissue [46, 47]. Furthermore, consistent with an oncogenic role in this disease, *EHF*

knockdown inhibited proliferation, survival, migration and invasion of gastric cancer cell lines *in vitro* and *in vivo*. Mechanistically, EHF was shown to drive gastric cancer progression through direct transactivation of the HER2 promoter, and activation of downstream MAPK and PI3K/AKT signalling [45, 47].

Similarly, Gong et al. reported that knockdown of *EHF* in gastric cancer cell lines decreased the size of gastric spheres and attenuated clonogenicity [48]. Interestingly, overexpression of *EHF* in gastric cancer cell lines conferred resistance to 5-FU, and increased cell motility and invasiveness. Collectively, these studies establish a role for EHF in gastric cancer progression and suggest EHF may be a potential therapeutic target in this disease.

Thyroid cancer: EHF mRNA and protein expression are upregulated in papillary thyroid cancer (PTC) compared with normal tissue [49]. As observed in gastric cancer, EHF mRNA expression is correlated with HER2 and HER3 expression in PTC patients, and EHF can directly transactivate the HER2 and HER3 promoters. Consistent with a role for EHF in tumour progression in thyroid cancer, knockdown of *EHF* in PTC cell lines inhibited proliferation, colony formation, migration and invasion and increased apoptosis *in vitro* and *in vivo*.

1.2 The intestinal epithelium

A major focus of this thesis is to investigate the role of EHF in the intestinal epithelium, and specifically in the colonic epithelium where EHF expression is highest [26]. As described above, EHF is highly expressed in proliferative stem cells and microfold cells in the intestinal epithelium. Complete ablation of the *Ehf* gene in mice decreases LGR5+ stem cell numbers in the small intestine and impairs the ability of the intestinal epithelium to self-renew following irradiation. However, the impact of *Ehf* deletion on colonic homeostasis, or tumour progression was not investigated in this study.

The role of the related ESE family members SPDEF and ELF3 have also been studied in the intestinal epithelium. Specifically, terminal differentiation of goblet cells in the intestinal epithelium of *Spdef* $^{-/-}$ mice is impaired [50], while transgenic *Spdef* overexpression resulted in an expanded number of goblet cells in the intestinal epithelium [51] establishing SPDEF as a goblet cell lineage determinant.

Likewise, constitutive deletion of *Elf3* in mice (*Elf3* $^{-/-}$) results in partial embryonic lethality and the majority of surviving mice suffer from malnourishment leading to premature death [52]. The phenotype is caused by disrupted structural and functional intestinal barrier integrity as

manifested by impaired enterocyte morphology and reduced number of differentiated goblet cells.

Comparatively, the impact of *Ehf* deletion on maintenance of colonic homeostasis is unknown and will be investigated in Chapter 4 of this thesis. A detailed review of the hierarchy of intestinal epithelial cell differentiation and turnover, and the pathways involved in regulating this process is presented below.

1.2.1 Hierarchy of the intestinal epithelium

The intestinal epithelium is highly specialised to perform the basic functions of food digestion, nutrient absorption and protection against pathogens [53]. In humans the intestine is anatomically divided into the small intestine and colon, with the small intestine further subdivided into the duodenum, jejunum and ileum. The intestinal tract of mice additionally comprises the caecum which assists with breakdown of plant-based materials such as cellulose.

Morphologically the small intestine is organised into crypts of Lieberkühn and villi. The villi protrude into the intestinal lumen which dramatically increases the surface area of the epithelium and allows for efficient nutrient absorption. Comparatively, the colon consists only of crypts of Lieberkühn.

Proliferative stem cells reside in the base of the crypts in both the small intestine and colon. Stem cells give rise to transit-amplifying cells, which undergo several rounds of cell division. The progeny of these cells then undergoes terminal differentiation into one of the highly specialised epithelial cells of either the absorptive or secretory lineages. These cells differentiate as they migrate up the crypts/crypt-villous axis towards the luminal surface, where they ultimately undergo spontaneous apoptosis and are shed into the gut lumen. This whole process of terminal differentiation takes 3-5 days to complete [54, 55]. The exception is the differentiation of Paneth cells (small intestine) or deep crypt secretory cells (colon), which differentiate as the migrate downwards to the crypt base. Currently, it is understood that intestinal stem cells can give rise to at least seven unique and highly specialised epithelial cell types in the intestine (Figure 1.2). These cell types are described below.

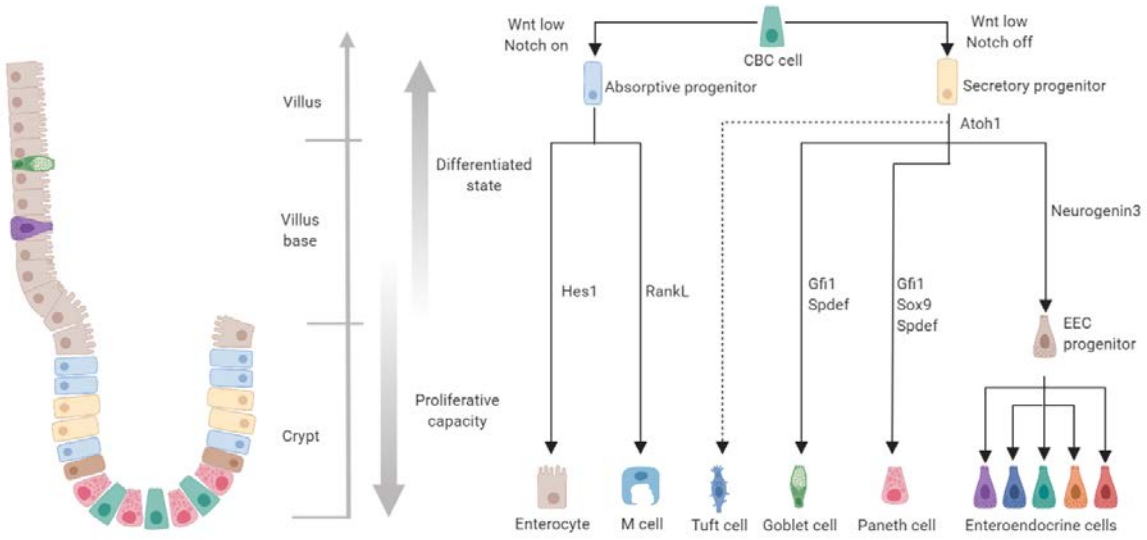

Figure 1.2. Hierarchy of the intestinal epithelium and the factors contributing to epithelial cell fate specification. The crypts of Lieberkühn contain proliferative crypt base columnar (CBC) stem cells interspersed between Paneth cells (or deep crypt secretory cells in the colon), and as cells migrate up the crypt-villous axis towards the luminal surface they undergo terminal differentiation. Activation/de-activation of the Wnt and Notch pathways determine absorptive or secretory lineage commitment, while expression of specific genes give rise to the specialised epithelial cell types lining the intestine. EEC: enteroendocrine cell.

Intestinal stem cells: The exact number of stem cells in each crypt is unclear, but a study that relied on tracing mutation-induced clonal marks during DNA replication, estimated the number to be between five and seven per crypt [56]. The first identified stem cells (crypt-base columnar (CBC) stem cells) which give rise to all cell types of the intestinal epithelium exhibited high expression of the canonical Wnt pathway target gene LGR5 [57]. These cells were highly proliferative, however, ablation of these cells demonstrated that they are dispensable for intestinal homeostasis [58], indicating there is another cell type that can compensate for loss of the $LGR5^{+}$-population. BMI1 is a marker of this second population of stem cells (often denoted +4 cells due to their location from the crypt base) which reside in a quiescent state and repopulate the intestinal epithelium in response to injury [59, 60].

Paneth cells: Unlike other cells of the intestinal epithelium, Paneth cells only exist in the small intestine. They are located at the base of the crypts of Lieberkühn interspersed between the $LGR5^{+}$ stem cells and are only renewed every 3-6 weeks [61]. These granulated cells are important for innate immunity as they are the main producers of antimicrobial proteins and peptides including crypt defensins (cryptdins) and lysozyme [62]. The Paneth cells also contribute to the CBC stem cell niche by producing growth factors required for stem cell maintenance such as EGF, WNT3 and NOTCH ligands. This was identified through *in vivo* ablation of Paneth cells which resulted in

concomitant loss of LGR5$^+$ CBC stem cells [63, 64]. Comparatively, *Atoh1*-null mice with complete and sustained loss of Paneth cells retained LGR5$^+$ stem cell function and proliferation, suggesting that Paneth cells are not the only cell type to contribute to the stem cell niche [65].

The colonic equivalent of Paneth cells are the REG4$^+$ deep crypt secretory (DCS) cells which contribute to the colonic stem cell niche. This was established through *in vivo* studies where ablation of REG4-expressing cells resulted in loss of LGR5$^+$ stem cells, and by *in vitro* studies where sorted REG4$^+$ DCS cells promoted organoid formation of single LGR5$^+$ colon stem cells [66].

Enterocytes: Enterocytes are highly polarised cells that constitute over 80% of the intestinal epithelial cells [53]. These cells develop a brush border consisting of negatively charged microvilli responsible for nutrient and antigen absorption and transport of these nutrients across the epithelium [67].

Goblet cells: The proportion of goblet cells increases from the duodenum (~4%) [54] to the distal colon (~16%) [68]. These cells secrete mucins (mainly MUC2) and trefoil proteins that protect the epithelium against shear stress and chemical damage and ensures movement of gut contents. The mucous layer also creates a protective barrier between the epithelium and contents of the colonic lumen including the microbiota, and knockout mouse models with reduced/absent mucous production (e.g. *Muc2*-null) spontaneously develop colitis and adenomas in the small intestine [69, 70].

Enteroendocrine cells: Enteroendocrine cells (EECs) is the collective name for the variety of different hormone producing cells scattered throughout the intestinal epithelium [71], and comprise approximately 1% of all epithelial cells lining the intestinal tract [54]. In the intestinal epithelium all enteroendocrine cells are dependent on Neurogenin3 (NGN3) as *Ngn3*-deficient mice fail to develop any EECs, although differentiation of the other major intestinal lineages remains intact [72]. *Ngn3*-deficient mice develop diabetes shortly after birth due to a failure to generate any islet cells and endocrine progenitors in the pancreas, illustrating the importance of these cells in homeostasis.

Tuft cells: Tuft cells constitute around 0.4% of all the intestinal epithelial cells [73], but accumulate during parasite colonization and infection. Furthermore, the number of tuft cells varies depending on the microbiota present at animal facilities [74]. Tuft cells express a taste-chemosensory machinery and cooperates with the innate immune system to mount responses to parasitic infections [75]. There are a variety of tuft cell markers, of which DCLK1 is the most commonly used to [73]. The DCLK1$^+$ tuft cells are long-lived quiescent cells that remain quiescent even following conditional *APC* mutation [76]. These cells only become active upon mucosal injury, and ablation of tuft cells by intestinal-specific deletion of *Dclk1* (*Villin* ^{Cre};*Dclk1* $^{Lox/Lox}$) causes impaired recovery

following small intestinal and colonic irradiation-induced injury [77]. The authors showed that these mice have a weakened epithelial barrier function evidenced by reduced expression of tight junction proteins and increased permeability of a FITC-labelled dextran tracer, however the the mechanism by which this occurs is not yet known.

Microfold cells: Throughout the intestinal tract there are organised lymphoid follicles known as gut associated lymphoid tissue (GALT) or Peyer's patches, which are located beneath the epithelial cell layer. A small portion of cells in the follicle-associated epithelium are microfold (M) cells. These cells perform phagocytosis and transcytosis of gut luminal macromolecules and particulate antigens across the epithelium [78]. Another population of M cells have also been identified which are not associated with the lymphoid follicles, termed villous M cells [79]. These cells sample antigens and elicit immune responses independent of Peyer's patches.

Cup cells: Cup cells are not well studied, and their role in the intestinal epithelium is unclear. About 6% of the intestinal villous epithelium consist of cup cells, and these cells can undergo pinocytosis and are therefore members of the absorptive lineage [80].

1.2.2 Signalling pathways involved in intestinal homeostasis

There are four main pathways that determine the commitment of $LGR5^+$ stem cell-derived progenitor cells into terminally differentiated cells of the absorptive or secretory lineages; the Notch, Wnt, Hedgehog and BMP pathways. The contribution of each pathway to intestinal stem cell renewal and epithelial cell differentiation is described below.

1.2.2.1 The Notch signalling pathway

The Notch signalling pathway is relatively unique in that it relies on cell-cell contact for signalling. The pathway is initiated by binding of transmembrane protein Notch ligands (Delta/Serrate/Lag-2 families) to its receptors (Notch 1-4) on adjacent cells [81]. Ligand binding promotes two proteolytic cleavage events in the Notch receptor catalysed by the ADAM-family of metalloproteases and y-secretase. This releases the Notch intracellular domain which subsequently translocates to the nucleus and cooperates with DNA-binding proteins to promote transcription [82].

In the intestinal epithelium Notch signalling is active in stem and progenitor cells and there is increased expression of the Notch ligands Dll1, Dll4, Jagged1 and the Notch receptors Notch1 and Notch2 [83] in intestinal crypts where these cells reside. Notch signalling is important for CBC stem cell renewal as shown by loss of the stem cell marker OLFM4 upon Notch inhibition [84].

Furthermore, Notch signalling is a key determinant of intestinal epithelial cell fate, as inhibition of the pathway in mice by treatment with γ-secretase inhibitors caused a lack of absorptive cells and an overproduction of secretory goblet and enteroendocrine cells [85-87]. These findings were subsequently verified through genetic deletion of Notch signalling components (e.g., *Dll1*/*Dll4* knockout mice) which induced a similar increase in secretory cell types [88, 89], thus indicated an essential role for Notch signalling in establishment of the absorptive cell lineage.

Key transcriptional targets of Notch signalling in the intestinal epithelium are Hes1 and Atoh1. Hes1 is a transcriptional repressor important for lineage commitment of absorptive enterocytes, however, a recent study demonstrated that Hes3 and Hes5 can compensate for loss of Hes1 in the adult intestine [90]. *Hes1*-null mice die soon after birth due to a surplus of goblet, Paneth and enteroendocrine cells [91, 92], but conditional knockout of *Hes1* demonstrated that the distribution of secretory and absorptive lineages reverted to normalcy at two months of age [90]. Mutation of all three Hes-genes, however, led to long-term abnormal crypt/villi morphology with increased abundance of secretory cell lineages. Deletion of these genes did not impact the CBC stem cells, indicating that Hes1/3/5 specifically regulate absorptive cell fate determination.

In contrast to Hes1, expression of Atoh1 promotes differentiation along the secretory cell lineages in the intestinal epithelium, as demonstrated by complete loss of these lineages in *Atoh1*-null and *Atoh1* intestinal-specific knockout mice [93, 94]. Inhibition of Notch signalling had no phenotypic effect on *Atoh1*-deficient mice [95-97], indicating that Atoh1 is the master regulator of cell fate determination in the intestinal epithelium and that Notch/Hes1 functions as a negative regulator of Atoh1 to drive differentiation towards the absorptive lineage. Downstream of Atoh1 are several transcription factors that contributes to each specific secretory cell lineages. Ngn3 is essential for the differentiation of enteroendocrine cells [72], Gfi1 directs progenitor cells toward a Paneth cell fate [98], while Spdef and Klf4 are goblet cell lineage determinants [50, 99].

1.2.2.2 The Wnt signalling pathway

The Wnt signalling pathway is highly conserved and activated through approximately 20 secreted Wnt ligands [100]. The Wnt ligands interact with 10 human Frizzled (Fzd) transmembrane receptors to mediate downstream signalling by either canonical or non-canonical pathways. The canonical pathway is the best described Wnt signalling pathway and relies on β-catenin as its main effector protein. Absence of Wnt signalling leads to degradation of β-catenin, while active Wnt signalling blocks this degradation through a destruction complex that involves Axin, adenomatous polyposis coli (APC), casein kinase I (CK1) and glycogen synthase kinase 3β (GSK3β) [101].

Stabilised β-catenin is translocated to the nucleus where it binds to transcription factors such as TCF4 to transactivate expression of Wnt target genes such as c-MYC and LGR5.

Wnt signalling is required for maintaining correct ISC function, as deregulation of the pathway in ISCs through *Apc* mutations leads to development of epithelial hyperplasia and polyposis [102]. Furthermore, genetic deletion of the Wnt effector proteins β-catenin and TCF4 results in rapid loss of the $LGR5^{+}$ stem cell compartment [103, 104]. Wnt signalling is also implicated in lineage specification as impaired Wnt signalling in mice results in reduced Atoh1-positive precursor cells in intestinal crypts (i.e. reduced secretory lineages) [105]. Furthermore, Wnt signalling is actively involved in Paneth cell differentiation through the Wnt target gene SOX9. Conditional deletion of *Sox9* in the intestinal epithelium of mice results in complete ablation of Paneth cells, which are replaced with Ki67-positive cells [106, 107].

1.2.2.3 The Hedgehog signalling pathway

There are three Hedgehog (Hh) ligands in mammals, Indian Hedgehog (Ihh), Desert Hedgehog (Dhh) and Sonic Hedgehog (Shh). Dhh and Shh are mainly expressed in the stomach, although Shh is expressed at low levels in epithelial cells at the bottom of intestinal crypts [108]. Ihh is expressed in intestinal epithelial cells located at the bottom of small intestinal villi and in mature colonocytes suggesting a role in differentiation [109, 110].

Hedgehog signalling is important for intestinal homeostasis as conditional deletion of *Ihh* causes ISC hyperproliferation, crypt fission, expansion of the Wnt-responsive compartment and up-regulation of Wnt target genes such as c-MYC, SOX9 and LGR5 [111]. Similarly, rats treated with a Hh-inhibitor resulted in loss of colonic differentiation markers and restricted Wnt signalling in colonic crypts [110]. Collectively, these data indicate cross-talk between Wnt and Hh signalling in the intestinal epithelium.

1.2.2.4 Bone morphogenic protein signalling pathway

The bone morphogenic protein (BMP) pathway constitutes signalling molecules belonging to the TGFβ cytokine family. As with some of the other signalling pathways (Wnt and Hh) BMP members are expressed both in the epithelium and the surrounding mesenchyme in the intestine [112] and influence lineage-specific differentiation. Disruption of BMP signalling in mice by treatment with the BMP inhibitor noggin resulted in ISC hyperproliferation and ectopic crypt formation which eventually led to development of intestinal polyposis [113], although this effect was likely due to mesenchymal rather than epithelial BMP signalling [114]. BMPs prevent intestinal stem cells

proliferation by antagonising Wnt signalling [115] or by negative regulation of cell cycle progression through stabilisation of the cyclin-dependent kinase inhibitor, p21 [116].

BMPs can also influence intestinal epithelial lineage differentiation as shown by BMP receptor type IA (*Bmpr1a*) conditional intestinal knockout mice, which demonstrate impaired maturation of goblet and Paneth cells and reduced number of enteroendocrine cells in the intestinal epithelium [114]. This effect on intestinal epithelial differentiation occurred independent of the Hh and Wnt signalling pathways.

1.3 Pathologies of the intestinal epithelium

A second focus of this thesis is to investigate the role of EHF in pathologies associated with the intestinal epithelium, particularly inflammatory bowel disease (IBD) and colon tumourigenesis. The role of EHF in inflammation of the colonic epithelium is unknown, although there have been some *in vitro* studies that suggest a role of EHF in airway inflammation [11, 12]. As for the role of EHF in colorectal cancer, there are conflicting data obtained from cultured cell lines as described earlier. Studies by Tanuie et al. and Wang et al. suggested that EHF is required for the survival of colon cancer cells and that EHF over-expression promotes cell proliferation, migration and invasion [34, 35], whereas unpublished data from our own laboratory suggests that loss of *EHF* increases migratory and invasive properties of colon cancer cells [117]. The role of EHF in IBD and CRC *in vivo* has not been investigated. A detailed review of our current understanding of these diseases is presented below.

1.3.1 Inflammatory bowel disease

Inflammatory bowel disease (IBD) is characterised by sustained inflammation of the intestine and can be sub-divided into two main diseases; ulcerative colitis (UC) and Crohn's disease (CD). UC is mostly restricted to the colonic mucosa, while CD affects the colon and small intestine with transmural inflammation [118]. Genome-wide association studies have identified 163 IBD-associated loci, many which are shared between UC and CD [119]. Animal studies have highlighted the importance of the genes, and their contribution towards the severity of IBD, although it must be noted that animal studies typically investigate gene ablation while the human studies are identifying SNPs. For instance, conditional deletion of hepatocyte nuclear factor 4a (*Hnf4a*) and *Stat3* increases the susceptibility and severity of chemically induced colitis [120, 121]. These genetic associations however, do not fully explain IBD, implying there is a role for environmental factors, particularly those that alter the composition of the gut microbiota [122].

The physical barrier of the intestinal epithelium is maintained through tight junctions (TJs) between neighbouring cells. Weakening of these TJs may contribute to IBD by increasing permeability and thereby inducing mucosal inflammation. Several factors may contribute to TJ weakening including the pro-inflammatory cytokines TNF-α and interferon-γ [123]. Indeed, it has been demonstrated that anti-TNF therapy alleviates the inflammation in IBD patients [124]. Another potential contributor to IBD is a reduced mucus layer. *Muc2*-deficient mice spontaneously develop colitis [69] and some IBD patients present with diminished mucus secretion [125].

1.3.1.1 Mouse models of inflammatory bowel disease

There are a variety of mouse models available to study IBD/colitis. These include genetic mouse models harbouring genetic deletion of key IBD-associated genes, adoptive transfer of T cells, Interleukin-10 (*Il10*) knockout, and treatment with the inflammation-inducing agents dextran sodium sulphate (DSS), trinitrobenzene sulfonic acid (TNBS) or oxazolone [126]. While none of these models fully recapitulate human IBD, each covers a specific initiating feature of the disease (Figure 1.3) and are described below.

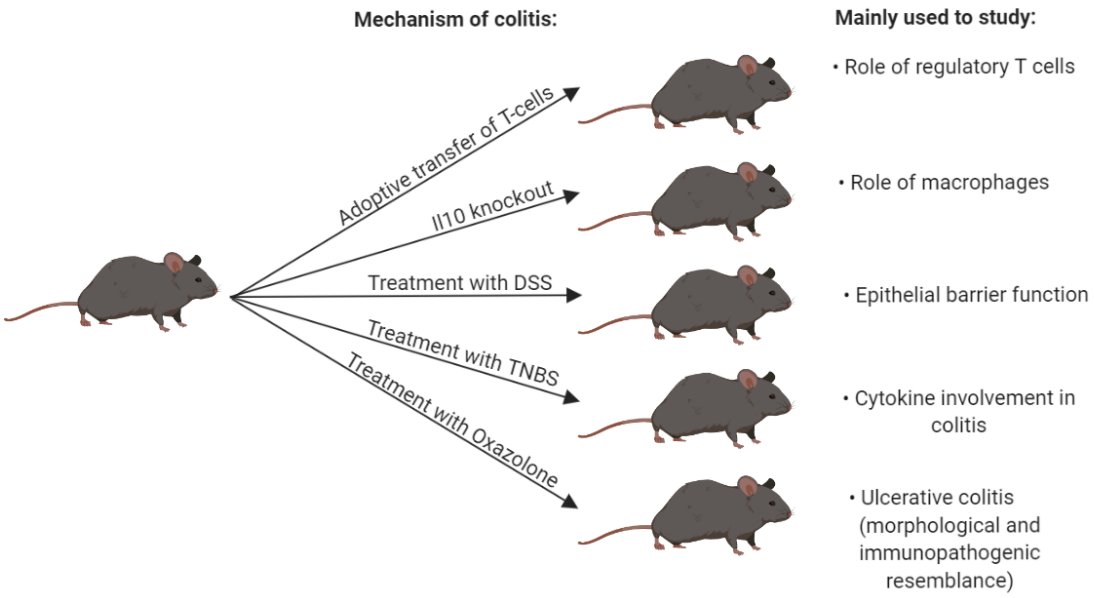

Figure 1.3. Mouse models of IBD. Figure illustrates the different mechanisms by which IBD can be initiated in mice and what feature of IBD each of these typically have been used to study. DSS: Dextran sodium sulphate. TNBS: Trinitrobenzene sulfonic acid.

Genetic deletion: There are a number of mouse models that involve conditional deletion of specific genes in the intestine which spontaneously develop colitis and may therefore be used to study the disease. Mice with genetic deletion of the multiple drug resistance gene, *Mdr1a* (*Mdr1a* $^{-/-}$),

develop spontaneous colitis as a result of a defective intestinal epithelial barrier [127]. Intestinal core 1-derived O-glycan (C1GALT1), the predominant form of mucin-like O-linked oligosaccharides which are principal components of the intestinal mucous layer, have been reported as impaired in UC patients [128]. Consistent with this finding, mice with intestinal-specific deletion of *C1galt1* (*C1galt1* $^{Lox/Lox}$; *Villin* ^{Cre}) spontaneously develop colitis in the rectum and distal colon caused by an impaired mucous barrier function, enabling rapid breach of the mucous layer by bacteria [129]. These models can be useful for the purpose of understanding the pathology of IBD, however have limited use in studying the impact of genetic modifications in colitis susceptibility and severity.

Adoptive transfer of T cells: The transfer of naïve T cells ($CD4^{+}CD45RB^{high}$) into syngeneic immunodeficient SCID or $Rag^{-/-}$ mice results in primary colonic inflammation 5-10 weeks after treatment, whereas transfer of mature T cells ($CD4^{+}CD45RB^{low}$) does not cause colitis [130]. The reason for this difference is likely due to the absence of T_{reg} cells in the mice transferred with naïve T cells, which suppress inflammation through production and secretion of cytokines including *Il10* and *Tgfβ* [131, 132]. The development of colitis in the adoptive transfer model does not occur when donor mice are housed in a germ-free facility [133]. This suggests that the microbiome plays a major role in colitis development, despite the inflammation being initiated through immune cells and the cytokines they produce.

Il10 knockout: Genetic polymorphisms in the IL-10 locus have been identified which are associated with increased risk of developing UC and CD [134, 135], while mutations in the IL-10 receptor subunits IL10RA and IL10RB have been associated with a familial form of early onset CD [136]. Consistent with these findings, *Il10* knockout mice develop spontaneous enterocolitis at 7-11 weeks [137] which is mediated mostly through macrophage dysfunction [138, 139]. This model of colitis also depends on the presence of the intestinal microbiota, as the inflammation phenotype is lost in a germ-free facility [140].

Dextran sodium sulphate: DSS is a detergent which causes colitis by disrupting the epithelial barrier, thereby enabling entry of bacteria and bacterial antigens into the mucosa. Administration of DSS occurs through the drinking water and histopathological features induced include erosions/ulcers, crypt loss and infiltration of lymphocytes [141]. This model has been widely used to study the role of the innate immune system (macrophages, neutrophils and mast cells) in the development/recovery of intestinal inflammation [142-145] and the factors that maintain and re-establish epithelial integrity during or post-injury [146, 147]. A summary of the model is presented in Figure 1.4.

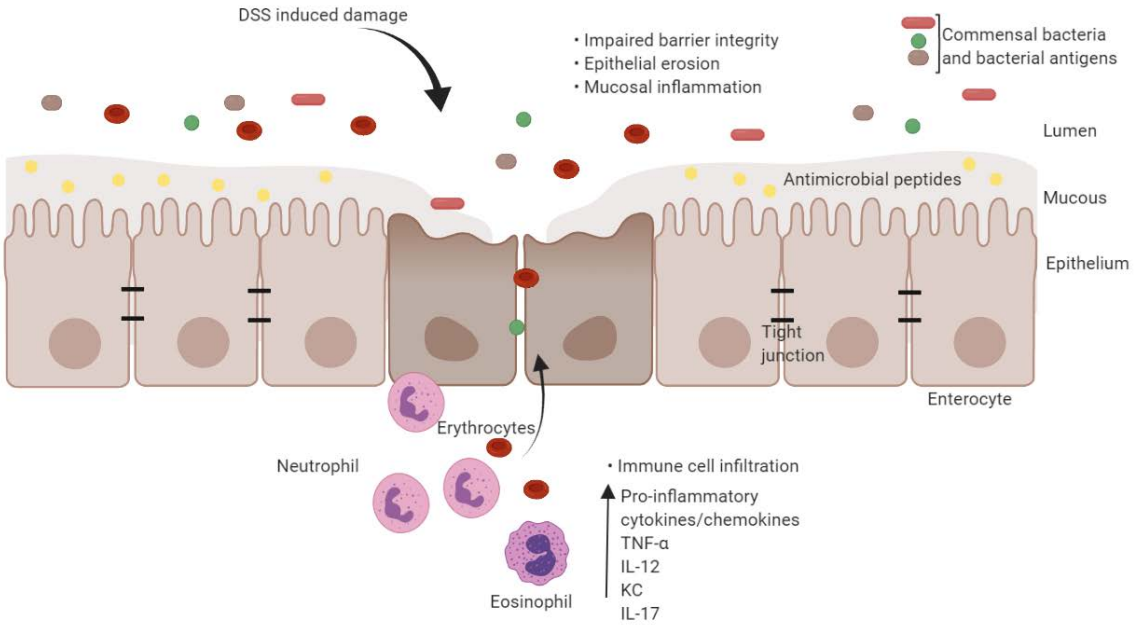

Figure 1.4. DSS colitis mouse model. Addition of DSS causes damage to the epithelial barrier, thereby enabling entry of bacteria and bacterial antigens into the mucosa. This elicits an immune response and subsequent upregulation of proinflammatory cytokines.

Trinitrobenzene sulfonic acid (TNBS): TNBS is a contactant, is administered intra-rectally and initiates a mucosal immune response by rendering colonic proteins immunogenic, through haptenating body proteins with trinitrophenyl groups [148]. The resulting colitis is transmurally driven by T_H1-mediated immune responses and causes weight loss, diarrhoea and rectal prolapse in recipient animals [149]. This model is used to study CD due to similarities in the characteristics of the disease [126], and successful mouse studies in blocking IL-12 cytokine response [149-151] have led to the development of IL-12 antibody treatment for CD patients [152, 153].

Oxazolone: Finally, as with TNBS, oxazolone is a haptenating agent administered intrarectally, but unlike TNBS it induces colitis of the distal colon that resembles UC rather than CD. The disease is characterised by immune infiltration of lymphocytes, oedema and ulcerations [154] believed to be caused by the presence of natural killer T cells that produce an abundance of Il13 [155].

1.3.2 Colorectal cancer

Colorectal cancer (CRC) is the third most commonly diagnosed cancer in Australia and is the second leading cause of cancer-related deaths, with an estimated 4,129 deaths in 2018 [156]. The overall five-year survival rate is 69% in Australia, but there is a clear correlation between survival rate and the stage of disease at diagnosis. For localised disease (stage I) the survival rate is around 90%, while it drops to below 15% for patients with metastatic disease (stage IV) [157].

Most colorectal cancers are sporadic (70-80%), while the remaining cases have a strong familial or hereditary component. These include Lynch Syndrome and familial adenomatous polyposis [158]. A small subset of patients (1-2%) present with CRC on account of inflammatory bowel disease [159].

1.3.2.1 Staging and treatment

Colorectal cancers are typically classified according to the TNM system which considers the depth to which the tumour has invaded into the underlying muscularis (T stage), lymph node involvement (N stage) and presence of distant metastases (M stage). These factors combined informs the stage of disease which forms the basis of therapeutic decisions [160].

Surgery remains the most common treatment for early-stage disease (stage I and II), while some stage II and stage III colon cancers are treated by adjuvant chemotherapy following surgery to lower the risk of recurrence. Comparatively, rectal cancers are commonly treated with neoadjuvant chemotherapy and radiation therapy [161]. For patients with advanced disease, treatment options are limited to chemotherapy, targeted therapy and in a small subset of patients, immunotherapy.

1.3.2.2 Molecular pathogenesis

Colorectal cancer is a heterogenous disease that arises from genetic and/or epigenetic alterations. Underlying the accumulation of genetic alterations (e.g. mutations, amplifications, deletions) is an increase in genomic instability which can be due to chromosome instability (CIN) or microsatellite instability (MSI) [162]. These pathways are described below and are summarised in Figure 1.5.

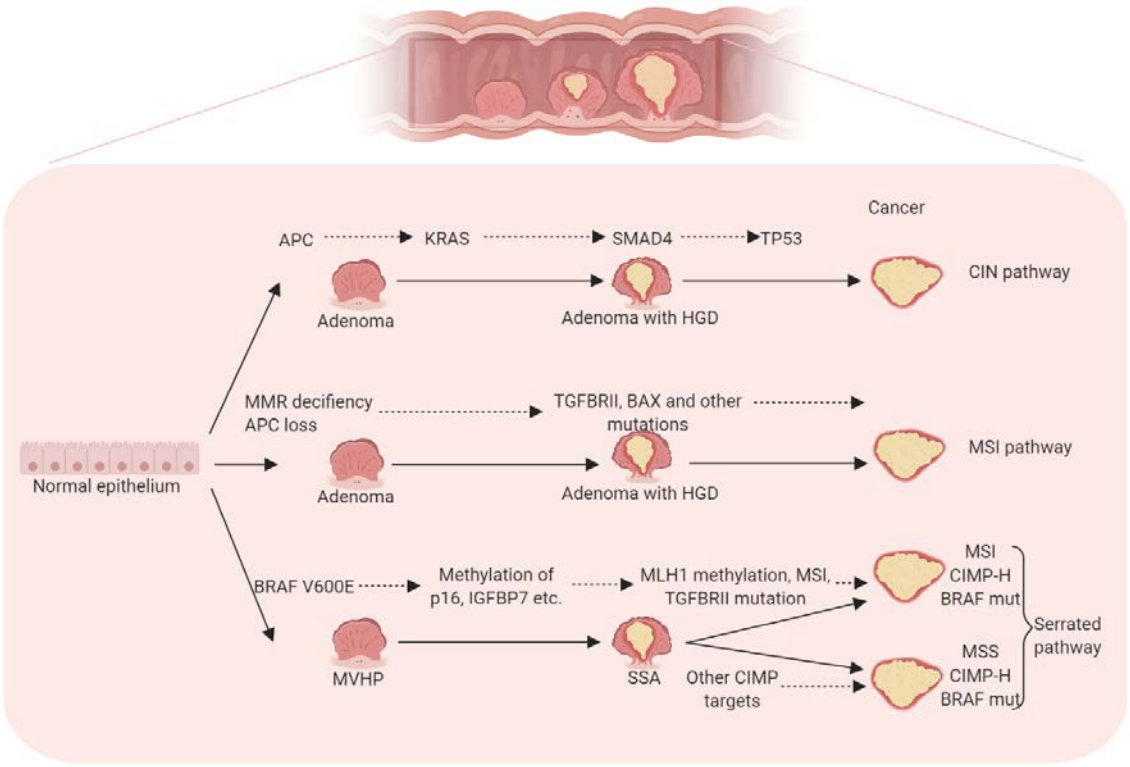

Figure 1.5. Overview of the different pathways leading to colorectal cancer initiation and progression. MMR: Mismatch repair. SSA: Sessile serrated adenomas. CIN: Chromosomal instability. CIMP-H: CpG island methylator phenotype – High. MSS: Microsatellite stability. MSI: Microsatellite instability. HGD: High-grade dysplasia. MVHP: Microvesicular hyperplastic polyp.

Chromosome instability: CIN occurs in about 85% of CRCs and are characterised by high numbers of chromosomal gains or losses (aneuploidy) as well as more focal regions of amplifications and deletions [163]. These tumours have high rates of Wnt pathway activation (80-85% of cases) mostly due to inactivating mutations and loss of heterozygosity (LOH) of the *APC* tumour suppressor gene, or occasional activating mutations of β-catenin [164]. The resultant constitutive activation of Wnt signalling initiates tumour formation by inducing epithelial hyperplasia and polyp formation. Subsequent (1) mutations in oncogenes belonging to the Extracellular signal-regulated kinase (ERK)-Mitogen-activated protein kinase (MAPK) pathway (*RAS*, *BRAF*); (2) inactivating mutations of the *TP53* gene; (3) inactivation of TGF-β signalling through *SMAD2-4* mutations; and (4) activating mutations of *PIK3CA* which activates PI3K signalling [165] enables these pre-malignant lesions to progress to adenocarcinomas with a capacity to metastasise [166].

Microsatellite instability: The second form of genomic instability which gives rise to CRC is deficient DNA mismatch repair (MMR). These tumours are initiated by mutations or epigenetic silencing of DNA mismatch repair genes such as *MSH2*, *MLH1*, *hPMS1*, *hPMS2*, and *hMSH6*/*GTBP*, however mutations in either *MLH1* or *MSH2* are most common [167]. Consequently, cells lose the ability to repair DNA, which results in a hypermutator phenotype. This most commonly manifests in

repetitive sequences of DNA (microsatellites) hence these tumours are also referred to as harbouring microsatellite instability (MSI). Mutations inevitably arise in components of the same signalling pathways described above for CIN tumours, however the specific genes which are mutated does differ. The genes that are more commonly mutated harbour repetitive elements in their coding sequence, e.g. *TGFBRII*, *PTEN* and *BAX* which impact the TGFβ, PI3K and TP53 signalling pathways respectively [168, 169]. MSI tumours initiated by epigenetic silencing of DNA mismatch repair genes (most commonly *MLH1*), often harbour methylation of multiple other loci, and are consequently referred to as having CpG island methylation phenotype (CIMP) [170, 171].

Serrated pathway: While the majority of colorectal cancers follow the classical adenoma-carcinoma sequence pathway described above, about 10% of colorectal carcinomas are initiated by the serrated pathway [172]. The serrated polyps which arise from this pathway are a heterogenous group of colorectal lesions that includes hyperplastic polyps (HPs), sessile serrated adenomas (SSA) and traditional serrated adenoma (TSA). These lesions are characterised by "saw-toothed" infoldings of the crypt epithelium. The majority of SSAs are initiated by mutations in the *BRAF* gene, and they frequently harbour CIMP with epigenetic silencing of genes including *MLH1*, *p16INK4a* and *IGFBP7* [173, 174]. Serrated carcinomas without *BRAF* mutations often harbour *KRAS* mutations and due to a lower rate of promoter methylation are referred to as CIMP-low [175]. Silencing of the DNA repair gene methylguanine methyltransferase (*MGMT*) by promoter hypermethylation has been associated with *KRAS* mutation and CIMP-low [176].

1.3.2.3 Mouse models of colorectal cancer

There are a variety of different models in use to study the initiation and progression of colorectal cancer in mice. However, most are limited by the failure to completely recapitulate the human disease, mainly due to the complexity of modelling the temporal accumulation of somatic mutations or other aberrations such as promoter methylation and mismatch repair defects. Furthermore, susceptibility of CRC development in mice highly depend on the background used [177, 178]. Nevertheless, mouse models remain an important tool in understanding CRC biology and for testing new treatments for this disease. A short description of some of these mouse models is given below.

Apc-initiated mouse models of CRC: The observations that the *APC* gene is inactivated in the majority of sporadic CRCs [164] and that these mutations are an early event in colorectal neoplasia [179], triggered the pursuit of a model of *Apc*-initiated CRC. The first such model was developed in the mid-1990s through a screen of mice treated with the mutagen *N*-ethyl-*N*-nitrosourea, where a mouse strain was identified which developed ~30 adenomas mostly throughout the small

intestine. It was subsequently identified that these mice harboured a heterozygous nonsense mutation in the *Apc* gene [180]. These mice were designated as *Apc* $^{Min/+}$ (Min=multiple intestinal neoplasia). Since then, multiple mouse strains have been generated using genetic approaches to introduce targeted inactivating mutations in specific regions of the *Apc* gene. Depending on the severity of the mutation (amount of *Apc* deleted), adenoma number (5-41 in the small intestinal and colonic epithelium) and latency (3 weeks to 8 months) varies significantly [181-184]. However, none of these models develop metastatic disease, and only long-lived mice will present with locally invasive adenocarcinomas [185]. To overcome this, researchers began combining *Apc* loss with other genetic modifications in genes known to be mutated in human CRC including Smad2/4 [186, 187], Kras [188] and Tp53 [189]. Combining *Apc* deletion with mutations in either of these genes led to development of locally invasive, but not metastatic adenocarcinomas. Interestingly, in a study where both *Apc* and *Kras* was modified using an adenoviral Cre, 20% of the mice developed metastasis to the liver after approximately 6 months [190]. Metastasis was achieved by restricting tumour multiplicity in the colon which enabled mice to live long enough to develop metastases. This was achieved by injection of Cre-expressing adenovirus into select regions of the colon and limitation of its spread by the surgical implantation of clips. Another metastatic model involved deletion of *Apc* and *Tp53* followed by doxycycline-inducible expression of mutant *Kras* [191]. In this model metastasis was observed after approximately 6 weeks in 25% of cases.

Mouse models of MSI CRC: The MSI phenotype is caused by mutations or more frequently, epigenetic silencing of DNA mismatch repair genes, Knockout mouse models of the constituents of the MMR machinery has been developed, however most of these gene deletions results in premature death due to haematopoietic malignancies such as lymphomas (e.g., *MLH1* [192], *MSH2* [193, 194], *MSH6* [195] and *PMS* [196]). Consequently, only a small fraction of the mice develop intestinal tumours [197, 198]. To overcome this limitation, a mouse model which allows for conditional deletion of *Msh2* was generated (*Msh2* $^{Lox/Lox}$). Crossing these mice with *Villin* ^{Cre} deleter mice limited tumour formation to the small intestinal epithelium [199]. Kucherlapati et al. combined mice with floxed *Msh2* alleles with mice harbouring a Lynch Syndrome related missense mutation (*Msh2* $^{G674D/+}$) or an *Msh2Δ7* null mutation (*Villin* ^{Cre};*Msh2* $^{Lox/G674D}$ and *Villin* ^{Cre};*Msh2* $^{Lox/null}$) and showed that these mice develop chemo-resistant intestinal tumours typical for MSI-high tumours.

Mouse models of Braf-initiated CRC: Recently, a number of mouse models of mutant *Braf*-initiated colon cancer have been developed. These models have a long latency of adenoma formation [200] which can be accelerated upon loss of differentiation-promoting genes such as *Cdx2* and *Smad4* [201]. *Braf*-driven CRC can also be accelerated by *Tp53* mutation that resulted in adenocarcinoma formation with metastasis to lymph nodes, pancreas and lungs in about 20% of cases [200].

Other genetic models of CRC: Other genetic mouse models of colon cancer include *Tgfbr2* inactivation combined with either hyperactivation of the PI3K signalling pathway initiated by *Pten* deletion [202] or hyperactivation of the MAPK pathway by *Kras* mutation [203]. In both models, mice developed adenocarcinomas with occasional metastasis.

Carcinogen-induced mouse models of CRC: The most common carcinogen-induced mouse model of CRC is administration of azoxymethane (AOM). Mice typically develop locally confined tumours [204] however, rapid progression may occur under a state of inflammation typically achieved through administration of DSS [205]. However, whole exome sequencing studies have shown that AOM-induced tumours have a distinct mutational landscape to that observed in human CRC [206]. In this study, most of the top significantly mutated genes (17/21) in AOM/DSS tumours were not classical cancer-related genes. While this model give rise to tumours which morphologically mimic human CRC, the applicability of this model for studying the contribution of specific signalling pathways to tumour progression is limited.

1.4 The mammary gland

A further focus of this thesis is to understand the role of EHF in mammary gland development. EHF has not been previously studied specifically in this context, however the EHF homologue ELF5 which is located only ~110kB apart on chromosome 11p13 is a critical determinant of mammary development. This is evidenced by conditional deletion of *Elf5* in the mammary glands of mice which blocks alveologenesis and lactation during pregnancy due to impaired terminal differentiation [207-210]. Interestingly, a study of the cell specific active enhancer states and associated transcription factor networks in mammary epithelial cells (MECs) identified EHF and ELF5 DNA binding sites as the most prevalent in luminal progenitor cells, and revealed a transcriptional regulatory network driven by EHF and ELF5 in luminal progenitors [211]. Consistent with this study, scRNA-seq mapping of cellular dynamics of human mammary epithelial cells demonstrated the transcription factors FOXS1, ELF5 and EHF to be most increased in the secretory lineage during gestation and lactation [42]. A similar study on adult mouse MECs uncovered a rare mixed-lineage cluster amongst basal cells expressing a subset of luminal genes, including EHF, suggesting the presence of cellular intermediates that may serve as transit or lineage-primed cells, and supporting the notion that EHF may play a role in commitment to a luminal cell fate in the post-natal mammary gland [212]. Here, we will undertake a review of the current knowledge of the histological changes and underlying molecular events which drive mammary gland development (summarised in Figure 1.6).

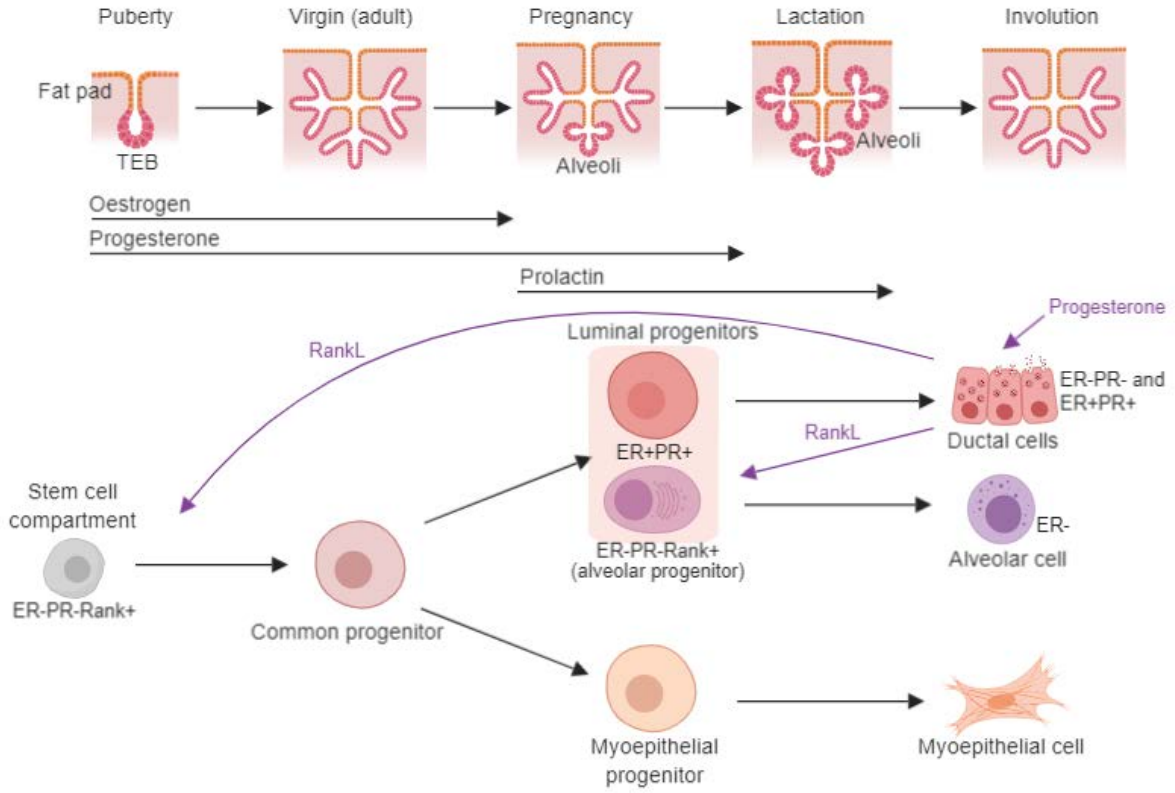

Figure 1.6. Mammary gland development and epithelial cell hierarchy. Top panel shows the stages of mammary gland development and the hormones involved in each process. The bottom panel shows the hierarchy of the mammary epithelium. ER: Oestrogen receptor. PR: Progesterone receptor.

1.4.1 Mammary gland development

Development of the mammary gland anlage begins between embryonic day (E) 10.5 and E18.5 in mice [213], and is composed of apically oriented luminal epithelial cells that line the ducts, also known as duct cells, and basally oriented myoepithelial cells in contact with the basement membrane [214].

Branching morphogenesis: After birth, the rudimental ductal tree remains quiescent until puberty when hormonal cues from oestrogen and progesterone (PR) initiate invasion of the anlage into the mammary fat pad, known as branching morphogenesis [215]. The importance of the oestrogen receptor α (ERα) and progesterone receptors (both PR-A and PR-B isoforms) in branching morphogenesis is highlighted by impaired ductal development of mice in which these genes have been deleted [216, 217].

The invading front is composed of highly proliferative terminal end buds (TEBs) [218], and the process is stopped through activation of the TGFβ pathway once the fat pad is filled [219]. The

outer compartment of the TEBs is composed of a single-cell layer of cap cells at the growing tip of the TEB, which differentiate into myoepithelial cells as the duct elongates, while the inner compartment consists of body cells that either apoptose to form the lumen or differentiate into duct cells [220]. Every oestrus cycle the mammary epithelium undergoes a burst of proliferation and apoptosis [221].

Alveologenesis and lactation: Upon pregnancy, the hormones PR and prolactin (Prl) initiate a proliferation and terminal differentiation program that results in the development and maturation of secretory milk-producing alveolar cells that constitute the lobuloalveolar compartment of the gland [220]. Epithelial-specific knockout of PR results in complete absence of alveologenesis indicating its essential role in this process [222]. Furthermore, the importance of Prl signalling is highlighted by knockout mouse studies of constituents of the downstream JAK2-STAT5 pathway [223, 224]. For example, *Stat5a* null mice have impaired alveolar differentiation [223]. Notably, this phenotype is partially overcome by exposure to multiple pregnancies due to compensatory signalling through STAT5b [225]. This was confirmed by conditional *Stat5a/b* mammary gland knockout mice which showed complete failure to form alveoli over multiple pregnancies [226].

Lactation occurs by contraction of the surrounding myoepithelial cells which causes the release and transport of milk through the ductal tree, a process stimulated by oxytocin.

Involution: Finally, once the hormonal stimulation is lost at the end of lactation, the expanded epithelial compartment undergoes apoptosis, termed involution, and is remodelled by proteases to resemble its pre-pregnant state [227].

1.4.2 Hierarchy of the mammary epithelium

Mammary luminal and myoepithelial cells arise from multipotent mammary stem cells (MaSCs). Single-cell sequencing studies have demonstrated that these cells exist during embryogenesis where the majority of mammary epithelial cells exhibit dual expression of both luminal and myoepithelial signature genes [228-230]. At birth, many cells retain this dual expression profile, however whether these are bipotent mammary progenitor cells [231] or cells spanning various transitional stages of lineage restriction is unclear. By puberty, these cells have bifurcated into lineage-restricted unipotent luminal and myoepithelial progenitor cells [212], although one study showed this lineage restriction occurs as early as four days after birth [228]. Luminal progenitors eventually differentiate to generate a secretory alveolar lineage (ER-) and a hormone sensitive lineage (ER+) [232, 233]. During pregnancy, the secretory alveolar lineage expands to produce mature alveolar cells required for lactation.

1.5 Hypothesis and aims

The EHF transcription factor is involved in the maintenance of multiple epithelial tissues including the skin, cornea, prostate, mammary gland and intestine. Furthermore, EHF can act as a tumour suppressor gene or an oncogene depending on the tissue in which the tumour arises. However, most of the current knowledge regarding the role of EHF in normal tissue homeostasis and cancer is derived from cultured cell lines, and there is therefore much that remains to be learned regarding the biological role of EHF. The aims of this PhD thesis therefore were to:

1. Generate a mouse model which allows for conditional deletion of the *Ehf* gene and study the impact of *Ehf* deletion on epithelial tissue homeostasis.
2. Determine the impact of *Ehf* deletion in the small intestinal and colonic epithelium on the onset of colitis and colorectal tumourigenesis.

Chapter 2: Materials and Methods

2.1 Generation of the *Ehf* floxed mice

Ehf $^{Lox/Lox}$ mice were generated by Ozgene (Perth, WA) prior to commencement of this PhD thesis. Briefly, mice were generated by flanking exon 8 and the coding region of exon 9 with loxP sites in C57Bl/6 embryonic stem (ES) cells. The targeting vector contained a neomycin cassette for selection in ES cells and was flanked by FRT sites for Flp-recombinase-mediated removal of the neomycin cassette (Figure 2.1). ES cell clones were selected based on neomycin resistance, screened by Southern hybridisation, and correctly targeted clones were microinjected into C57BL/6 murine blastocysts, and implanted into pseudo-pregnant females. Resulting chimeras were bred to wildtype C57Bl/6 mice to generate mice heterozygous for the floxed allele. Heterozygous mice were then crossed with C57Bl/6 OzFLP mice to induce removal of the neomycin cassette. Mice heterozygous for the floxed *Ehf* allele were subsequently mated to generate homozygous *Ehf* $^{Lox/Lox}$ mice.

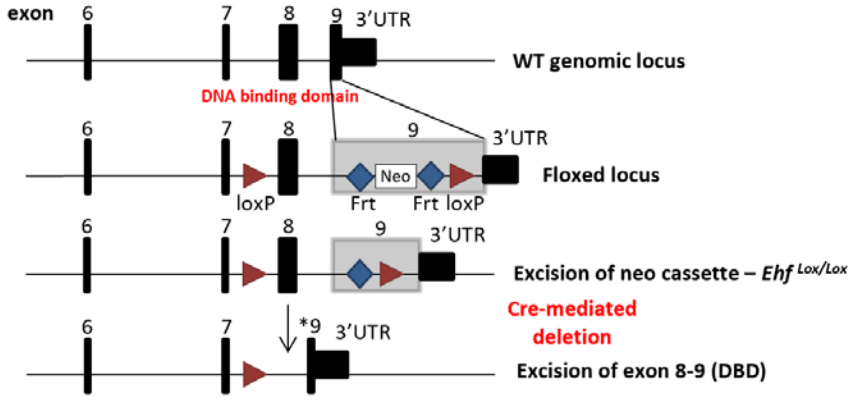

Figure 2.1. Generation of the *Ehf* floxed genomic locus and the impact of Cre-mediated deletion. *:disrupted exon.

2.2 Mouse breeding and maintenance

Breeding of the five mouse strains used in this thesis (Table 2.1) was undertaken at the AgriBio facility at the La Trobe Animal Research and Teaching Facility (La Trobe University, Bundoora, Melbourne). For experimental purposes, mice of the desired genotype were transferred to the Bio-Resource Facility (BRF) at the Austin Hospital. All animal studies performed in this thesis were approved by the Austin Health Animal Ethics Committee and conformed to the Australian Code of

Practice for the Care and Use of Animals for Scientific Purposes. Mice were housed in open-top boxes at the Bio-Resource Facility (BRF) at Austin Health (ONJCRI) unless otherwise stated.

Table 2.1. List of mouse strains used in this thesis.

Strain	Treatment and genotype	Gene deletion	Source	Background
1. *Ehf*$^{Lox/Lox}$	*Ehf*$^{Lox/Lox}$	No gene deletion	Ozgene	C57Bl/6
2. *CMV*^{Cre}	*CMV*^{Cre}	No gene deletion	Prof Warren Alexander (Walter and Eliza Hall Institute, Melbourne, Australia); *OS: Mouse Genetics Cologne (MGC) Foundation	C57Bl/6
3. *Villin*^{CreERT2}	Tamoxifen treated, *Villin*$^{CreERT2\text{-}TMX}$	No gene deletion, but activated Cre-recombinase	Dr. Sylvie Robine (Institut Curie-CNRS, Paris, France) [234]	C57Bl/6
4. *Ehf*$^{-/-}$	*Ehf*$^{-/-}$	*Ehf* deleted in all cells of the animal	In-house	C57Bl/6
5. *Ehf*$^{+/+}$	*Ehf*$^{+/+}$	No gene deletion	In-house	C57Bl/6
6. *Ehf*$^{Lox/Lox}$; *Villin*^{CreERT2}	Tamoxifen treated, *Ehf*^{IKO}	*Ehf* deleted in the small intestinal, caecal and colonic epithelial cells	In-house	C57Bl/6
	Oil treated, *Ehf*^{WT}	No gene deletion - wildtype	In-house	C57Bl/6
7. *Apc*$^{Lox/Lox}$; *Cdx2*^{CreERT2}	Tamoxifen treated, *Apc*^{CKO}	Mosaic *Apc* deletion in caecal and colonic epithelial cells	Prof. Matthias Ernst (Olivia Newton-John	C57Bl/6

8. *Apc* $^{Lox/+}$; *Cdx2* ^{CreERT2}	Tamoxifen treated, *Apc* $^{CKO/+}$	One allele of *Apc* deleted in caecal and colonic epithelial cells	Cancer Research Institute, Heidelberg, Australia); *OS: *Apc* $^{Lox/Lox}$ [183] and *Cdx2* ^{CreERT2} [235]	C57Bl/6
9. *Ehf* $^{Lox/Lox}$; *Apc* $^{Lox/Lox}$; *Cdx2* ^{CreERT2}	Tamoxifen treated, *Ehf* ^{CKO}; *Apc* ^{CKO}	Mosaic *Ehf* and *Apc* deletion in caecal and colonic epithelial cells	In-house	C57Bl/6
10. *Ehf* $^{Lox/Lox}$; *Apc* $^{Lox/+}$; *Cdx2* ^{CreERT2}	Tamoxifen treated, *Ehf* ^{CKO}; *Apc* $^{CKO/+}$	*Ehf* and one allele of *Apc* deleted in caecal and colonic epithelial cells	In-house	C57Bl/6

*OS: Original source

2.2.1 Animal monitoring

Mice used for experiments in this thesis were weighed and monitored at least once per week between the ages of 4 to 52 weeks. Any mice showing signs of ill health were monitored more frequently and were provided with mashed chow to facilitate feeding. Any mouse with a *Severe* score in any of the categories listed in Table 2.2 or any mouse with a *Moderate* score in more than four categories was euthanized immediately.

Table 2.2. Mouse monitoring: symptoms and severity scores.

Symptoms	**Normal**	**Mild**	**Moderate**	**Severe**
Activity	Normal	Isolated, abnormal posture	Huddled/inactive OR overactive	Moribund OR fitting
Alertness/Sleeping	Normal	Dull or depressed	Little response to handling	Unconscious
Coat	Normal	Coat rough	Unkempt, wounds, hair thinning	Bleeding or infected wounds

				OR severe hair loss OR self-mutilation
Faeces general	Normal	Faeces moist	Loose, soiled perineum	Presence of diarrhoea for 48h OR no faeces for 48h
Movement/gait	Normal	Slight OR abnormal gait	Walking on tiptoe OR reluctance to walk	Staggering OR limb dragging OR paralysis
Nose	Normal	Wetness	Discharge	Obstruction of nasal passages OR constant purulent discharge
Vocalisation	Normal	Squeaks when palpated	Struggles and squeaks loudly in response to handling of a body part and signs of aggression	Persistent and repetitive vocalisation without handling
Faeces blood	Normal (no blood in stool)	Slight discolouring of stool	Evidence of blood passing with faeces when examining bedding	Stool stained consistently red indicating significant blood, appearance of blood on bedding, blood around anus
Body condition	Normal	Thin	Loss of body fat, failure to grow	Loss of muscle mass that enables palpation of the spine
Body weight	Normal weight and growth rate	Reduced growth rate	Chronic weight loss >10%	Acute weight loss >15%, chronic weight loss >20% OR failure to grow for juveniles or

				failure to stabilise body weight
Breathing	Normal	Rapid, shallow	Rapid, abdominal breathing	Laboured, irregular or gaping mouth breaking, and/or blue skin
Dehydration	None	Skin less elastic	Skin tenting/ sunken abdomen	Skin tenting and eyes and abdomen sunken
Drinking	Normal	Increased OR decreased intake over 24h	Increased OR decreased intake over 48h	Constantly drinking OR not drinking over 24h
Eating	Normal	Increased OR decreased intake over 24h	Increased OR decreased intake over 48h	Obese OR not eating over 48h
Eyes	Normal	Wetness or dullness	Discharge	Severe eye infection with vision obstructed and signs of pain

2.3 Tamoxifen treatment

Tamoxifen (Sigma Aldrich, USA) was dissolved in molecular grade ethanol at a concentration of 100mg/mL. The solution was placed on a heat-block at 37°C in the dark and vortexed every 3-5 minutes until dissolved. The tamoxifen solution was then transferred to a 15mL Falcon tube under sterile conditions and diluted 10-fold with sunflower seed oil from *Helianthus annuus* (Sigma Aldrich, USA) to a final concentration of 10mg/mL, and stored at 4°C in the dark for up to one week. Vehicle only (i.e. sunflower seed oil) solution was prepared in the same way without the inclusion of tamoxifen.

- Experimental *Ehf* $^{Lox/Lox}$; *Villin* ^{CreERT2}, *Ehf* $^{Lox/Lox}$; *Apc* $^{Lox/+}$; *Cdx2* ^{CreERT2} and *Ehf* $^{+/+}$; *Apc* $^{Lox/+}$; *Cdx2* ^{CreERT2} mice at 4 weeks of age were given a total of 9 mg tamoxifen solution (10mg/mL) via intraperitoneal injections over four consecutive days (300µl, 200µl, 200µl, 200µl) using a 26-gauge needle. Control mice were given the same dose regimen of sunflower seed oil solution.

- Experimental *Ehf* $^{Lox/Lox}$; *Apc* $^{Lox/Lox}$; *Cdx2* ^{CreERT2} and *Ehf* $^{+/+}$; *Apc* $^{Lox/Lox}$; *Cdx2* ^{CreERT2} were administered a low dose of tamoxifen to induce mosaic gene deletion of *Ehf* and/or *Apc* specifically in caecal and colonic epithelial cells. Mice at 4 weeks of age were given a total of 2 mg tamoxifen solution (10mg/mL) via intraperitoneal injection over two consecutive days (100µl, 100µl) using a 26-gauge needle. Control mice were given the same dose regimen of sunflower seed oil solution.

2.4 BrdU treatment

5-bromo-2'-deoxyuridine (BrdU, Sigma Aldrich, USA) and 5-fluoro-2'-deoxyuridine (FdU, Sigma Aldrich, USA) were dissolved in sterile phosphate-buffered saline (PBS) at a concentration of 10mg/mL and 1.2mg/mL respectively, in a 15mL Falcon tube. The tube was wrapped in aluminium foil and placed on a roller at room temperature to dissolve. The dissolved solution was then aliquoted into Eppendorf tubes and stored at -80°C long-term, and -20°C short-term (up to two weeks). Aliquots were freeze-thawed a maximum of two times. Experimentally, mice were given an intraperitoneal injection of BrdU solution (10µL/g mouse) using a 29-gauge insulin syringe two hours prior to cull.

2.5 DSS-induced colitis

For the DSS studies, eight-week-old littermates were given dextran sodium sulphate (DSS, 2.5% (w/v), Lot#Q8378, MP Biomedicals, Canada) in autoclaved drinking water *ad libitum* for 5 consecutive days. Untreated mice served as controls and were given autoclaved water without DSS for 5 consecutive days. During the experimental period the mice were weighed and monitored daily for colitis as assessed by the criteria listed in Table 2.3.

Table 2.3. Colitis disease scoring criteria.

Colitis disease score	
Weight loss	0: Normal 1: <5% 2: 6-10% 3: 11-20% 4: >20%
Faeces	0: Normal 1: Pasty, semi-formed

	4: Liquid, sticky or unable to defecate >5 minutes
Blood	0: No blood 1: Traces of blood in stool or in rectum 2: Free-flowing blood from rectum, blood on fur
General appearance	0: Normal 1: Piloerection, hunching 2: Lethargy and piloerection 4: Motionless

2.6 High cholesterol diet

The high cholesterol diet (SF00-245, Specialty Feeds, Australia) used in this thesis was stored at -20°C to prevent rancidification and was weighed and changed daily for the entire experimental period. The caloric content of the diet is given in Table 2.4.

Table 2.4. Caloric content of high cholesterol diet.

Calculated Nutritional Parameters	
Protein (%)	19.4
Total Fat (%)	16
Crude Fibre (%)	4.7
AD Fibre (%)	4.7
Digestible Energy (MJ/Kg)	18.2
Total calculated digestible energy from lipids (%)	32
Total calculated digestible energy from protein (%)	19

2.7 Irradiation

For the irradiation study, eight-week old mice were irradiated with 8Gy using a Gammacell 1000A irradiator (MDS Nordion, Canada) fitted with a caesium-137 core. The mice were then housed in microisolator cages with filtered air and were monitored daily until the final experimental time point of either:

- 2h post irradiation: Maximal DNA damage;

- 24h post irradiation: Maximal apoptosis;
- 72h post irradiation: Significant loss of epithelial cells in the intestine;
- 120h post irradiation: Robust epithelial regeneration.

2.8 Timed pregnancies

To determine the effect of *Ehf* deletion on mammary gland development, mammary glands of *Ehf* $^{+/+}$ and *Ehf* $^{-/-}$ littermates were collected at day 18.5 of pregnancy (18.5dP). To accurately determine the day of gestation, female mice were subjected to timed pregnancies by placing a male mouse with one of two female mice for one night. Three nights prior soiled bedding material was placed in the female cage to promote the oestrus cycle. The following morning the male was separated from the female(s) and the females checked for plugs. If a plug was observed, this was counted as 0.5dP. Pregnancy was confirmed by an atypically large weight gain starting around 12dP. Timed pregnancies were performed once per week.

2.9 Collection of intestinal epithelial cells

On the day of tissue collection, Buffer 1 and Buffer 2 (Appendix A) were pre-heated for 10 minutes at 56°C to activate the RNA secure, then aliquoted into 50mL Falcon tubes (approx. 3mL per tube).

For isolation of intestinal epithelial cells, mice were culled and the small intestine (duodenum, jejunum and ileum) and colon removed and opened longitudinally using a ball-scissor. The tissue was washed in PBS to remove the intestinal contents and placed in pre-warmed Buffer 1 at 37°C on a shaker for 10 minutes. Samples were then vortexed, the smooth muscle removed from the tubes, and the suspended epithelial cells centrifuged at 1400 x *g* for 5 minutes at 4 degrees. The supernatant was discarded, and the pellet washed in 1-2mL of Buffer 2 (depending on the size of the pellet) and transferred to Eppendorf tubes. Samples were then centrifuged at 17000 x *g* in a Heraeus Pico 17 tabletop centrifuge (Thermo Fisher Scientific, Australia) for 1 minute and the supernatant discarded. Pellets were snap-frozen on dry ice and stored at -80°C.

2.10 Tissue fixation and processing

Harvested tissue was placed in cassettes and fixed in 10% neutral buffered formalin (Fronine General Chemicals, Australia) for 24-48 hours (depending on the thickness of the tissue), following which samples were transferred into 80% ethanol. Fixed samples were then submitted to the Department of Anatomical Pathology (Austin Hospital, Australia) for processing and paraffin

embedding. Sections (4µm) were cut using a Leica Biosystems RM2245 Semi-Automated Rotary Microtome (Leica Biosystems, Australia) onto SuperFrost slides (Thermo Fisher Scientific, Australia).

2.11 Tissue staining

2.11.1 Mammary gland whole mounts

Inguinal mammary glands were carefully resected and spread across a SuperFrost slide (Thermo Fisher Scientific, Australia). Sections were then fixed overnight at 4°C in Carnoy's fixative (60% ethanol, 30% chloroform and 10% glacial acetic acid). On the second day, slides were gradually hydrated through serial ethanol incubation steps, then stained in carmine alum solution (Appendix B) overnight at room temperature. On the third day, slides were gradually dehydrated through serial ethanol incubation steps, then left in xylene (VWR International, USA) for 24-72 hours at room temperature until the fat had rendered. Once the fat had rendered, the mammary glands were mounted using Entellan (Merck Millipore, Australia).

2.11.2 Haematoxylin and eosin staining

Formalin-fixed paraffin embedded sections were deparaffinised and rehydrated through serial xylene and ethanol washes. Slides were rinsed in RO water and stained in filtered Mayer's haematoxylin (Sigma Aldrich, USA) for 1-6 minutes. The incubation time depended on the number of times the haematoxylin solution had been used. The slides were then washed in warmed tap water and incubated in Scott's solution for the same time as used for the haematoxylin stain. The slides were then rinsed in water, counterstained in acidified aqueous eosin Y solution (Sigma Aldrich, USA) for 2-5 minutes before being dehydrated through serial ethanol and xylene washes. Slides were then mounted using Dibutylphthalate Polystyrene Xylene (DPX, Sigma Aldrich, USA).

2.11.3 Periodic Acid Schiff – Alcian Blue staining

Formalin-fixed paraffin embedded sections were deparaffinised and rehydrated through serial xylene and ethanol washes, then rinsed in RO water and stained with Alcian blue 8GX (ProSciTech, Australia) for 15 minutes. Slides were then rinsed thoroughly in tap water and stained in 0.5% periodic acid (Sigma-Aldrich, USA) in Milli-Q water for 5 minutes. Slides were again rinsed in tap water, then stained with Schiff's reagent (VWR International, USA) for 10 minutes. Sections were then counterstained with haematoxylin, dehydrated through serial ethanol and xylene washes, and mounted using DPX (Sigma Aldrich, USA).

2.11.4 Immunohistochemistry

Formalin-fixed paraffin embedded sections were deparaffinised and rehydrated through serial xylene and ethanol washes, then rinsed in tap water. Endogenous peroxidase was quenched by incubating the sections in 3% H_2O_2 (Science Supply Associates, Australia) in RO water at room temperature for 10 minutes. The method of antigen retrieval depended on the primary antibody used but was most commonly citric acid buffer (Appendix C). Occasionally, Tris-Hcl or EDTA buffers were used. The antigen retrieval was performed in a water bath at 100°C for 30 minutes, and the slides were left to cool to below 65°C. Slides were then washed in TBST and stained with primary antibody (Table 2.5) overnight at 4°C. On the following day, the slides were washed in TBST and incubated with Dako envision anti-rabbit or anti-mouse labelled polymer-HRP (Dako, USA) secondary antibody for 30 minutes at room temperature. Slides were washed in TBST, then incubated with 3, 3-diaminobenzidine (DAB) solution (Dako, USA) for between 30 seconds and 3 minutes until sufficient brown colour could be observed by eye. In all cases, sections from control and experimental groups were analysed in parallel. The stained slides were counterstained with haematoxylin, dehydrated through serial ethanol and xylene washes and mounted using DPX (Sigma Aldrich, USA).

Stained slides were scanned on an Aperio Scanscope XT slide scanner (Aperio Technologies, USA) onto an online server where the slide could be accessed and analysed. Image analysis was performed using the Aperio ImageScope software v12.0.1.5027, using the specifically designed Nuclear v9.1 or Positive Pixel Count v9.1 algorithms. The algorithm was tested on three separate slides before being applied to all slides to be analysed.

Table 2.5. List of antibodies used for immunohistochemistry.

Antibody	**Host species**	**Company**	**Dilution**
Anti-Chromogranin A (ab85554)	Rabbit	Abcam, USA	1:500
Lysozyme/Muramidase Ab-1 (RB-372-A)	Rabbit	Thermo Fisher Scientific, UK	1:300
Phospho-Histone H2A.X (Ser139) (CST.9718)	Rabbit	Cell Signaling Technology, USA	1:450
Phospho-Stat5 (Tyr694) (CST.9359)	Rabbit	Cell Signaling Technology, USA	1:100

Ki-67 Monoclonal Antibody (MA5-14520)	Rabbit	Thermo Fisher Scientific, UK	1:150
PCNA Antibody (sc-56)	Mouse	Santa Cruz Biotechnology, USA	1:400
Purified Mouse Anti-BrdU (555627)	Mouse	BD Biosciences, Australia	1:100
Mouse Milk Specific Protein (YNRMMSP)	Rabbit	Accurate Chemical and Scientific Corporation, USA	1:12000
Olfm4 (D6Y5A) Rabbit mAb (CST.39141)	Rabbit	Cell Signaling Technology, USA	1:400
Keratin 20 (D9Z1Z) XP® Rabbit (mAb #13063)	Rabbit	Cell Signaling Technology, USA	1:500
Anti-DCLK1 antibody (ab31704)	Rabbit	Abcam, USA	1:600
Elf-5 Antibody (G-2) (sc-166653)	Mouse	Santa Cruz Biotechnology, USA	1:200

2.11.5 Immunofluorescence

Formalin-fixed paraffin embedded sections were deparaffinised and rehydrated through serial xylene and ethanol washes, then rinsed in tap water and TBST. The antigen retrieval was performed in citric acid buffer in a water bath at 100°C for 15 minutes, and the slides were left to cool to below 65°C. Slides were then washed in TBST and stained with primary antibody (Table 2.6) overnight at 4°C. On the following day, the slides were washed in TBST and incubated with Alexa Fluor® 594 AffiniPure Goat Anti-Rabbit IgG (H+L) (Abacus DX, Australia) with DAPI added (1/1000) (Perkin Elmer, USA) for one hour at room temperature. Sections were then washed in TBST and mounted using DPX/Vectashield mounting media (Vector Laboratories, Burlingame, CA). Stained slides were scanned on an Olympus IX-81 inverted fluorescence microscope slide scanner (Olympus Corporation, Japan) and imaged using the HALO software v3.1.1076.

Table 2.6. List of antibodies used for immunofluorescence.

Antibody	**Host species**	**Company**	**Dilution**
	Rabbit	BioLegend, USA	1:300

Purified anti-Keratin 14 Antibody (905304)			
Purified anti-mouse Keratin 6A Antibody (905701)	Rabbit	BioLegend, USA	1:300
Purified anti-Loricrin Antibody (905104)	Rabbit	BioLegend, USA	1:300

2.12 Mouse genotyping

2.12.1 DNA extraction

Crude DNA extraction: DNA was extracted from the tails of mice by submerging the tissue in 30µL Quick Extract DNA Extraction solution (Astral Scientific, Australia) in Eppendorf tubes, and incubating on a heat-block at 65°C for 10 minutes. The tubes were then transferred to a 98°C heat-block for a further 5 minutes. Samples were then vortexed, and the solution centrifuged using a LabStar mini personal centrifuge (LabGear, Australia). Extracted DNA was used immediately.

Clean DNA extraction: DNA extraction was performed using the column-based ReliaPrep gDNA Tissue Miniprep system (Promega, USA) as per manufacturer's instruction. Extracted DNA was stored at -20°C.

2.12.2 PCR amplification of DNA

DNA amplification mastermix

- 12.5µL Forward primer
- 12.5µL Reverse primer
- 500µL MyTaq Red Mix 2x (Bioline, Australia)
- 475µL Nuclease free water

For genotyping, 18-19µL of the master mix and 1-2µL extracted DNA were added to PCR strip tubes to a final volume of 20µL. The amount of DNA added to the tubes depended on the extraction method as the crude extraction method was less efficient at extracting DNA compared with the clean extraction method. The PCR strip tubes were subsequently spun down using a LabStar mini personal centrifuge (LabGear, Australia), and the DNA amplified using a MasterCycler Thermal

Cycler (Eppendorf, USA). The specific cycling conditions depended on the primer pair used, as these have different optimal annealing temperatures. The cycling condition of the *Ehf* $^{Lox/Lox}$ reaction is given below. In all PCR reactions, DNA from mice of known genotype were used as a positive control and water was used as a negative control.

1. 94°C 2:00 minutes
2. 94°C 0:30 minutes ┐
3. 68°C 1:00 minutes ├ x35 cycles
4. 72°C 1:20 minutes ┘
5. 72°C 3:00 minutes
6. 4°C ∞

2.12.3 Gel electrophoresis

A 1.5% w/v agarose (Bioline, Australia) solution was prepared in TAE buffer by heating in a microwave until fully dissolved. The solution was subsequently poured into a mould with two 20 well gel combs and allowed to solidify. The solidified gel was then immersed in TAE buffer in a gel tank, and 10µL of the amplified DNA loaded into the wells. Where needed, 2µL of a 1kb plus DNA ladder (Invitrogen, Australia) was added to enable accurate determination of the size of bands. The loaded gel was run at 90V for 60-75 minutes depending on the expected sizes of the PCR products being investigated. Gels were visualised on a ChemiDoc^{TM} XRS+ Molecular Imager (Bio-Rad, USA).

2.12.4 Primers

The primers used for DNA genotyping are listed in Table 2.7.

Table 2.7. DNA genotyping primer sequences and target site.

Target gene	**Forward primer sequence**	**Reverse primer sequence**	**Exon/intron targeted**
Ehf	GTCCAAAATGAAGCCCAGGGTA	CGTCCGGTTCTTCATTGATCAG	Exon 8 (outside floxed region)-intron 6
	TGTGTCTTGCTTTCCACCAG	CGTCCGGTTCTTCATTGATCAG	Exon 8 (inside floxed region)- intron 6

CMV-Cre	CTGACCGTACACCAAAATTGCCTG	GATAATCGCGAACATCTTCAGGTT	-
Villin-CreERT2	CAAGCCTGGCTCGACGGCC	CGCGAACATCTTCAGGTTCT	-
Apc	GTTCTGTATCATGGAAAGATAGGTGGTC	CACTCAAAACGCTTTTGAGGGTTGATTC	Intron 14- exon 15
Cdx2-CreERT2	CATGGTGAGGTCTGCTGATG	CATGTCCATCAGGTTCTTGC	-

2.13 Quantitative real time polymerase chain reaction (q-RT-PCR)

2.13.1 RNA extraction

RNA was extracted from isolated cells or tissue using the filter column-based ReliaPrep RNA Tissue Miniprep System (Promega, USA) as per manufacturer's instructions with one exception. To homogenise the tissue, we used 2.4mm diameter Omni Metal Beads (Capella Science, Australia) rinsed in ethanol and RNaseZap RNase Decontamination Solution (Thermo Fisher Scientific, Australia). Five beads were added to each Eppendorf tube containing tissue and lysis buffer, and the tubes placed on a Tissuelyser II (Qiagen, USA) and shaken at a frequency of 30 shakes per second for 2x1 minute. RNA was eluted off the column in a final volume of 10-30µL nuclease free water depending on size of the starting material. Purified RNA was stored at -20°C for short term or -80°C for long term storage.

2.13.2 Determination of RNA concentration and quality

RNA concentration and quality was determined spectrophotometrically using the Nanodrop ND-2000 (NanoDrop Technologies, USA). RNA purity was determined by the ratio of absorbance at 260nm and 280nm, with ratios of >1.8 deemed of sufficient purity for cDNA synthesis. RNA quality was also assessed by loading samples onto an agarose gel (1.5%), running at 90V for 40 minutes. Samples which separated into 18S and 28S rRNA bands were deemed good quality.

2.13.3 cDNA synthesis

RNA was converted to cDNA using the High-Capacity cDNA Reverse Transcription Kit (Applied Biosystems, USA) as per manufacturer's instruction. A total of 500ng RNA was converted into cDNA and no RNase inhibitor was used for the final reaction. Each reaction consisted of 5µL RT

master mix (1µL 10X RT Buffer, 0.4µL 25X 100mM dNTP Mix, 1µL 10X RT Random Primers, 0.5µL MultiScribe™ Reverse Transcriptase and 2.1 µL Nuclease-free water) and 5µL RNA and nuclease free water solution in PCR strip tubes. The reaction was carried out using the following program on a MasterCycler Thermal Cycler (Eppendorf, USA).

1. 25°C 10 minutes
2. 37°C 120 minutes
3. 85°C 5 minutes
4. 4°C ∞

After the reaction had completed, the newly synthesised cDNA was diluted 1:10 and stored at -20°C for short term or -80°C for long term storage.

2.13.4 Quantitative Real Time Polymerase Chain Reaction

The synthesised cDNA was used as template to determine gene expression levels by quantitative real time PCR (q-RT-PCR). The PCR reaction mixture consisted of the following components:

- 0.75µL forward primer
- 0.75µL reverse primer
- 1µL cDNA
- 2.5µL 2xPower SYBR Green PCR Master Mix (Thermo Fisher Scientific, Australia)

Samples were then amplified using the following cycling conditions on the Viia 7 Real Time PCR system (Applied Biosystems, USA):

1. 95C 10 minutes
2. 95C 15 seconds
3. 60C 1 minute

} 40 cycles

Expression level of genes of interest were normalised to levels of expression of the house-keeping genes β-Actin, β-Tubulin or Gapdh using the ΔCT method.

2.13.5 Primers

Primers for q-RT-PCR were based on published sequences or designed using the Primer3 program (bioinfo.ut.ee/primer3-0.4.0/). In case of the latter, the murine cDNA sequence of the gene of interest was obtained from the University of California, Santa Cruz (UCSC) Genome Browser (htts://genome.ucsc.edu/). Primers were selected based on their GC composition (45-55%) and

similarity of melting temperature. All primers were purchased from Sigma-Aldrich, Australia. For q-RT-PCR, primers were diluted in nuclease free water to a working concentration of 500 nM. A list of the primer sequences used in this thesis is given in Table 2.8.

Table 2.8. List of genes and primer sequences used for q-RT-PCR.

Target genes	Forward primer sequence	Reverse primer sequence
β-Actin	ACTGGGACGACATGGAGAAG	GGGTGTTGAAGGTCTCAAA
β-Tubulin	AAACAGCACAGCCATCCAG	GCTTCGGTGAACTCCATCTC
Gapdh	CGACCCCTTCATTGACCTTA	GCCTTGACTGTGCTGTTGAA
Ehf	AAGTCCCACACCAAAAAGCA	TCTCGGATGAACTCCCATAA
Ndrg2	TCAAAGGCAAGTGAAGGTGG	CAGTCTCGGGTGTTTGTCCA
Cobll1	GCTGTCGTCACAGAGCAACA	ACGAGCAAGTCCATCATTGG
Klk13	TCTCTGCAGATGACTGCCTG	CACTGCAGGGTTTTGGGATA
Krt4	GATGATGCAGGACAGTGTGG	CTGCAGCTGTACGCTTGTTG
Lyz1	GCAAAGAGGGTGGTGAGAGA	GAAAGCGAGGAAGTGTGACC
Chga	CAGAAAAGCCAAGCAAGAGG	ATGGAAGTGGGAACTGGATG
Lgr5	GGACCAGATGCGATACCGC	CAGAGGCGATGTAGGAGACTG
Muc2	GGACCCACACTTTGTCACCT	GGTAATCTCCTCCACCAGCA
Myc	GTGCTGCATGAGGAGACACC	AGGGGTTTGCCTCTTCTCC
Vil1	AAATGGTGGATGACGGGAGT	TAGAGCAGCAGGTAGCAGTC
Alpi	CTGGGTGCTGCTGTTGTTTT	GCTGATGTCTGAATGGGCTG
Vim	ATTTCTCTGCCTCTGCCAAC	CCTGTCCATCTCTGGTCTCAA
Acta2	CCGATAGAACACGGCATCAT	AGCAGTGTCGGATGCTCTTC
Fap	CGAGTATGCTTGCACTGGCT	GCTTTCTTCTACATGCTCCTGG
Elf3	GAAGGCAAGCTGGACTAGCG	GGAGCTGGCGTCATACTTGTT
Elf5	GACTCCGTAACCCATAGCACC	GCTGAACAGATCGGTCCAAGG
Cdx1	GGCTCCTTGGCCCGGCGG	CCGAGCTGGCTGCTAACC
Cdx2	GAAACCTGTGCGAGTGGATG	ACACCACCCGGTATTTGTCTT
Il6	TGATGGATGCTACCAAACTGG	TGGTACTCCAGAAGACCAGAGG
Pcna	GAATGGGGTGAAGTTTTCTG	CAGTGGAGTGGCTTTTGTGA
Mki67	GAAGCAGCAGCAGATGAGTG	GGTGATGGGCTCAGGTATGT
Cdh1	CAGTTCCGAGGTCTACACCTT	TGAATCGGGACTCTTCCGAAAA
Ccnd1	TCCTCTCCAAAATGCCAGAG	AGGGTGGGTTGGAAATGAAC
Smad4	GCTCATCCTAGCAAGTGTGTCA	AGGAAATCCTTTCCGACCAG
Tnc	GGGCTATAGAACACCGATGC	CATTTAAGTTTCCAATTTCAGGTTC

Il17	CTCCAGAAGGCCCTCAGACT	CTTCCCAGATCACAGAGGGA
Tnf	TTATGGCTCAGGGTCCAACT	TGTCCCAGCATCTTGTGTTT
Cxcl1	GTGCCCCAAGTAACGGAGA	ACAGGTGCCATCAGAGCAGT
Ifng	GCGTCATTGAATCACACCTG	GCTGGACCTGTGGGTTGTT
Il33	TCAGCCTTGCTCTTTCCTTT	ACTGTGGTGCCTGCTCTTCT
Tjp1	ATTTACCCGTCAGCCCTTCT	CGAAACCCACACTATCTCC
Abcg5	TACGTGCTACACGTCCTCCC	CCAAATCTGGCAACTTCAGG
Abcg8	CTATAGCAACCCTGCGGACTT	CTAGGAACAGGGCTGCAAGA

2.14 RNA sequencing analysis

RNA isolated from colonic epithelial cells was prepared for next-generation sequencing using the stranded RNA library preparation kit with rRNA depletion (Illumina) and sequenced using an Illumina HiSeq 2500 with 100bp single reads. Library preparation, sequencing and initial data analysis (read mapping) was performed by an external service provider (Australian Genome Research Facility, Australia). Gene set enrichment analyses were performed using the publicly available GSEA v4.1.0 software from the Broad institute (Subramanian et al., 2005), by comparison to the MSigDB "HALLMARKS" gene set signatures (Liberzon et al., 2015). The "Signal2Noise" metric was used for gene ranking and the threshold for false discovery rate (FDR) was set at $q<0.05$.

2.15 Statistical analysis

Statistical analyses were performed using GraphPad Prism v8.0 software (GraphPad Software, La Jolla, CA, USA). Groups were typically compared using the student's T-test with Welch's correction or Chi-square analysis. In cases where the data was assumed to be non-Gaussian distributed, groups were analysed using the Mann-Whitney test. In all cases $P<0.05$ was considered statistically significant.

Chapter 3: Role of EHF in tissue homeostasis

3.1 Introduction

Ets homologous factor (EHF) is a member of the ESE subfamily of ETS transcription factors which is highly expressed in multiple epithelial tissues. The other ESE members have been extensively studied using mouse models which have shown that SPDEF is a regulator for goblet cell differentiation in epithelial tissues including the intestine [50], ELF5 is a key driver of alveolar differentiation in the mammary gland [207, 208], while ELF3 is required for goblet cell differentiation and intestinal barrier function [52]. Comparatively, EHF has only been studied using cultured cell lines. These studies have suggested that EHF plays an important role in epithelial tissue homeostasis [16, 19, 21]. Specifically, EHF was shown to be highly expressed during differentiation of human epidermal keratinocytes and EHF depletion impaired the expression of key differentiation-related genes [21]. Another study found that *Ehf* is highly expressed in the adult mouse corneal epithelium and expression increases with age. Knockdown of *Ehf* in human corneocytes caused significant transcriptional changes including down-regulation of SPRR proteins involved in barrier function [19].

The impact of *Ehf* deletion on development and tissue homeostasis *in vivo* has not been previously investigated. We therefore crossed *Ehf* floxed mice generated in our laboratory with *CMV* ^{Cre} deleter mice to induce *Ehf* deletion in all tissues. The aim of this chapter was to assess the phenotype of these mice.

3.2 Results

3.2.1 Generation of *Ehf* whole-body knockout mice

To induce gene deletion of *Ehf* in all cells of the mouse, *Ehf* $^{lox/lox}$ mice were crossed with *CMV* ^{Cre} mice. *Ehf* heterozygous offspring lacking *CMV* ^{Cre} were subsequently intercrossed to generate progeny with germline deletion of *Ehf* (*Ehf* $^{-/-}$) and control wildtype (*Ehf* $^{+/+}$) littermates. The colony was maintained by *Ehf* heterozygous (*Ehf* $^{+/-}$) matings.

We generated 658 pups from 100 litters born to heterozygous parents, averaging out to a litter size of 6.6 pups. Of these, 649 pups were genotyped at weaning, of which 175 were *Ehf* $^{+/+}$, 332 were *Ehf* $^{+/-}$ and 142 were *Ehf* $^{-/-}$ (Table 3.1). The smaller percentage of *Ehf* $^{-/-}$ mice born compared to the expected Mendelian ratio of 1:2:1 was not statistically significant (χ^2 test, two-sided p=0.314), indicating that ubiquitous deletion of *Ehf* does not cause embryonic lethality.

Table 3.1. Number of *Ehf* wildtype, heterozygote and knockout mice born to *Ehf* $^{+/-}$ parents.

Stage	Number of litters	Number of mice	Ehf genotype		
			+/+	+/-	-/-
Expected ratio			25%	50%	25%
Postnatal					
P21	99	649	175 (26.9%)	332 (51.2%)	142 (21.9%)

Next, to confirm successful deletion of *Ehf*, we collected multiple organs from 14-week-old *Ehf* $^{+/+}$ and *Ehf* $^{-/-}$ littermates and assessed *Ehf* DNA deletion by genotyping (Figure 3.1A) and *Ehf* mRNA expression by q-RT-PCR (Figure 3.1B). Genotyping of *Ehf* across 18 tissues revealed successful gene deletion of *Ehf* in all cases in the *Ehf* $^{-/-}$ mice. Consistent with these results, examination of *Ehf* mRNA expression across 14 tissues revealed a complete absence of *Ehf* mRNA (exon 7-8) in all tissues of the *Ehf* $^{-/-}$ mice, confirming constitutive *Ehf* deletion in this strain. Consistent with previous findings, *Ehf* mRNA expression was highest in salivary glands, preputial glands, prostate, colon and stomach in *Ehf* $^{+/+}$ mice [26].

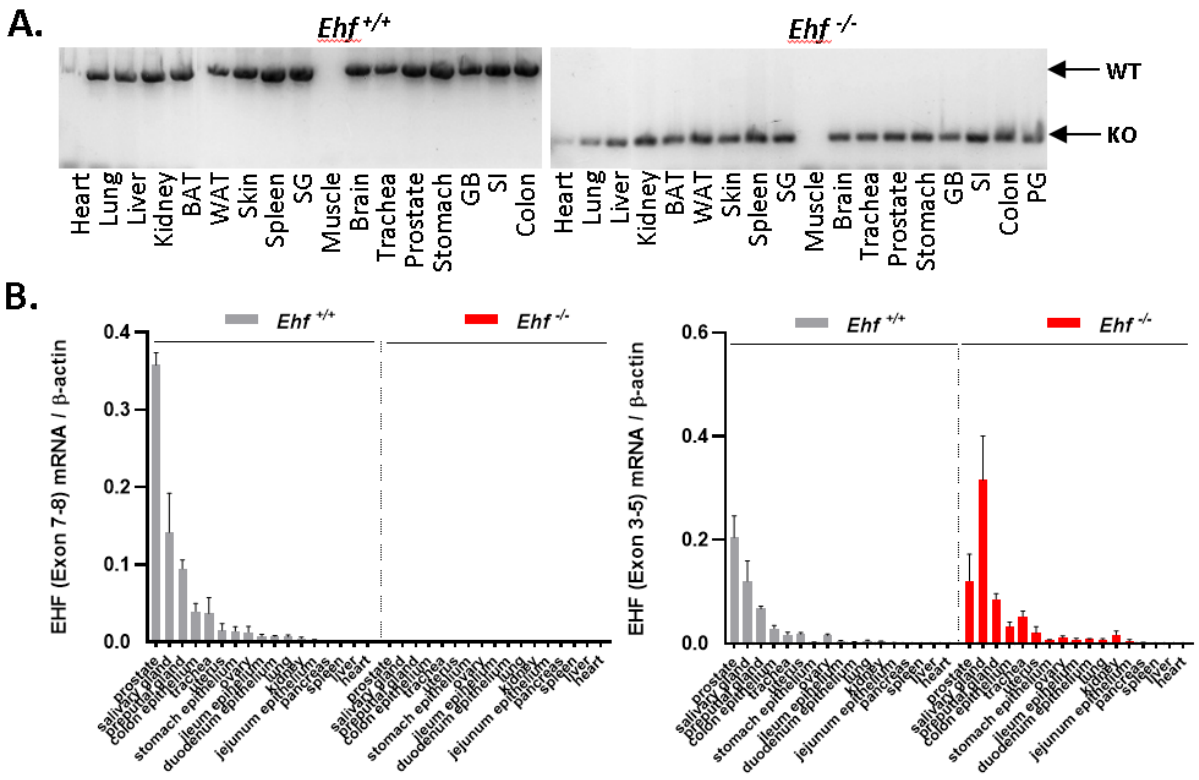

Figure 3.1. Confirmation of *Ehf* deletion in *Ehf* $^{-/-}$ mice. (A) *Ehf* genotyping and (B) *Ehf* mRNA expression in 14-18 tissues derived from 14 week old *Ehf* $^{+/+}$ and *Ehf* $^{-/-}$ littermates (BAT = brown adipose tissue; WAT = white adipose tissue; SG = salivary gland; GB = gall bladder; SI = small intestine; PG = preputial gland). Values shown are mean ± SEM from n= 3 *Ehf* wildtype and *Ehf* knockout mice.

3.2.2 Histological analysis of epithelial tissues

To determine the impact of *Ehf* deletion on tissue homeostasis we performed a gross histological assessment of the tissues in which *Ehf* is most highly expressed, i.e. the salivary glands, preputial glands, prostate, stomach and intestine (Figure 3.2, the impact of *Ehf* deletion on intestinal epithelial homeostasis will be investigated in detail in Chapter 4). For this purpose, tissues were collected from *Ehf* $^{+/+}$ and *Ehf* $^{-/-}$ littermates at 6 weeks of age. Unless specified, all parts of the tissue was examined but only certain areas are highlighted here for the purpose of the histological comparison.

Salivary glands: The salivary gland consists of three glands, the parotid, submandibular and sublingual glands. The submandibular glands of the *Ehf* $^{+/+}$ and *Ehf* $^{-/-}$ mice had a similar number of convoluted ducts (CD) while the sublingual glands had normal appearance of mucous acini (M) and striated excretory ducts (black arrows). The parotid gland was not examined.

Preputial glands: The preputial glands of mice are lobulated glands with large, cavernous ducts. Examination of the preputial glands of *Ehf* $^{+/+}$ and *Ehf* $^{-/-}$ revealed similar gland appearance with normal sebaceous secretory cells (SC) forming acini and excretory ducts (D) lined by squamous epithelium.

Prostate: The mouse prostate is composed of four lobes: anterior, dorsal, lateral and ventral. The lobes are fundamentally similar, although there are differences in the amount and biochemical composition of secretions. Examination of the anterior and dorsolateral lobes of *Ehf* $^{+/+}$ and *Ehf* $^{-/-}$ mice did not reveal any significant differences. The anterior lobe in both cohorts of mice displayed acini lined with cuboidal to columnar epithelium with centrally located nuclei and ample infoldings. Additionally, there was abundant eosinophilic luminal secretion present. Furthermore, the dorsolateral lobe of the prostate displayed small acini mostly lined by simple columnar epithelium with centrally located nuclei and sparse infoldings. Occasional eosinophilic luminal secretion was noted.

Stomach: The stomach of mice can be divided into the corpus, antrum and forestomach. We examined the histology of stomachs from *Ehf* $^{+/+}$ and *Ehf* $^{-/-}$ mice but did not observe any significant changes upon *Ehf* deletion. The forestomach of both cohorts of mice consisted of folded keratinised stratified squamous epithelium of similar height and the gastric glands of the corpus consisted of similar straight long tubules.

Collectively, these findings indicate that at the age of 6 weeks, loss of *Ehf* does not impact the differentiation and maturation of these tissues.

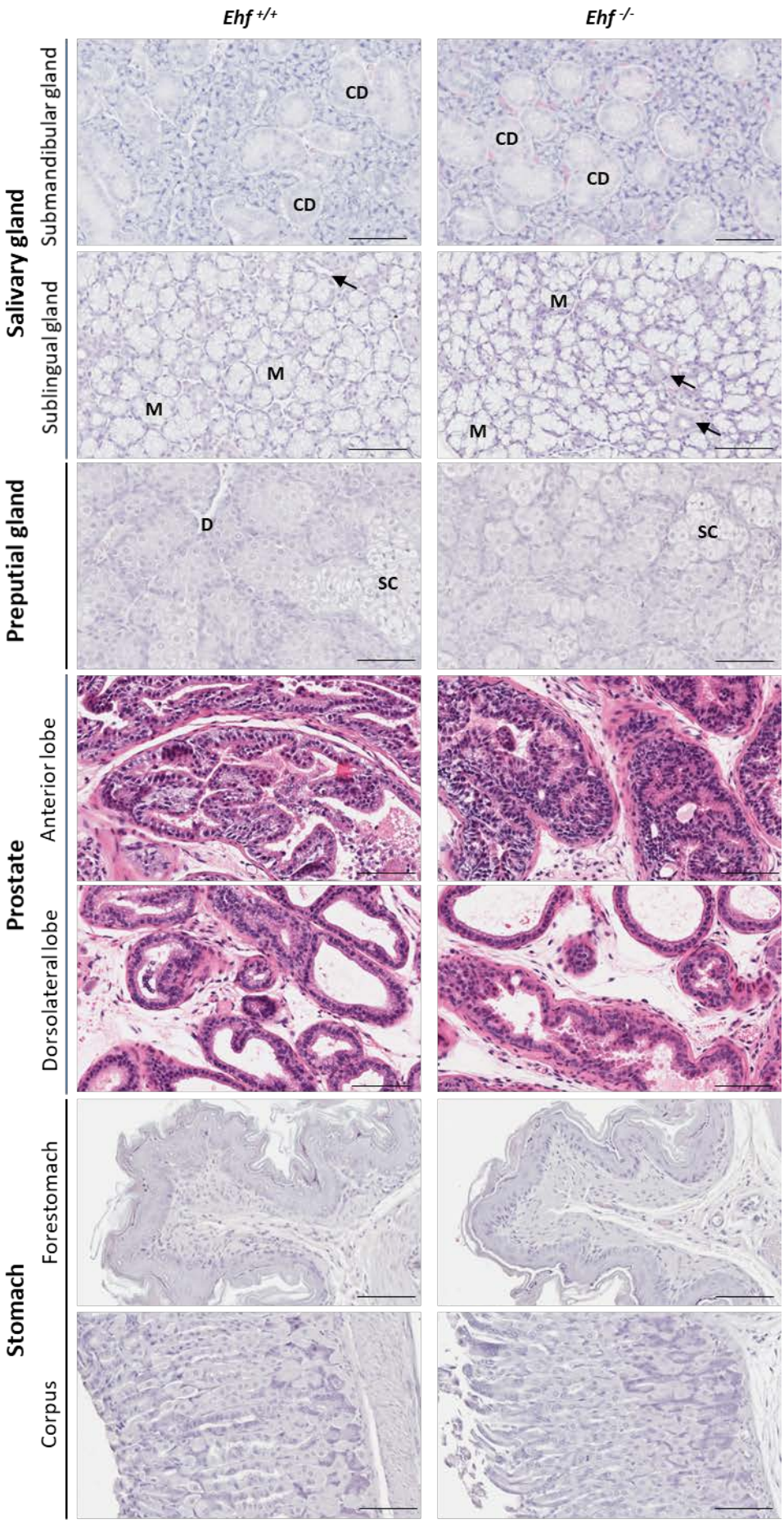
Ehf +/+
Ehf -/-
Salivary gland
Submandibular gland
Sublingual gland
Preputial gland
Prostate
Anterior lobe
Dorsolateral lobe
Stomach
Forestomach
Corpus
CD
CD
CD
CD
M
M
M
M
D
SC
SC

Figure 3.2. Impact of *Ehf* deletion on the histology of epithelial tissues with high *Ehf* mRNA expression from 6 weeks old *Ehf* $^{+/+}$ and *Ehf* $^{-/-}$ littermates. Scale bar 50µm.

3.2.3 Overall health of *Ehf* $^{-/-}$ mice

To assess the impact of *Ehf* deletion on overall animal health, *Ehf* $^{-/-}$ and *Ehf* $^{+/+}$ control mice were monitored and weighed weekly for 27 weeks (Figure 3.3A). Male *Ehf* $^{-/-}$ mice weighed less than their wildtype littermates at 4 weeks of age, and the weight discrepancy became progressively more pronounced as the mice aged. Comparatively, female *Ehf* $^{-/-}$ mice weighed the same as their wildtype littermates at 4 weeks of age however, like the males, gained weight at a significantly slower rate over the 27-week-long experimental period. The reduced body weight gain of *Ehf* $^{-/-}$ mice was not due to differences in daily food intake (Figure 3.3B).

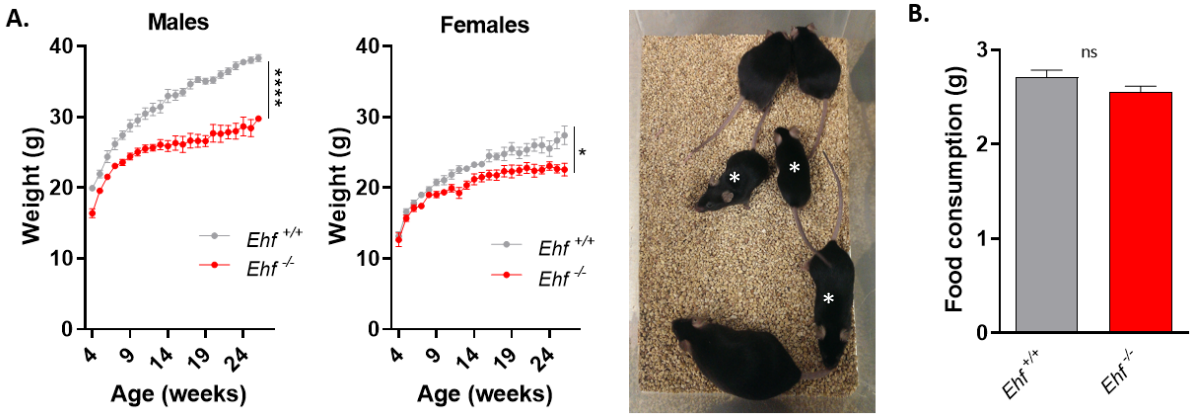

Figure 3.3. Impact of *Ehf* deletion on body weight. (A) Body weight of males and females between 4 and 27 weeks of age. Values shown are mean ± SEM from n= 10 *Ehf* $^{+/+}$ and *Ehf* $^{-/-}$ male mice and n= 10 *Ehf* $^{+/+}$ and *Ehf* $^{-/-}$ female mice. Image shows 3 *Ehf* $^{+/+}$ and 3 *Ehf* $^{-/-}$ (*) female mice together in a cage. (B) Average daily food intake of n=5 *Ehf* $^{+/+}$ and *Ehf* $^{-/-}$ female mice over a two-week period.

A second cohort of *Ehf* $^{-/-}$ and *Ehf* $^{+/+}$ littermates were aged to 52 weeks of age with weekly monitoring for any differences in overall health. This study revealed that *Ehf* $^{-/-}$ mice developed a series of ailments including (1) abscesses (in 19/20 mice) typically located in the preputial glands of male mice and vulva of female mice, with occasional abscesses presenting in the ear canal; (2) warts, wounds and swelling around the chin and mouth (in 9/20 mice) which would resolve then reappear; and (3) corneal ulcers (in 5/20 mice) (Figure 3.4A,B). The median age of onset of abscesses and facial warts was 16 weeks, while the corneal ulcers presented later, with a median age of onset of 36 weeks (Figure 3.4C).

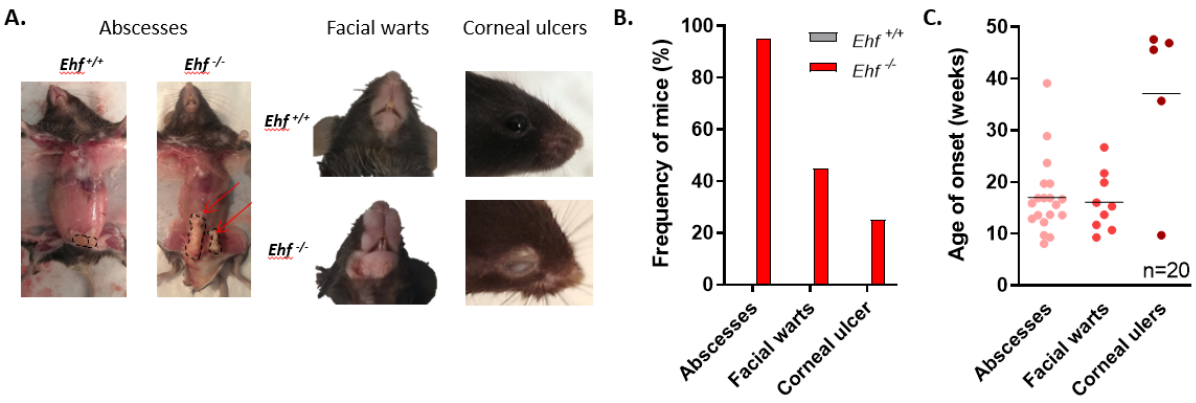

Figure 3.4. Impact of *Ehf* deletion on animal health. (A) Representative images of preputial gland abscesses (red arrows), facial warts and corneal ulcers in *Ehf* $^{-/-}$ mice. (B) Frequency of mice that develop these conditions. (**C**) Age at which *Ehf* $^{-/-}$ mice developed these ailments.

Due to the development of these various ailments, the majority of *Ehf* $^{-/-}$ mice had to be humanely euthanised before the designated experimental endpoint of 52 weeks (Figure 3.5A). The most common reason for euthanasia was the development of genital abscesses, which resulted in self-mutilation or restricted urination in 20% (4/20) and 40% (8/20) of mice respectively (Figure 3.5B). The median ethically determined lifespan was 17 weeks for *Ehf* $^{-/-}$ males and 48 weeks for *Ehf* $^{-/-}$ females.

The main reason for this gender difference in lifespan was that the preputial gland abscesses were larger due to the large surface area of the glands and therefore impacted the male mice more severely compared with the vulval abscesses of female mice. Preputial glands are susceptible to bacterial infections [236], and once infected can cause pain, self-mutilation, restricted urination, penile prolapse and fistulation. Despite the high incidence of facial warts, these did not severely impact the overall health of the animals.

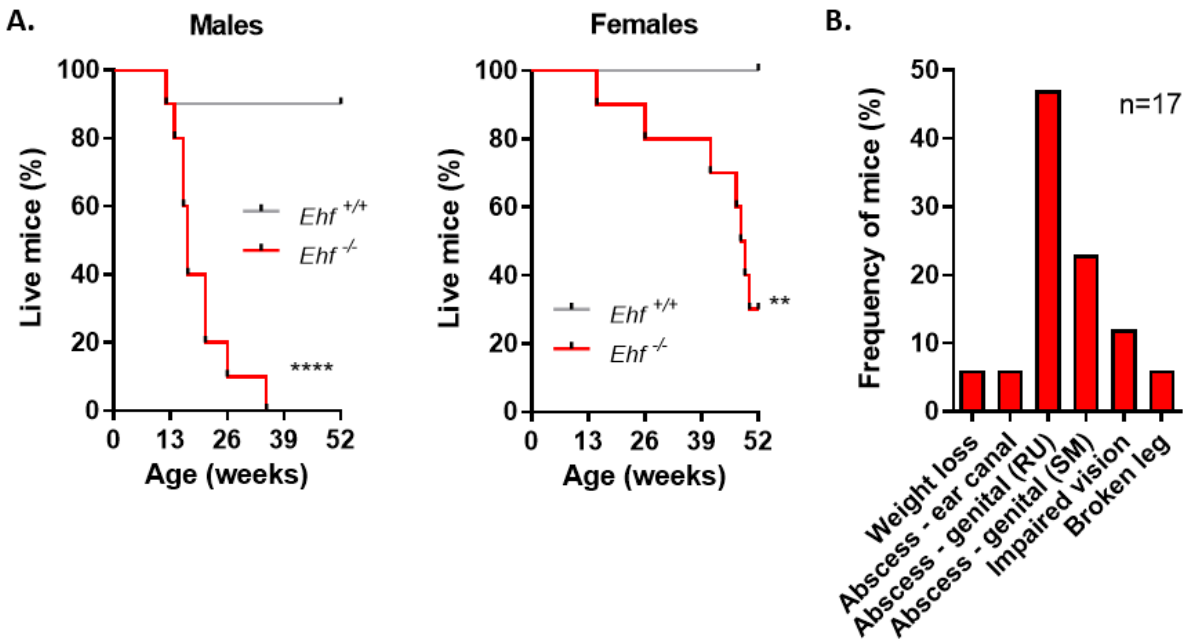

Figure 3.5. Impact of *Ehf* deletion on ethically determined lifespan. (A) Percentage of live male and female *Ehf* $^{+/+}$ and *Ehf* $^{-/-}$ aged for 52 weeks. Kaplan-Meier graph of n= 10 *Ehf* $^{+/+}$ and *Ehf* $^{-/-}$ male mice and n= 10 *Ehf* $^{+/+}$ and *Ehf* $^{-/-}$ female mice (B) Reason for euthanasia of *Ehf* $^{-/-}$ (RU = restricted urination; SM = self-mutilation).

3.2.4 *Ehf* deletion disrupts normal epidermal histology in adult mice

To understand the underlying cause of these observed phenotypes we first performed bacterial analyses of the genital abscesses and facial warts, which revealed heavy growth of the commensal bacteria *Staphylococcus aureus* and *Proteus mirabilis*. These are opportunistic bacterial species unlikely to cause infections in the absence of either an impaired immune system or a defective epithelial barrier. As EHF is predominantly an epithelial-restricted transcription factor [7, 8] and has been implicated as a key driver of basal keratinocyte differentiation [21], we therefore sought to determine whether the epidermal structure was impacted by *Ehf* deletion.

To investigate this, we first examined the skin histopathology of mice presenting with warts or swelling around chin and mouth (Figure 3.6). Histological assessment of these lesions revealed them to be in an inflamed state with histopathological features such as hyperplasia, hyperkeratosis and immune cell infiltrates into all layers of the epidermis. Furthermore, we also noted histological features reminiscent of squamous cell carcinoma such as keratinous pearls, enlarged nuclei and intercellular bridging.

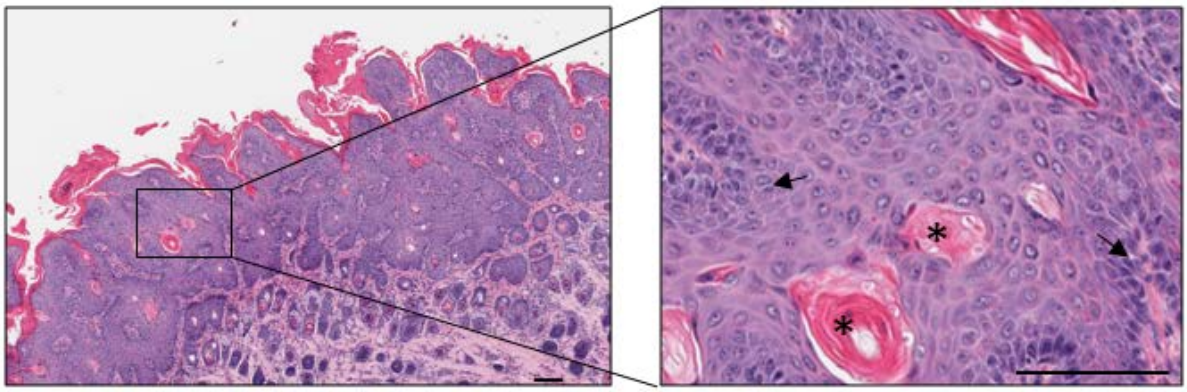

Figure 3.6. Histopathology of a chin skin lesion from an *Ehf* $^{-/-}$ adult mouse presenting with warts showing hyperplasia and hyperkeratosis of the epidermis. Insert shows Arrow: intercellular bridging and *: keratinous pearls. Scale bar = 200µm.

These findings prompted us to collect skin from the dorsal and chin region of mice at 6 weeks and 27 weeks of age to assess the impact of *Ehf* deletion on normal skin histology. At the 6 week timepoint both dorsal and chin skin from *Ehf* $^{+/+}$ and *Ehf* $^{-/-}$ mice appeared mostly normal. The epidermis consisted of a well-defined single basal cell layer and a thin layer of the stratum corneum (Figure 3.7A,B).

Comparatively, at the 27 week timepoint the chin skin of *Ehf* $^{-/-}$ mice (3/5) displayed areas of hyperplasia and hyperkeratosis despite not displaying macroscopic facial warts. Furthermore, a few *Ehf* $^{-/-}$ mice also developed Munro's microabscesses (1/5) and small keratinous pearls (2/5). The chin skin of *Ehf* $^{+/+}$ mice was normal (Figure 3.7A).

Assessment of the dorsal skin of these mice at the 27 week timepoint revealed the *Ehf* $^{+/+}$ dorsal skin to be mostly normal although one mouse displayed mild hyperkeratosis and a second mouse displayed Munro's microabscesses. Comparatively, the majority of *Ehf* $^{-/-}$ mice (4/5) displayed abnormal dorsal skin histology (Figure 3.7B). The mice had varying degrees of hyperkeratosis and hyperplasia. Furthermore, two of these mice also developed Munro's microabscesses and wounds accompanied by the presence of immune cell infiltrates in the dermal and epidermal skin layers.

As EHF has recently been shown to be required for the terminal differentiation of keratinocytes *in vitro*, we stained the dorsal skin for Keratin 14 (K14) and Loricrin to determine whether keratinocyte differentiation was impaired. K14 stained the basal keratinocyte layer in both *Ehf* $^{+/+}$ and *Ehf* $^{-/-}$ mice, while there was clear staining of Loricrin in the stratum corneum (Figure 3.7C,D), demonstrating that *Ehf* deletion does not impact on the capacity of basal keratinocytes to differentiate into corneocytes. We also stained the dorsal and chin skin with Keratin 6a (K6a), which is typically only expressed in hair follicles but will also be expressed during epidermal hyperproliferation as part of the wound healing response. At 6 weeks there was no K6a staining

in the epidermis however, at 27 weeks clear K6a staining was observed in areas of damaged skin in *Ehf* $^{-/-}$ mice (Figure 3.7E) demonstrating this feature of epidermal regeneration is also not impacted by *Ehf* deletion.

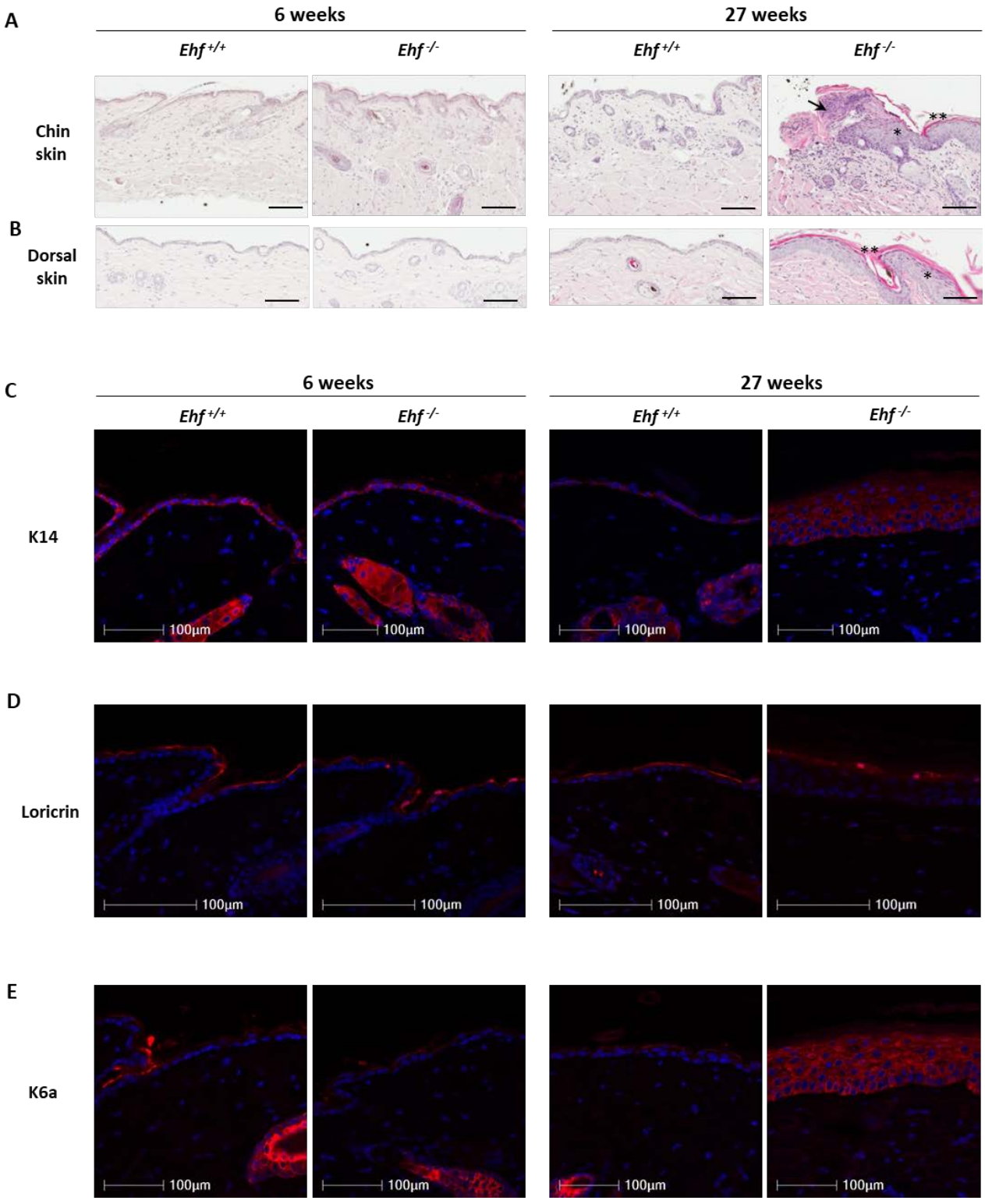

Figure 3.7. Impact of *Ehf* deletion on epidermal histology. (A, B) Representative haematoxylin and eosin stained sections showing the histology of the skin taken from the (A) chin or (B) dorsal region of *Ehf* $^{+/+}$ and *Ehf* $^{-/-}$ littermates at 6 and 27 weeks. * Hyperplasia, ** Hyperkeratosis, Arrow:

Munro's microabscess. Scale bar = 300µm. (C-E) Immunofluorescence staining for (C) K14, (D) Loricrin and (E) K6a in the dorsal skin of *Ehf* $^{+/+}$ and *Ehf* $^{-/-}$ mice at 6 and 27 weeks. Scale bar = 100µm.

3.2.5 *Ehf* $^{-/-}$ mice are fertile, but breeding of *Ehf* $^{-/-}$ female mice results in high neonatal mortality

As part of the characterisation of the *Ehf* $^{-/-}$ strain, *Ehf* $^{-/-}$ male and female mice were bred to *Ehf* $^{+/+}$ or *Ehf* $^{+/-}$ counterparts to determine whether loss of *Ehf* impacts fertility. While *Ehf* $^{-/-}$ males produced healthy and viable offspring, only 4/9 (44%) were successful breeders. It is possible that the reduced breeding success is related to the development of preputial gland abscesses typically seen in male *Ehf* $^{-/-}$ mice. Comparatively, 18/18 (100%) of the *Ehf* $^{-/-}$ female mice fell pregnant despite some of them presenting with genital abscesses at the time of conception.

Strikingly however, the neonatal mortality rate of first litters born to *Ehf* $^{-/-}$ female mice (n=10) was 85.7% (48/56) compared to 22.1% (21/96) and 7.8% (9/114) for *Ehf* $^{+/-}$ (n=16) and *Ehf* $^{+/+}$ (n=17) female mice respectively (Figure 3.8A). Notably, the 8 pups born to *Ehf* $^{-/-}$ mice which survived were fostered by *Ehf* $^{+/-}$ surrogate mothers.

DNA genotyping of the neonates born to *Ehf* $^{-/-}$ female mice which did not survive revealed an even distribution of *Ehf* $^{+/+}$ and *Ehf* $^{-/-}$ genotypes (Figure 3.8B) indicating the high mortality was likely due to a deficiency in the ability of *Ehf* $^{-/-}$ female mice to feed their pups. Consistent with this conclusion, pup mortality occurred within 24-48 hours of birth. Notably, the mortality rate of litters born to *Ehf* $^{-/-}$ mice decreased to 60% at the second pregnancy (n=6, 24/40), indicating partial compensation for EHF loss by exposure to multiple pregnancies (Figure 3.8C).

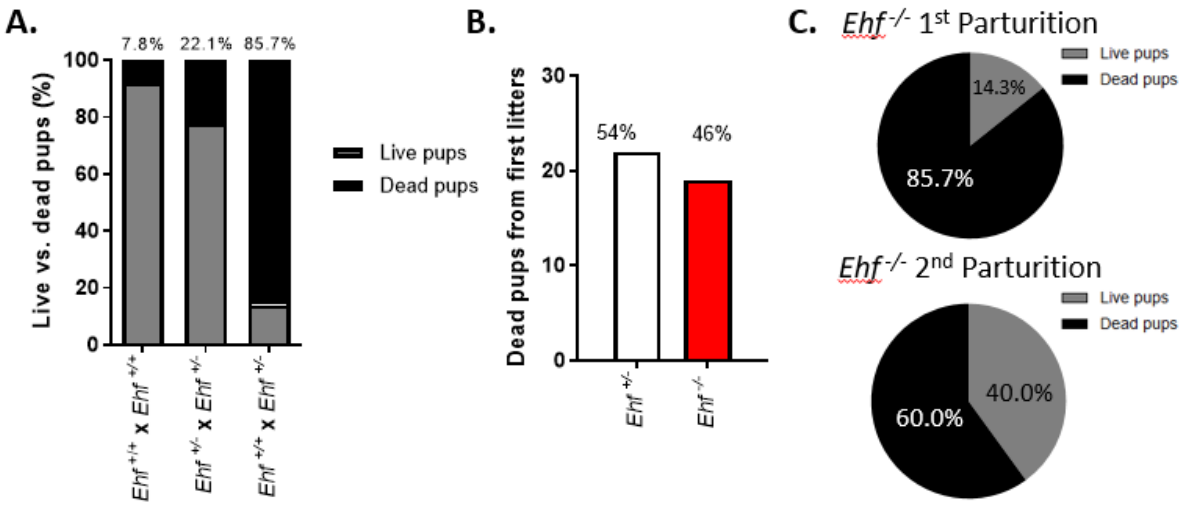

Figure 3.8. Impact of *Ehf* deletion on neonatal survival rate of pups born to uniparous female mice. (A) Neonatal mortality rate of first litters born to *Ehf* $^{+/+}$ (n=17), *Ehf* $^{+/-}$ (n=16) and *Ehf* $^{-/-}$ (n=10) female mice. (B) Genotypes of neonates born to *Ehf* $^{-/-}$ female mice which did not survive. (C) Neonatal mortality from *Ehf* $^{-/-}$ female mice after first (n=10) and second parturition (n=6).

3.2.6 Ehf expression during mammary gland development

To investigate the potential role of EHF in mammary gland development, we first interrogated publicly available single cell gene expression data derived from various stages of mammary gland development. This analysis revealed high Ehf expression in luminal progenitor cells (C6 and C7), and a further increase in expression in alveolar progenitor cells (C9 and C10), and differentiated alveolar cells (C8 and C11) (Figure 3.9, data mined from mammary gland developmental portal, Maroni lab, Cambridge, UK) [42]. This expression profile suggests a potential role for EHF in luminal cell differentiation. The expression profile of EHF was also remarkably similar to that of ELF5, a close homologue to EHF, and an established regulator of mammary gland differentiation.

Based on the observation that *Ehf* $^{-/-}$ female mice are unable to feed their pups and the expression profile of EHF during mammary gland development, we elected to investigate the role of EHF in mammary gland development at the alveologenesis phase (day 18.5 of pregnancy).

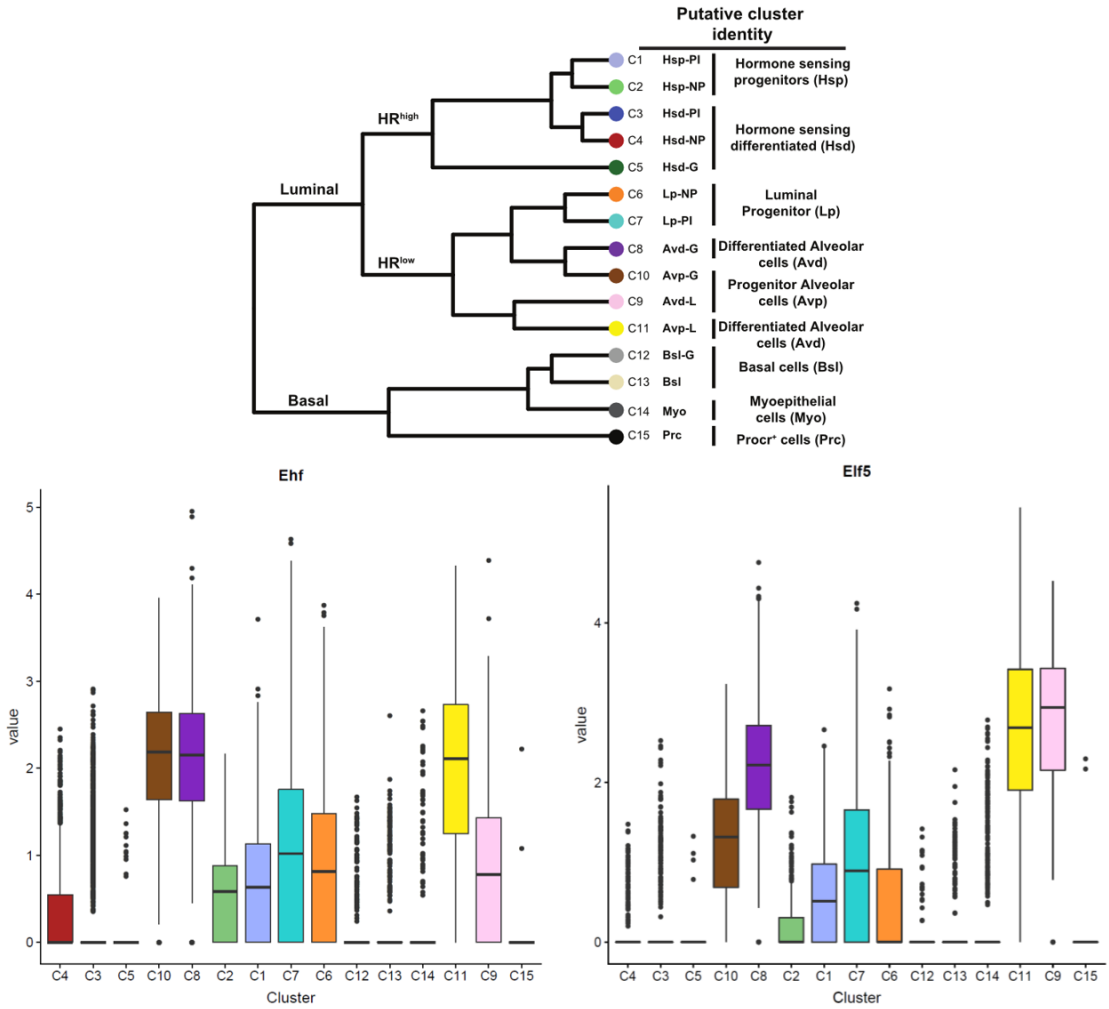

Figure 3.9. Ehf and Elf5 mRNA expression in 15 distinct cellular clusters identified during the various stages of mammary gland development by single cell RNA-seq analysis. NP: nulliparous, G: gestation, L: lactation, PI: post-involution and HR: hormone receptor.

3.2.7 Loss of *Ehf* impairs alveologenesis

To investigate the impact of *Ehf* deletion on mammary gland development at 18.5dP we performed timed pregnancies. For this, male bedding was added to female cages to initiate the oestrus cycle, and two days later, female and male mice were co-housed overnight. The following morning the mice were separated, and female mice checked for vaginal plugs. Plugged female mice were counted as 0.5dP, and mammary glands collected from *Ehf* $^{+/+}$ and *Ehf* $^{-/-}$ female mice at 18.5dP. At this stage of mammary gland development, alveolar differentiation has occurred where luminal progenitor cells differentiate to form secretory alveolar cells capable of milk production. Furthermore, the alveolar luminal space expands and is filled with milk precursor proteins and lipid droplets [237].

We first confirmed complete deletion of the DNA binding domain of *Ehf* in *Ehf* $^{-/-}$ mammary glands by q-RT-PCR (Figure 3.10A). Next, we examined the histology of *Ehf* $^{+/+}$ and *Ehf* $^{-/-}$ mammary glands. As expected, the mammary glands of *Ehf* $^{+/+}$ females at 18.5dP consisted of well-differentiated lobuloalveolar units of expanded alveoli with extensive cytoplasmic lipid droplets (Figure 3.10B). Comparatively, mammary glands of *Ehf* $^{-/-}$ females consisted of low-density lobuloalveolar-like structures with few cytoplasmic lipid droplets. Notably, blinded quantification of the histology confirmed a significant reduction in the number of alveoli, the average alveoli area and the percentage of the mammary gland comprising alveoli in *Ehf* $^{-/-}$ mice (Figure 3.10C), establishing a key role for EHF in alveologenesis.

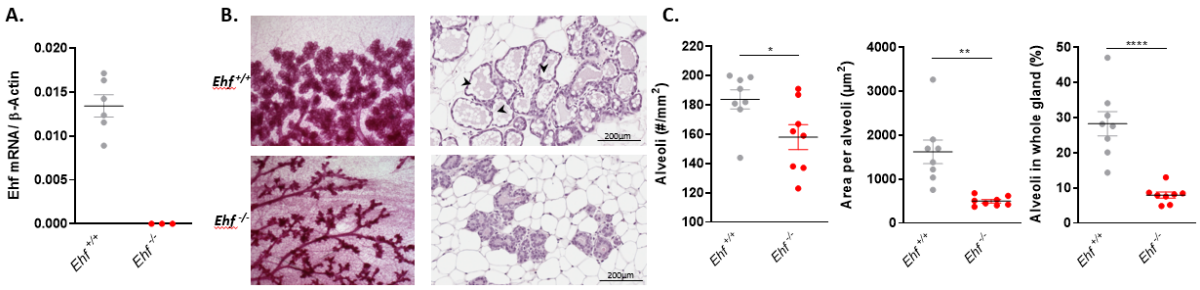

Figure 3.10. Impact of *Ehf* deletion on alveologenesis. (A) Confirmation of *Ehf* deletion in the mammary gland of *Ehf* $^{-/-}$ mice by assessment of *Ehf* mRNA expression by q-RT-PCR. Values shown are mean ± SEM from n= 6 *Ehf* $^{+/+}$ and n=3 *Ehf* $^{-/-}$ mice (B) Carmine alum and H&E stain of *Ehf* $^{+/+}$ and *Ehf* $^{-/-}$ mammary glands at day 18.5 of pregnancy. Black arrowheads indicate cytoplasmic lipid droplets, scale bar = 200μm. (C) Quantification of the number of alveoli, the average alveoli area and the percentage of the mammary gland comprising alveoli. Values shown are mean ± SEM from n= 8 *Ehf* $^{+/+}$ and *Ehf* $^{-/-}$ mice

To confirm these histological changes, mammary glands of *Ehf* $^{+/+}$ and *Ehf* $^{-/-}$ mice were first stained with anti-milk protein (Figure 3.11A). While milk was detected in the *Ehf* $^{-/-}$ mammary glands, the amount was reduced compared to the levels in *Ehf* $^{+/+}$ mice which was likely due to the reduced alveolar area of the *Ehf* $^{-/-}$ glands. Furthermore, no milk was observed in the stomachs of pups born to *Ehf* $^{-/-}$ females 24 hours after birth even though there was clear evidence of suckling. Collectively, these results demonstrate that *Ehf* deletion results in impaired milk production, secretion and/or composition.

Next, to gain insight into the potential underlying mechanisms driving the impaired alveologenesis of *Ehf* $^{-/-}$ mice, mammary glands from *Ehf* $^{+/+}$ and *Ehf* $^{-/-}$ mice were stained with anti-Ki67, anti-Elf5 and anti-p-Stat5 antibodies. Ki67 staining was significantly increased in the *Ehf* $^{-/-}$ mammary glands (Figure 3.11B) suggesting that the mammary epithelial cells of *Ehf*-deficient mice remain

proliferative throughout the pregnancy and are therefore less differentiated at this stage compared to their *Ehf* $^{+/+}$ counterparts.

We then examined whether *Ehf* deletion impacts expression of the highly related Elf5 gene, a key regulator of mammary gland development located immediately adjacent to Ehf in both the mouse and human genome. *Ehf* deletion resulted in a modest decrease in the number of cells expressing Elf5 protein in the mammary epithelium, however this was not statistically significant (Figure 3.11C). Notably, the intensity of Elf5 staining, expressed as an H score, was significantly reduced in *Ehf* $^{-/-}$ mice suggesting Ehf may lie upstream of Elf5.

Finally, as the prolactin/Jak2/Stat5 signalling pathway is a key regulator of alveologenesis, we examined p-Stat5 levels in *Ehf* $^{+/+}$ and *Ehf* $^{-/-}$ mice as a readout of the activation status of this pathway. Mammary epithelial cells from *Ehf* $^{-/-}$ mice had modestly reduced numbers and intensity of p-Stat5 staining compared to *Ehf* $^{+/+}$ mice, although these differences were not statistically significant (Figure 3.11D).

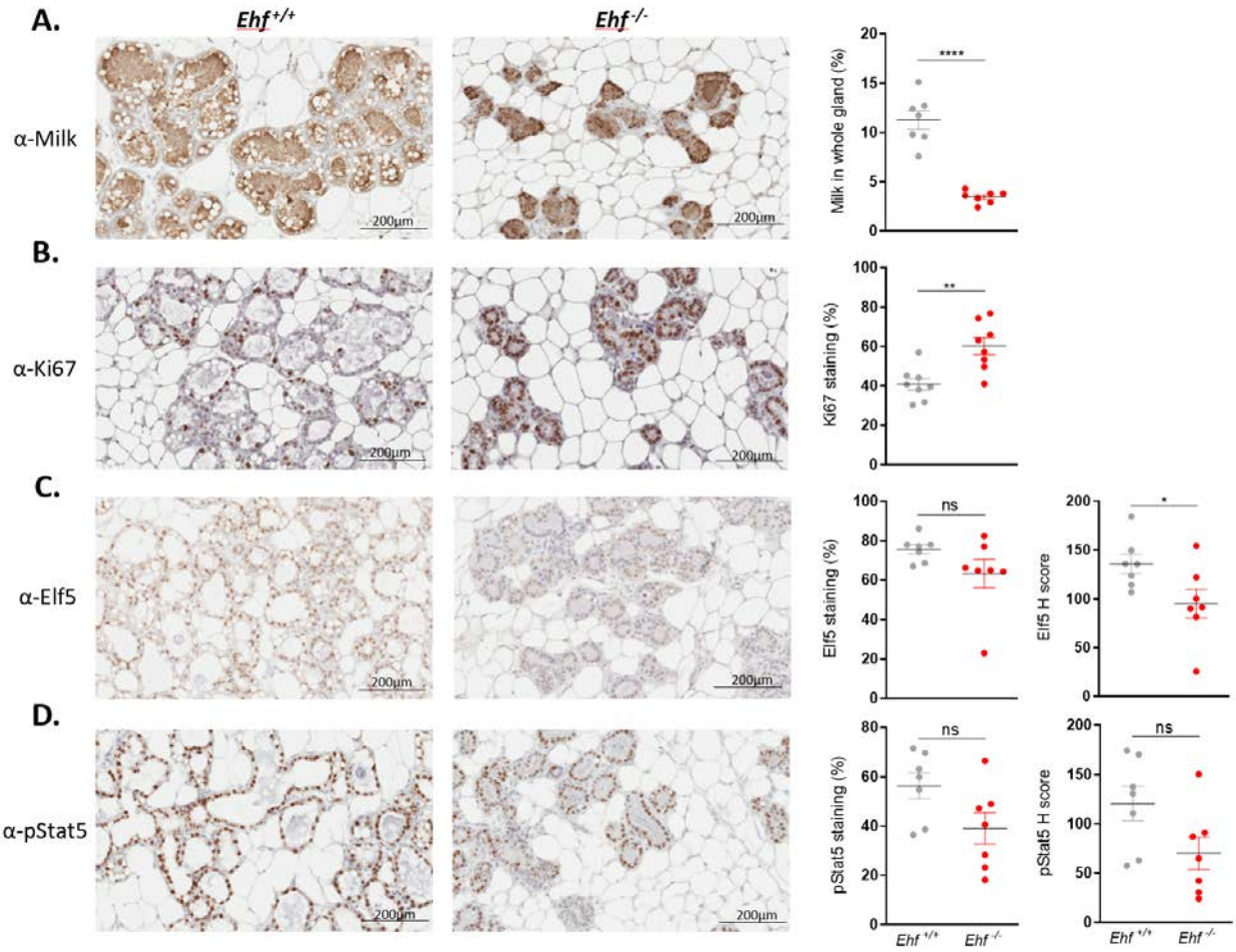

Figure 3.11. Impact of *Ehf* deletion on mammary gland development at 18.5dP. Mammary glands from *Ehf* $^{+/+}$ and *Ehf* $^{-/-}$ female mice stained with (A) anti-milk, (B) anti-Ki67, (C) anti-Elf5 and (D)

anti-p-Stat5, and stains quantified. Scale bar = 200µm. Values shown are mean ± SEM from n= 7 *Ehf* $^{+/+}$ and *Ehf* $^{-/-}$ mice.

3.2.8 Ehf does not profoundly impact branching morphogenesis

Having established an important role for EHF in alveologenesis, we next sought to determine the impact of *Ehf* deletion on branching morphogenesis. During this stage, highly proliferative terminal end buds (TEBs) direct ductal elongation through the mammary fat pad [237]. At approximately 10-12 weeks of age, the ducts reach the margins of the mammary fat pad, upon which the TEBs regress and ductal elongation ceases. To investigate the impact of *Ehf* deletion on branching morphogenesis, mammary glands from 8-10 week old nulliparous *Ehf* $^{+/+}$ and *Ehf* $^{-/-}$ mice were whole mounted and stained with carmine alum. Histological analysis of abdominal glands 4 and 9 revealed that the ductal tree was fully elongated in both *Ehf* $^{+/+}$ and *Ehf* $^{-/-}$ females (Figure 3.12A). However, in comparison to *Ehf* $^{+/+}$ mice, mammary glands from *Ehf* $^{-/-}$ mice contained a significantly higher number of TEBs (Figure 3.12B), although the size of the TEBs was similar (Figure 3.12C). Collectively, these results indicate that loss of *Ehf* does not impede ductal elongation however, the continued presence of TEBs in *Ehf* $^{-/-}$ mice at this time point warrants further investigation.

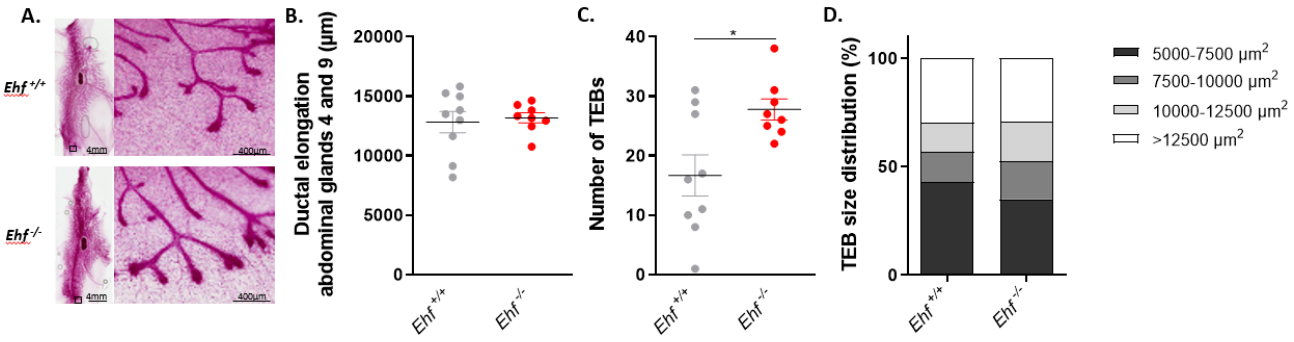

Figure 3.12. Impact of *Ehf* deletion on branching morphogenesis. (A) Carmine alum stained whole mounts of mammary glands from 8-10 week old nulliparous *Ehf* $^{+/+}$ and *Ehf* $^{-/-}$ (scale bar = 4mm) and higher magnification of terminal end buds (scale bar = 400µm). (B) Quantification of the ductal elongation length. Values shown are mean ± SEM from n= 9 *Ehf* $^{+/+}$ and n=8 *Ehf* $^{-/-}$ mice. (C) Quantification of the number of terminal end buds (TEBs). Values shown are mean ± SEM from n= 9 *Ehf* $^{+/+}$ and n=8 *Ehf* $^{-/-}$ mice. (D) The size distribution of the TEBs.

3.3 Discussion

While the role of EHF in homeostasis of a number of epithelial tissues and tumour types has been investigated in cellular model systems *in vitro* [26], the role of EHF in tissue homeostasis in vivo has not been systematically investigated.

To address this, we specifically inactivated the major known function of EHF, its ability to bind DNA and regulate transcription. This was achieved by targeted deletion of the ETS DNA-binding domain of EHF by crossing *Ehf* floxed mice with *CMV* ^{Cre} deleter mice. While successful deletion of the ETS DNA-binding domain was achieved, it should be noted that we detected the presence of residual Ehf mRNA transcripts in multiple tissues. It therefore remains possible that DNA-binding-independent functions of EHF may have been retained in this model. The EHF protein contains two functional domains: the pointed domain and the deleted ETS DNA-binding domain [2]. The pointed domain is required for protein-protein interactions and while it was initially shown that isolated pointed domains from ETS transcription factors do not retain functionality [238], a recent study of SPDEF demonstrated functionality of the pointed domain independent of the ETS domain [239]. Notably, when the ETS domain is deleted, the pointed domain of SPDEF was able to bind and sequester β-catenin in the cytoplasm more effectively. Comparatively, deletion of the ETS DNA-binding domain of ELF5 causes complete loss of the ELF5 protein [208]. It is currently unclear whether some functionality of the EHF protein is maintained in our *Ehf* $^{-/-}$ model, as despite making multiple attempts to assess EHF protein expression by Western Blot and immunohistochemistry, we were unsuccessful. However, our current findings establish that loss of EHF transcriptional activity is sufficient to induce a series of phenotypes in multiple tissues.

We began our characterisation of *Ehf* $^{-/-}$ mice by determining the impact of *Ehf* deletion on embryonic lethality, as deletion of the Ehf homologue *Elf5* results in embryonic lethality [210], while deletion of *Elf3* results in partial embryonic lethality [52]. We observed that although *Ehf* $^{-/-}$ mice were born at a lower-than-expected ratio, this difference was not significant, enabling us to conclude that EHF is not essential for embryonic development.

Most notable amongst the phenotypes of *Ehf* $^{-/-}$ mice was reduced body weight gain of both male and female *Ehf* $^{-/-}$ mice compared to *Ehf* $^{+/+}$ littermates, the development of abscesses in the preputial gland of male mice and vulva of female mice, as well as the development of facial warts and corneal ulcers. Notably, abscesses of the preputial glands of male mice and vulva of female mice meant that most of the *Ehf* $^{-/-}$ mice had to be euthanised within one year.

Consistent with our observation that *Ehf* deletion results in the development of corneal ulcers, a recent study by Stephens et al [19] in which the gene expression changes in the mouse corneal epithelium were profiled over time, identified Ehf as one of the few genes significantly up-

regulated during ageing. ChIP analysis revealed EHF binding to Plaur and Tcf4, genes involved in stem cell maintenance. Furthermore, knockdown of *EHF* in human corneal epithelial cells resulted in decreased expression of SPRR proteins which are required for keratin cross-linking and maintenance of the barrier function of skin. It is therefore possible that the corneal defects observed in *Ehf* $^{-/-}$ mice may be due to a defect in corneal differentiation during ageing which requires further investigation.

A major phenotype observed in *Ehf* $^{-/-}$ mice was the development of multiple facial warts and swelling of their facial skin. We therefore examined the histology of the skin of *Ehf* $^{-/-}$ and *Ehf* $^{+/+}$ littermates at multiple timepoints. While no gross histological abnormalities were observed at 6 weeks, at 27 weeks we observed a significantly higher rate of hyperplasia, hyperkeratosis and/or Munro's microabscesses in both the chin and dorsal skin of *Ehf* $^{-/-}$ mice. Furthermore, due to a recent study by Rubin et al that reported a central role for EHF in the in vitro differentiation of human keratinocytes [21] we also stained chin and dorsal skin sections for K14 and Loricrin. The presence of Loricrin in the stratum corneum of *Ehf* $^{-/-}$ mice demonstrates that *Ehf* deletion does not impact on the capacity of basal keratinocytes to differentiate into corneocytes. It is therefore unlikely that EHF is a regulator of keratinocyte differentiation in mice. Rather, the later onset of these lesions and the observation that they mostly occur in areas of high exposure to damage-inducing behaviours such as grooming and fighting, suggests a potential role for EHF in repair of the skin epithelium.

As these phenotypes were observed in mice in which *Ehf* was deleted in all cells, the possibility remains that defects in the immune system may play a role. In this regard, while *Ehf* is primarily expressed in epithelial tissues, it has also been reported to be expressed in mast cells and Langerhans cells [20, 22] which are key immune populations of the skin. Further studies such as bone marrow transplantation experiments are required to establish the role of the immune system in driving the phenotype of *Ehf* $^{-/-}$ mice.

While *Ehf* $^{-/-}$ mice frequently developed abscesses in the subcutaneous preputial glands (males) and vulva (females), we did not observe any gross histological differences in the epithelium of these tissues between *Ehf* $^{+/+}$ and *Ehf* $^{-/-}$ mice at 6 weeks. Again, these are areas frequently exposed to abrasions such as grooming or grazing against mouse bedding material, supporting a role for EHF in skin repair or maintenance of the skin barrier integrity.

In addition, we also examined the histology of other tissues in which *Ehf* mRNA is highly expressed. Histological analysis of the salivary gland, stomach and prostate in 6 week old mice revealed no gross abnormalities in these tissues at this time point. It remains possible, however, that EHF may

still play a key role in these tissues particularly under conditions of stress or in the context of cancer.

Finally, a major phenotype observed in *Ehf* $^{-/-}$ mice was the high mortality rate of pups born to *Ehf* $^{-/-}$ female mice, particularly after their first pregnancy. Interestingly, we did observe a decrease in the neonatal mortality rate with subsequent litters born to *Ehf* $^{-/-}$ females, indicating that the loss of *Ehf* could be at least partially compensated by exposure to multiple pregnancies. This phenomenon has been observed in other knockout mouse models, such as *Elf5* and *PrlR* heterozygous mice [208, 240], and has been postulated to be driven by an epigenetic memory retained from the first pregnancy that primes the activation of gene expression networks required for mammary gland development in subsequent reproductive cycles [241].

The high neonatal mortality of pups born to *Ehf* $^{-/-}$ females prompted us to investigate the mammary glands of *Ehf* $^{+/+}$ and *Ehf* $^{-/-}$ females. As mining of publicly available single cell RNA-seq data revealed Ehf to be highly expressed in luminal and alveolar progenitor cells and to be further increased in differentiated alveolar cells of the mammary gland [42, 211], we focussed on alveologenesis which occurs during pregnancy.

Analysis of the mammary glands at 18.5dP demonstrated a major defect in the development of lobuloalveolar units of *Ehf* $^{-/-}$ females at this time point, characterised by a higher rate of proliferation. While immunohistochemical staining revealed the presence of milk protein in the mammary glands of *Ehf* $^{-/-}$ females, the number of cytoplasmic lipid droplets was markedly reduced, suggesting the lipid composition of milk is likely compromised. Lipidomic profiling of milk from *Ehf* $^{+/+}$ and *Ehf* $^{-/-}$ females may provide more detailed insight into these differences. Collectively, these findings suggest a delay in the differentiation of luminal progenitor cells into terminally differentiated alveolar cells capable of proper milk production and secretion.

The mammary gland phenotype observed in *Ehf* $^{-/-}$ female mice is remarkably similar to that reported in *Elf5*-deficient mice [208-210]. Therefore, given the close proximity of the *Ehf* and *Elf5* genes, we investigated whether *Ehf* deletion may be impacting mammary gland development by disrupting ELF5 expression. While the number of ELF5-positive cells were not altered in *Ehf* $^{-/-}$ female mice, the staining intensity of ELF5 was modestly decreased. ELF5 is induced by prolactin-Stat5 signalling, and pSTAT5 levels were also modestly reduced in *Ehf* $^{-/-}$ female mice. Collectively, these findings suggest that *Ehf* deletion may impact on prolactin-Stat5-Elf5 signalling, however, the extent to which these pathway components are deregulated suggest it is unlikely to completely explain the phenotype. Additional studies including transcriptional profiling of mammary epithelial cells isolated from *Ehf* $^{+/+}$ and *Ehf* $^{-/-}$ female mice are therefore required to

fully understand the downstream transcriptional program impacted by *Ehf* deletion which may contribute to the observed phenotype.

In addition to examining the effect of *Ehf* deletion on alveologenesis, we also examined its impact on branching morphogenesis during puberty. This analysis revealed that the ductal tree of nulliparous *Ehf* $^{+/+}$ and *Ehf* $^{-/-}$ female mice were both fully elongated, although we noted that the TEBs in *Ehf* $^{-/-}$ mice had regressed to a lesser extent compared to those in *Ehf* $^{+/+}$ mice. These findings may indicate a potential role for EHF in either branching migration, differentiation or apoptotic regression, although additional studies, particularly at earlier timepoints are required to resolve this.

In summary, this is the first study of the role of the EHF transcription factor in development and tissue homeostasis *in vivo*. We reveal an essential role for EHF in the maintenance of epidermal homeostasis and as a promoter of alveologenesis during pregnancy.

Chapter 4: Role of EHF in the intestinal epithelium

4.1 Introduction

EHF is highly expressed in the colonic epithelium, which consists of unique and highly specialised absorptive and secretory epithelial cells. These terminally differentiated cells are continuously replenished by proliferating stem cells located in the intestinal crypts of Lieberkühn. The equilibrium between proliferation, differentiation and apoptosis is essential for maintaining an efficient epithelial barrier.

The role of EHF in intestinal homeostasis has only been investigated in a small number of studies. Asai et al. used an *in vitro* model of follicle-associated epithelium to show that EHF is involved in the transcytosis of non-opsonised and SIgA-opsonised particles through TC7 monocultures [18]. More recently, Zhu et al. used CRISPR-CAS9 mediated genome editing to delete *Ehf* in the whole body of mice, and reported that *Ehf* deletion resulted in reduced *Lgr5+* intestinal stem cell numbers, impaired organoid formation and decreased ISC stem cell renewal in the small intestine [16]. However, none of these studies comprehensively investigated the role of *Ehf* in the colonic epithelium where EHF is most highly expressed.

To determine the role of EHF in colonic epithelial homeostasis we used the *Ehf* whole body knockout mouse model described in Chapter 3**,** and a conditional mouse model in which *Ehf* was specifically deleted in small intestinal and colonic epithelial cells. The conditional mouse model was generated by crossing *Ehf* $^{Lox/Lox}$ mice with *Villin* ^{CreERT2} mice. Using these models, we demonstrate that *Ehf* deletion increases cell proliferation and reduces goblet cell differentiation in the colonic epithelium. Furthermore, we reveal significant transcriptional changes in the colon following *Ehf* deletion.

4.2 Results

4.2.1 *Ehf* deletion specifically in the intestinal epithelium has minimal impact on overall animal health

To induce *Ehf* deletion specifically in the intestinal epithelium, *Ehf* $^{Lox/Lox}$; *Villin* ^{CreERT2} mice were treated with tamoxifen (*Ehf* ^{IKO}). *Ehf* $^{Lox/Lox}$; *Villin* ^{CreERT2} littermates treated with vehicle only (*Ehf* ^{WT}) served as controls. To confirm *Ehf* deletion, small intestinal and colonic epithelial cells were isolated from 6-week-old *Ehf* ^{WT} and *Ehf* ^{IKO} mice, and Ehf expression determined by genotyping and q-RT-PCR. Genotyping of isolated small intestinal epithelial cells confirmed that the floxed region of *Ehf* was deleted (252bp band) in the tamoxifen treated mice but remained intact in vehicle treated mice (912bp band) (Figure 4.1A).

Consistent with these results, mRNA expression of Ehf in small intestinal and colonic epithelial cells was absent in *Ehf* ^{IKO} but not *Ehf* ^{WT} mice, and expression remained absent when mRNA levels were re-assessed in mice older than six months (Figure 4.1B). Collectively, these results indicate that the ETS DNA-binding domain of Ehf is successfully deleted in the small intestinal and colonic epithelium of *Ehf* ^{IKO} mice, and that there is no compensatory repopulation by *Ehf* wildtype cells over time.

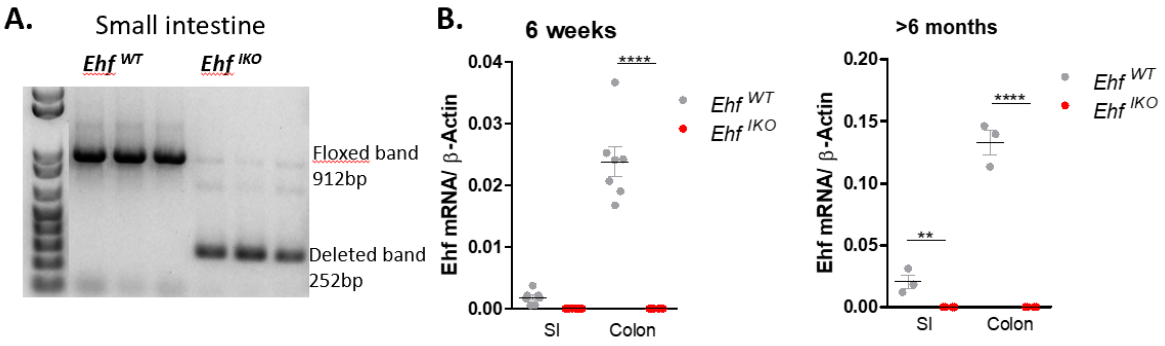

Figure 4.1. Confirmation of deletion of the DNA binding domain of EHF in the small intestinal and colonic epithelium of *Ehf* ^{IKO} mice at the (A) genomic level and (B) the mRNA level. SI = small intestine. Values shown are mean ± SEM from n= 6 and n=3 *Ehf* ^{WT} and *Ehf* ^{IKO} mice.

To determine the impact of intestinal-specific *Ehf* deletion on the overall health of the mice, male and female *Ehf* ^{WT} and *Ehf* ^{IKO} mice were aged for two years, and body weights monitored weekly. *Ehf* deletion did not impact body weight of male or female mice, which remained similar over the duration of the study (Figure 4.2A). Likewise, *Ehf* deletion had no effect on food intake which was similar between *Ehf* ^{WT} and *Ehf* ^{IKO} female mice (Figure 4.2B).

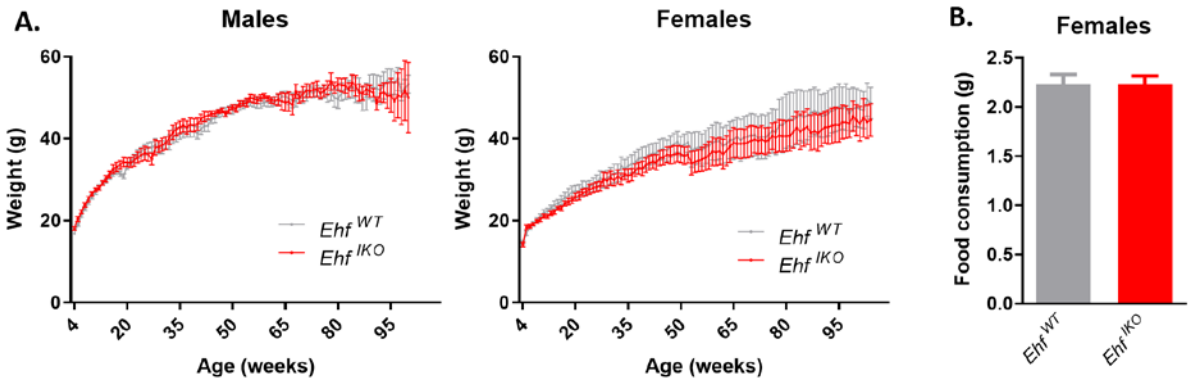

Figure 4.2. Body weight of *Ehf* ^{WT} and *Ehf* ^{IKO} mice. (A) Body weight of male and female *Ehf* ^{WT} and *Ehf* ^{IKO} littermates. (B) Daily average food intake of n=5 *Ehf* ^{WT} and *Ehf* ^{IKO} female mice measured over a two-week period.

As these mice were aged, they were monitored for signs of ill health as outlined in Chapter 2.2.1 Animal monitoring. Mice meeting the criteria of ill health were immediately culled and time point recorded. Based on these criteria, the median lifespan of both *Ehf* ^{WT} and *Ehf* ^{IKO} mice was approximately 23 months (Figure 4.3A), and there was no significant difference in the survival of *Ehf* ^{WT} and *Ehf* ^{IKO} mice. The major symptom of ill health requiring mice to be culled was weight loss for both *Ehf* ^{WT} and *Ehf* ^{IKO} mice (Figure 4.3B). Necropsy of these mice revealed this was most commonly associated with the onset of liver tumours (data not shown). These tumours were observed in 33 % (3/9) of both *Ehf* ^{WT} and *Ehf* ^{IKO} mice and were therefore considered unrelated to *Ehf* deletion. No evidence of tumour formation or other gross abnormalities were observed in the small intestinal or colonic epithelium in either *Ehf* ^{WT} or *Ehf* ^{IKO} mice at the time of death. Collectively, these results indicate that intestinal-specific *Ehf* deletion does not impact the overall health of the animals.

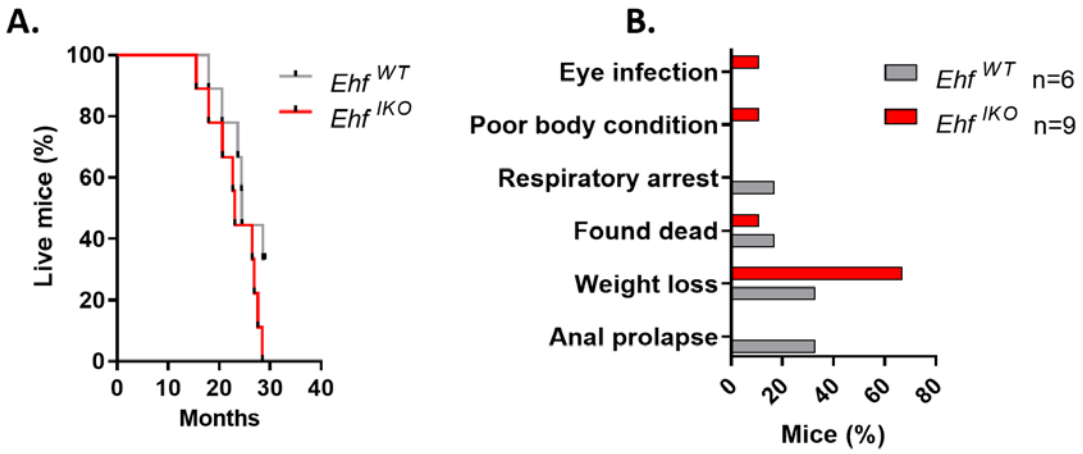

Figure 4.3. Lifespan of *Ehf* ^{WT} and *Ehf* ^{IKO} mice. (A) Kaplan-Meier survival analysis of *Ehf* ^{WT} and *Ehf* ^{IKO} mice over 29 months. (B) Symptoms of ill health displayed by *Ehf* ^{WT} and *Ehf* ^{IKO} mice requiring mice to be culled.

4.2.2 *Ehf* deletion does not impact on the stem cell compartment

To determine the impact of *Ehf* deletion on the stem cell compartment we analysed the expression of the stem cell marker Lgr5 in isolated small intestinal and colonic epithelial cells from 6-week-old *Ehf* ^{WT} and *Ehf* ^{IKO} mice by q-RT-PCR. This analysis revealed no difference in Lgr5 expression in either the colon or small intestine between *Ehf* ^{WT} and *Ehf* ^{IKO} mice (Figure 4.4A). To confirm this finding, we also examined protein expression of second stem cell marker, OLFM4, in the small intestine of 6-week-old *Ehf* $^{+/+}$ and *Ehf* $^{-/-}$ mice by IHC. This marker is expressed exclusively in stem cells of the small intestine in mice [242]. As expected, OLFM4 positively stained cells in the base of the small intestinal crypts where stem cells reside. Although *Ehf* deletion caused a modest increase in the number of OLFM4+ stem cells, this was not statistically significant (Figure 4.4B). Taken together, these findings demonstrate that *Ehf* deletion does not impact on the intestinal stem cell compartment.

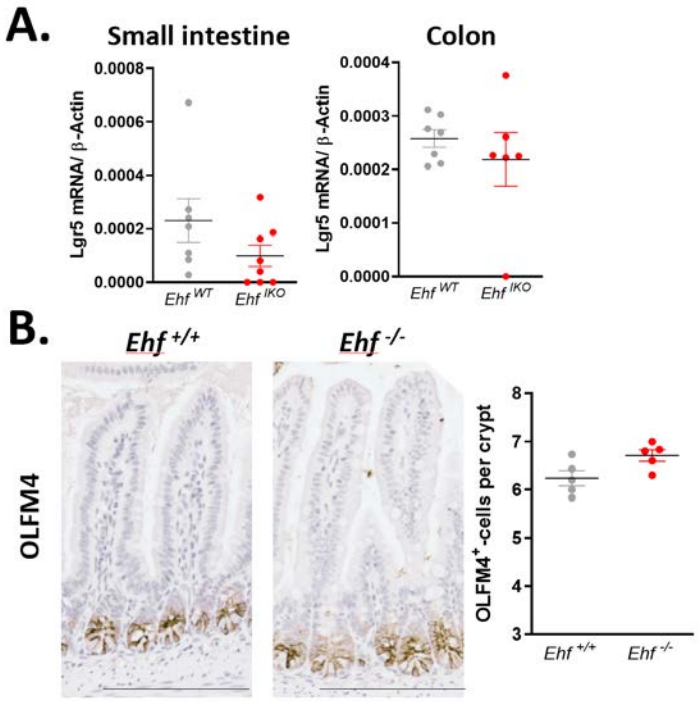

Figure 4.4. Analysis of the stem cell compartment in 6-week-old *Ehf* wildtype and *Ehf* knockout mice. (A) Gene expression of stem cell marker *Lgr5* in isolated small intestinal and colonic epithelial cells from *Ehf* ^{WT} and *Ehf* ^{IKO} mice. Values shown are mean ± SEM from n= 7 *Ehf* wildtype and n=8 *Ehf* knockout mice. (B) Staining and quantification of expression of the intestinal stem cell marker OLFM4 in the small intestinal epithelium of *Ehf* $^{+/+}$ and *Ehf* $^{-/-}$ mice. Values shown are mean ± SEM from n= 5 *Ehf* wildtype and *Ehf* knockout mice. Scale bar = 100µm.

4.2.3 *Ehf* deletion alters colonic epithelial cell proliferation and differentiation

To determine the impact of *Ehf* deletion of intestinal cell proliferation and differentiation, colon and small intestine were collected from 6-week-old *Ehf* ^{WT} and *Ehf* ^{IKO} littermates for molecular and histological analyses. To supplement these results, we also repeated all histological analyses using tissue collected from 6-week-old *Ehf* $^{+/+}$ and *Ehf* $^{-/-}$ (constitutive knockout) mice described in Chapter 3. The impact of *Ehf* deletion on epithelial cell proliferation and differentiation was mainly investigated in the colonic epithelium, where Ehf expression is highest.

First, *Ehf* ^{WT} and *Ehf* ^{IKO} mice at six weeks of age were culled and the small intestine and colon examined macroscopically for any intestinal abnormalities. This examination did not reveal any signs of inflammation or irregular growths following tamoxifen treatment, and the length of the small intestine and colon was unaltered (Figure 4.5).

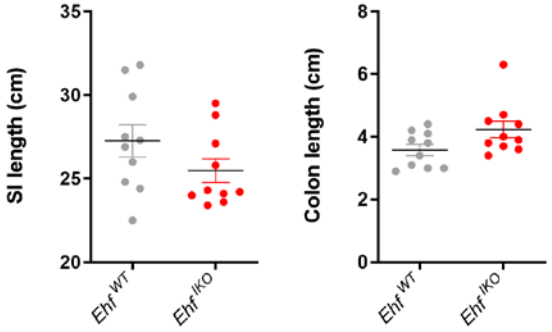

Figure 4.5. Length of small intestine (SI) and colon of 6-week-old *Ehf* ^{WT} and *Ehf* ^{IKO} mice. Values shown are mean ± SEM from n=10 *Ehf* ^{WT} and *Ehf* ^{IKO} mice.

Next, to determine the effect of *Ehf* deletion on epithelial cell proliferation, we generated organoids from isolated colonic crypts of *Ehf* ^{WT} and *Ehf* ^{IKO} mice and monitored their growth and morphology *in vitro*. No gross morphological differences were observed between *Ehf* ^{WT} and *Ehf* ^{IKO} organoids and the organoids appeared to grow at similar rates (Figure 4.6).

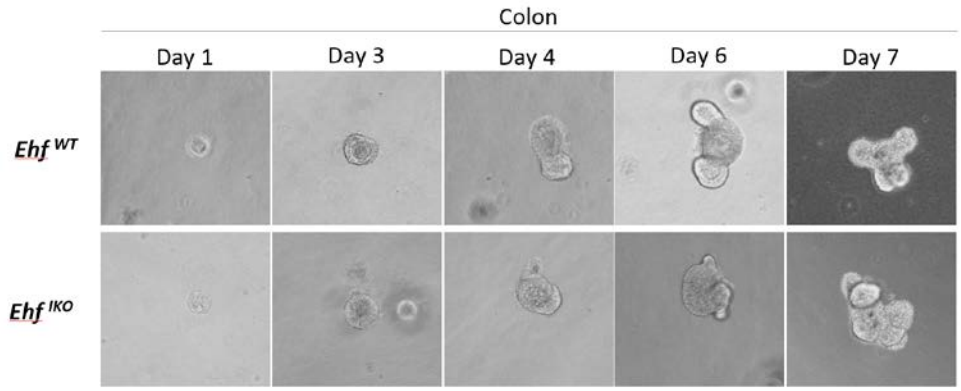

Figure 4.6. Growth of colonic organoids from 6-week-old *Ehf* ^{WT} and *Ehf* ^{IKO} mice.

Having seen no gross difference in *in vitro* growth, we sought to investigate differences in colonic epithelial cell proliferation more rigorously by analysing expression of cell proliferation markers in isolated colonic epithelial cells by q-RT-PCR, and on tissue sections by immunohistochemistry. For these analyses we used tissues from *Ehf* $^{+/+}$ and *Ehf* $^{-/-}$ (constitutive knockout) mice.

Notably, mRNA expression of the cell proliferation marker Pcna was significantly increased in isolated colonic epithelial cells from *Ehf* knockout mice, suggesting *Ehf* deletion may increases cell proliferation in the colon (Figure 4.7A). Consistent with this finding, staining and quantification of Ki67 protein expression in colonic sections confirmed an increase in cell proliferation in the colon of *Ehf* knockout mice (Figure 4.7B).

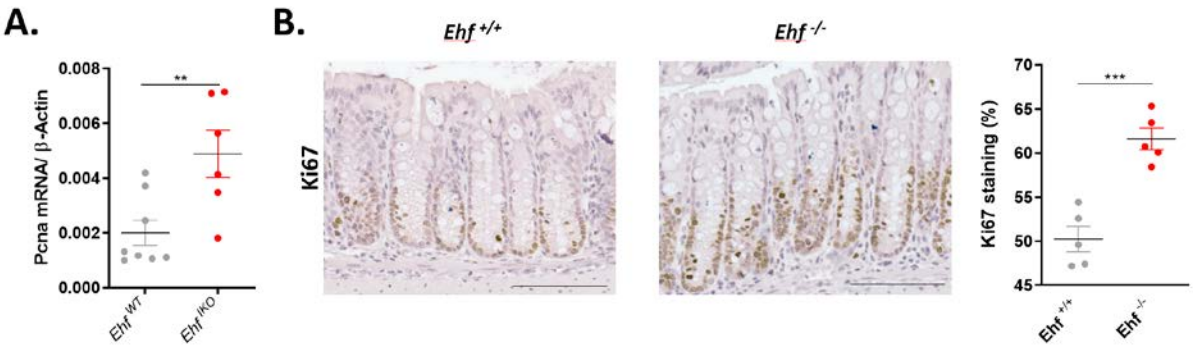

Figure 4.7. Epithelial cell proliferation in the colonic epithelium of 6-week-old *Ehf* wildtype and *Ehf* knockout mice. (A) mRNA expression of the cell proliferation marker *Pcna* in *Ehf* ^{WT} and *Ehf* ^{IKO} mice. Values shown are mean ± SEM from n= 8 *Ehf* wildtype and n=6 *Ehf* knockout mice. (B) Staining and quantification of Ki67 protein in *Ehf* $^{+/+}$ and *Ehf* $^{-/-}$ mice. Scale bar = 100µm. Values shown are mean ± SEM from n= 5 *Ehf* wildtype and *Ehf* knockout mice.

Finally, to determine the impact of *Ehf* deletion on intestinal cell differentiation we measured expression levels of markers of the major intestinal epithelial cell lineages by q-RT-PCR and immunohistochemistry.

Enterocytes: The levels of expression of keratin 20 (KRT20) was used as a measure of enterocyte differentiation. As expected, KRT20 stained differentiated enterocytes located at the top of the colonic crypts. Although expression of KRT20 was moderately decreased in the colonic epithelium of *Ehf* $^{-/-}$ mice compared to *Ehf* $^{+/+}$ mice, this difference was not significant (Figure 4.8A,B).

Enteroendocrine cells: Enteroendocrine cell differentiation was assessed by immunohistochemical detection of the enteroendocrine marker CHGA in the colonic epithelium. IHC staining revealed that as expected, these cells are sparsely located throughout the colonic and small intestinal

crypts, however no difference was observed in the number of CHGA-positive cells between *Ehf* $^{+/+}$ and *Ehf* $^{-/-}$ mice (Figure 4.8C,D).

Tuft cells: The effect of *Ehf* deletion on tuft cell differentiation was assessed by immunohistochemical detection of the tuft cell marker DCLK1 in the colon. As expected, these cells were sparsely located along the crypt axis, however there was no difference in the number of DCLK1+ cells between *Ehf* $^{+/+}$ and *Ehf* $^{-/-}$ mice (Figure 4.8E,F).

Goblet cells: The number of goblet cells was assessed by examining the amount of PAS/AB staining in the colon. Strikingly, PAS/AB staining was significantly reduced in the *Ehf* $^{-/-}$ mice compared to *Ehf* $^{+/+}$ mice, suggesting that *Ehf* deletion may reduce goblet cell differentiation and/or mucus production in the colon (Figure 4.8G,H).

Paneth cells: Finally, the impact of *Ehf* deletion on Paneth cell differentiation was assessed by immunohistochemical detection of the Paneth cell marker LYZ1 in the small intestine where these cells are localised. As expected, LYZ1 positive Paneth cells were located in the crypt base consistent with the known location of these cells. However, there was no difference in the number of LYZ1 positive Paneth cells between *Ehf* $^{+/+}$ and *Ehf* $^{-/-}$ mice (Figure 4.8I,J).

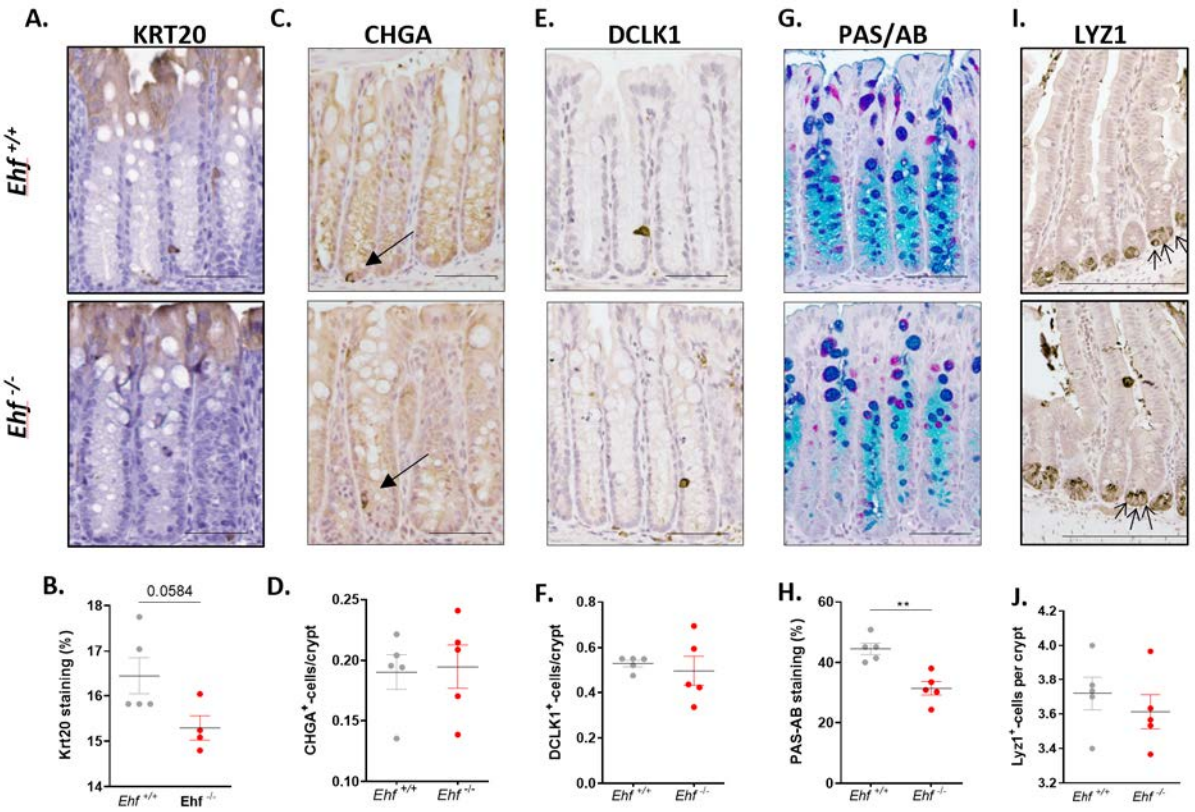

Figure 4.8. Lineage-specific epithelial cell differentiation in the small intestinal and colonic epithelium of *Ehf* $^{+/+}$ and *Ehf* $^{-/-}$ mice at 6 weeks of age. (A) Staining and (B) quantitation of the

enterocyte marker KRT20. (C,D) Staining and quantitation of the enteroendocrine marker CHGA; (E,F) Staining and quantification of the tuft cell marker DCLK1; (G,H) Staining and quantification of goblet cells using periodic acid-Schiff/ Alcian Blue (PAS/AB); and (I,J) Staining and quantification of the Paneth cell marker LYZ1. Scale bars: 100 μm. Values shown are mean ± SEM from n= 5 *Ehf* wildtype and *Ehf* knockout mice.

4.2.4 *Ehf* deletion does not alter the rate of cell migration along the colonic crypt

Having established a role for EHF in cell proliferation and goblet cell differentiation of colonic epithelial cells, we next sought to determine the impact of *Ehf* deletion on cell migration along the colonic crypt axis.

In the colon, terminally differentiated epithelial cells migrate along the crypt axis towards the luminal surface, in a process that takes 3-5 days to complete [54, 55]. To determine the impact of Ehf deletion on the rate of cell migration in the colon, we performed a BrdU-chase experiment. Here, BrdU is used to label the DNA of proliferating cells, thereby providing a means to track the location of these cells over time. *Ehf* ^{WT} and *Ehf* ^{IKO} mice were given a single intraperitoneal injection of BrdU at 6 weeks of age, and cohorts of mice culled at 2, 24, 48 and 72 hours post injection. The position along the crypt axis of each BrdU-positive cell was scored and plotted (Figure 4.9). The peak of each curve corresponds to the cell position along the crypt axis with the highest number of BrdU-positive cells at that timepoint, and a shift in the peak position between the *Ehf* ^{WT} and *Ehf* ^{IKO} curves would reflect a difference in cell migration. Consistent with the increase in colonic cell proliferation following *Ehf* deletion in mice, more colonic epithelial cells in the *Ehf* ^{IKO} mice were BrdU-positive compared with *Ehf* ^{WT} mice at all timepoints. However, comparison of the peak position of the curves corresponding to the *Ehf* ^{WT} and *Ehf* ^{IKO} mice revealed no difference in the rate of cell migration following *Ehf* deletion along the crypt axis in the colon.

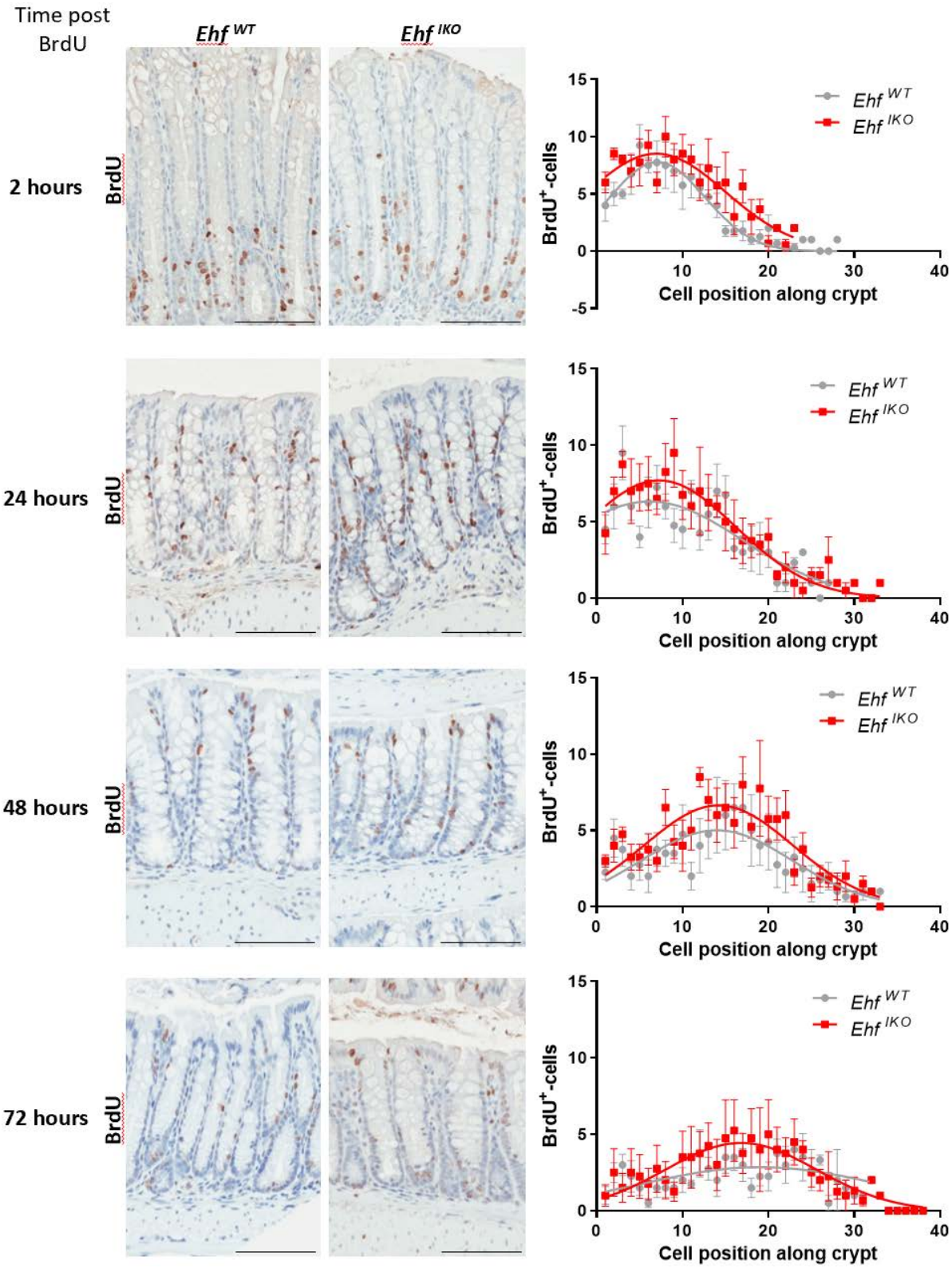

Figure 4.9. Effect of *Ehf* deletion on the rate of cell migration along the colonic crypt axis. 6-week-old *Ehf* ^{WT} and *Ehf* ^{IKO} mice were injected with BrdU and sections of colon stained for BrdU positivity after 2, 24, 48 and 72 hours. Corresponding quantification of BrdU-positive cells is shown on the right. Values shown are mean ± SEM from n= 4 *Ehf* wildtype and *Ehf* knockout mice.

4.2.5 Intestinal-specific deletion of *Ehf* causes major transcriptional reprogramming in the colonic epithelium

To further elucidate the role of EHF in the colonic epithelium, we performed RNA-seq analysis of colonic epithelial cells isolated from 6-week-old *Ehf* ^{WT} and *Ehf* ^{IKO} mice. To account for possible transcriptional changes induced by tamoxifen, *Villin* ^{CreERT2} mice treated with tamoxifen (*Villin* $^{CreERT2\text{-}TMX}$) were also analysed as a further control. Principal components analysis of the RNA-seq data resulted in clear separation of the *Ehf* ^{IKO} samples from the two control groups (Figure 4.10), indicating *Ehf* deletion induces extensive transcriptional reprogramming in the colonic epithelium. Analysis of the gene expression changes identified 146 differentially expressed genes between the *Ehf* ^{IKO} mice and both control strains, of which 75 were upregulated and 71 were downregulated in the *Ehf* ^{IKO} mice (Figure 4.11A, Appendix D). Of the top differentially expressed genes, increased expression of Reg4, Id4 and Pla2g2a, and reduced expression of Lpo in *Ehf* ^{IKO} mice was confirmed by q-RT-PCR, demonstrating the reproducibility of the RNA-seq data (Figure 4.11B).

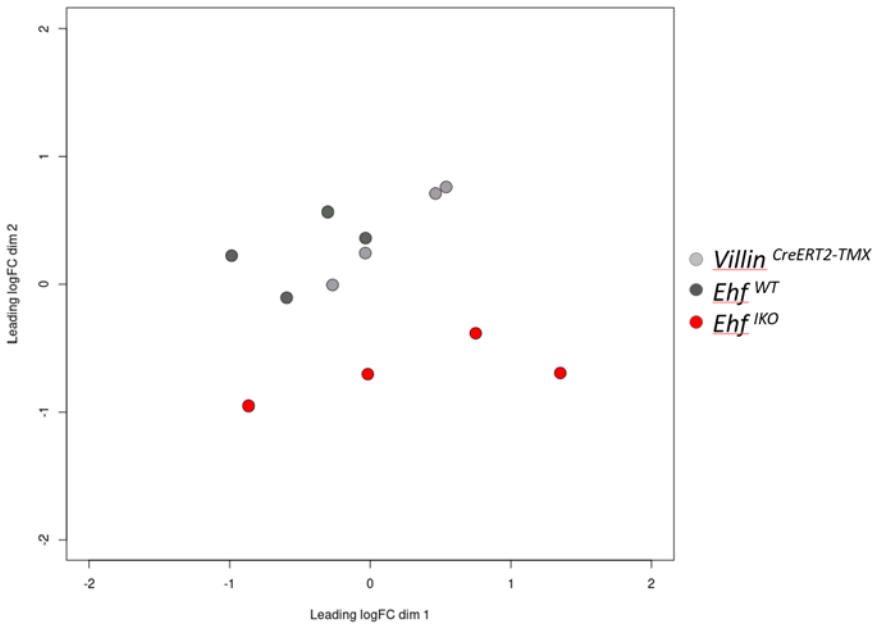

Figure 4.10. Unsupervised cluster analysis of gene expression profiling of colonic epithelial cells isolated from 6-week-old *Ehf* ^{WT}, *Ehf* ^{IKO} and *Villin* $^{CreERT2\text{-}TMX}$ mice (n=4 mice were analysed per genotype).

Consistent with the increase in colonic cell proliferation induced by *Ehf* deletion, gene set enrichment analysis (GSEA) using the 'Hallmark gene sets' in the MSigDB database identified an enrichment of the G2M checkpoint category, which included increased expression of genes involved in cell cycle progression (E2f3, Cenpf and Rad21) in *Ehf* ^{IKO} mice (Figure 4.11C, Appendix E). This analysis also identified an enrichment of the epithelial to mesenchymal transition (EMT)

gene signature, which included increased expression of Vcam1, Itgb3, Fap, Fbn2, Tfpi2, Adam12, Eln, Wnt5a, Spp1, Bgn, Slit3, Serpinh1, Fbln2, Plaur, Capg, Tnc, Timp3, Lamc1, Pmp22, Itgb5 and several collagens (Col1a1, Col1a2, Col3a1, Col4a1, Col4a2, Col5a1, Col5a2, Col6a2 and Col6a3) in *Ehf* ^{IKO} mice (Figure 4.11C, Appendix F). Similar enriched categories were identified following comparison to the 'Curated gene sets' in the MSigDB database, including "ECM proteoglycans", "ECM receptor interaction", "Zhou_cell cycle genes in IR response" and "Molenaar_targets of CCND1 and CDK4" (Appendix G).

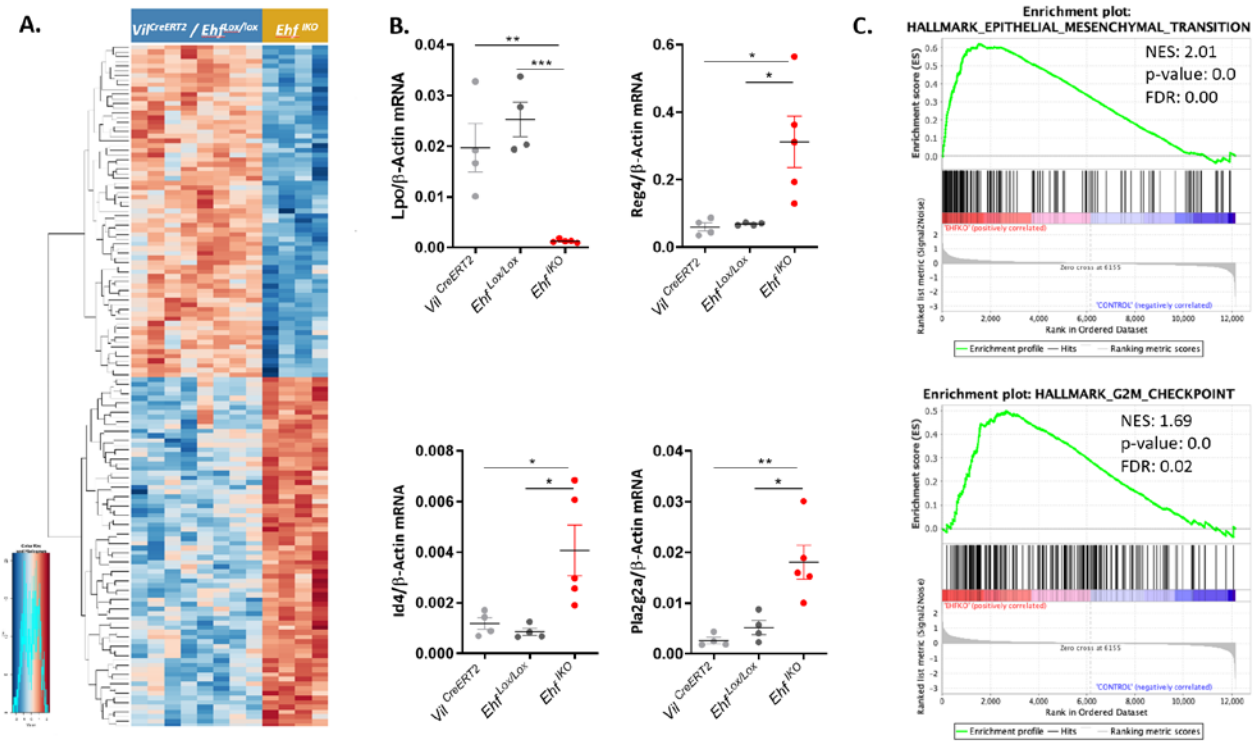

Figure 4.11. *Ehf* deletion induces extensive transcriptional reprogramming of the colonic epithelium. (A) Heatmap of genes differentially expressed between *Ehf* ^{IKO} and both *Ehf* $^{Lox/Lox}$ and *Villin* $^{CreERT2-TMX}$ mice. List of gene names is provided in Appendix D. (B) q-PCR validation of selected differentially expressed genes. Values shown are mean ± SEM from n= 4 *Villin* $^{CreERT2-TMX}$, n=4 *Ehf* ^{WT} and n=5 *Ehf* ^{IKO} mice. (**C**) Gene set enrichment plots showing significant enrichment of the epithelial to mesenchymal transition (146 genes) and G2M checkpoint (192 genes) hallmarks in *Ehf* ^{IKO} mice. NES, normalized enrichment score; FDR, False discovery rate q-value.

Additional gene expression changes: Finally, more detailed, manual examination of the genes differentially expressed between *Ehf* ^{WT} and *Ehf* ^{IKO} mice, revealed a number of other interesting genes which were altered in expression in *Ehf* ^{IKO} mice, although some of these did not satisfy the stringent cut-off criteria of statistical significance. Notable among these were reduced expression

in *Ehf* ^{IKO} mice of two genes involved in cholesterol efflux, Abcg5 and Abcg8. Importantly, qPCR analyses confirmed the significant downregulation of these genes in *Ehf* ^{IKO} mice (Figure 4.12).

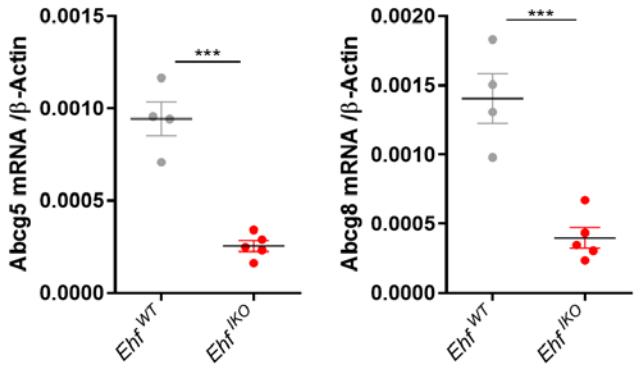

Figure 4.12. Gene expression of Abcg5 and Abcg8 involved in cholesterol efflux in isolated colonic epithelial cells from *Ehf* ^{WT} and *Ehf* ^{IKO} mice at 6 weeks of age. Values shown are mean ± SEM from n= 4 *Ehf* wildtype and n=5 *Ehf* knockout mice.

4.2.6 Intestinal deletion of *Ehf* does not adversely affect animals fed a high cholesterol diet

While the findings described above revealed that *Ehf* deletion in mice causes significant transcriptional changes in the colonic epithelium, increases epithelial cell proliferation, and decreases goblet cell differentiation, these alterations did not ostensibly impact animal health under normal homeostatic conditions. We therefore next sought to determine how *Ehf* deletion impacts on the response of mice to specific intestinal challenges.

First, as our gene expression profiling data revealed a decrease in expression of the cholesterol transport genes Abcg5 and Abcg8 in *Ehf* ^{IKO} mice, we examined the impact of *Ehf* deletion on the ability of these mice gain weight and thrive when fed a high cholesterol diet.

To test this, 8-week-old *Ehf* ^{WT} and *Ehf* ^{IKO} mice (n=8) were fed a high fat / high cholesterol (16% fat, 1% cholesterol) diet for 78 days. During the experimental period, the mice were monitored and weighed daily, and daily food intake calculated. No difference was observed in body weight or food intake between the *Ehf* ^{WT} and *Ehf* ^{IKO} mice fed this diet over the course of the experimental period (Figure 4.13A). At the end of the experimental period, mice were culled and the intestinal lengths measured, and the livers weighed. Consistent with the body weight data, there was no difference in intestinal length or liver weight between *Ehf* wildtype and *Ehf* knockout mice (Figure 4.13B). Collectively, these data indicate that intestinal-specific *Ehf* deletion does not adversely affect the capacity of mice to tolerate a high cholesterol diet.

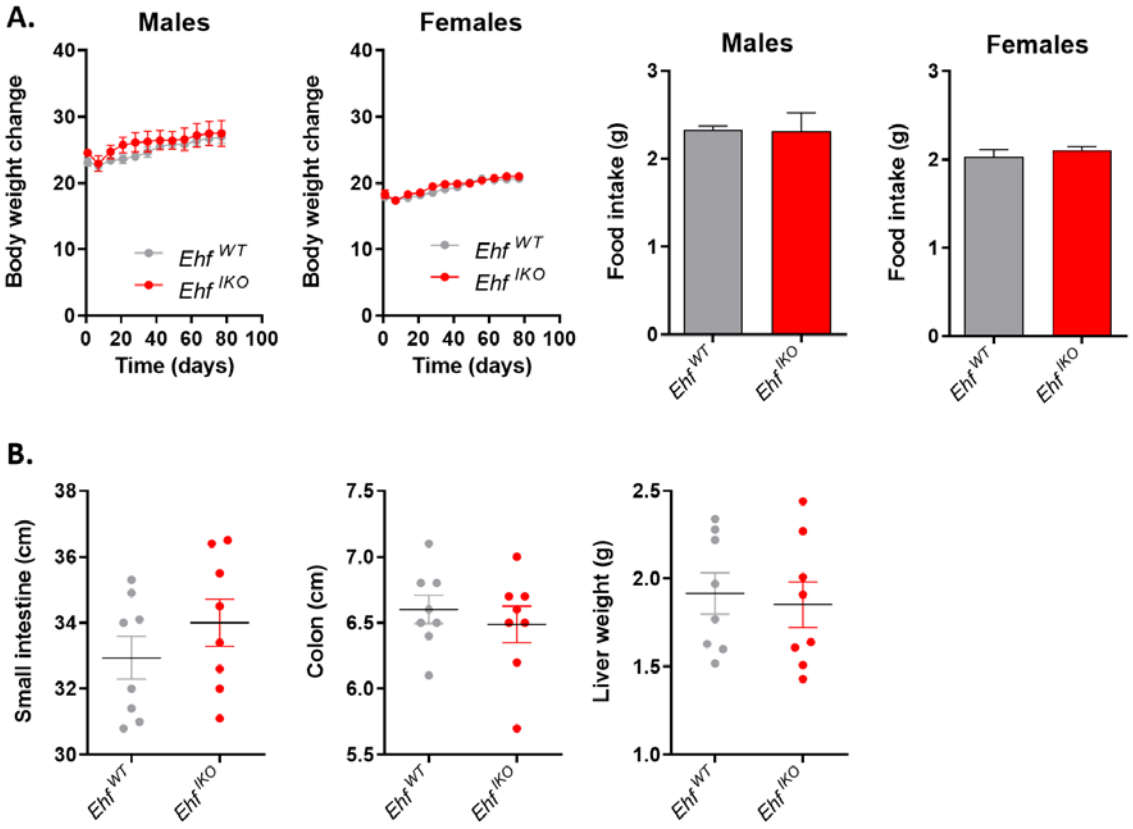

Figure 4.13. Effect of intestinal-specific *Ehf* deletion on overall health of mice fed a high cholesterol diet. (A) Body weight and average food intake of male and female *Ehf* ^{WT} and *Ehf* ^{IKO} mice monitored for 78 days. Values shown are mean ± SEM from n= 8 *Ehf* ^{WT} and *Ehf* ^{IKO} mice. (B) Length of small intestine and colon and liver weight of *Ehf* ^{WT} and *Ehf* ^{IKO} mice at the end of the experimental period. Values shown are mean ± SEM from n= 8 *Ehf* ^{WT} and *Ehf* ^{IKO} mice.

4.2.7 *Ehf* deletion does not impact response of the colonic epithelium to irradiation-induced DNA damage

Next, we compared the response of the colonic epithelium of *Ehf* ^{WT} and *Ehf* ^{IKO} mice to irradiation induced double-stranded DNA damage and epithelial regeneration.

To determine this, we subjected 8-week-old *Ehf* ^{WT} and *Ehf* ^{IKO} mice to a sub-lethal dose of γ-irradiation (8Gy). Mice were then culled at 2, 24, 72 and 120 hours post irradiation which has previously been shown to correspond to the time points at which DNA damage, apoptosis, epithelial cell loss and regeneration are maximal following irradiation [243].

Mice were monitored and weighed daily during the experimental period, and colonic tissue was collected for histological analyses at each time point. Following irradiation, both *Ehf* ^{WT} and *Ehf* ^{IKO} mice lost weight rapidly (Figure 4.14A), then as expected, began to re-gain weight at day five post irradiation. No difference in the rate of weight loss or recovery was observed between *Ehf* ^{WT} and

Ehf ^{IKO} mice. The length of colonic crypts and the number of epithelial cells per crypt at each timepoint were then quantified to assess the extent of irradiation-induced damage and epithelial regeneration in the two groups (Figure 4.14B,C). As expected, irradiation caused a significant reduction in colonic crypt length and the number of epithelial cells per crypt at 2, 24 and 72 hours post irradiation consistent with the induction of DNA damage, apoptosis and epithelial cell loss. Subsequently, colon crypt length and the number of epithelial cells per crypt returned to baseline levels after 120 hours, consistent with the completion of epithelial regeneration. However, no differences in either colon crypt length or the number of epithelial cells per crypt were observed between *Ehf* ^{WT} and *Ehf* ^{IKO} mice at any of the timepoints examined.

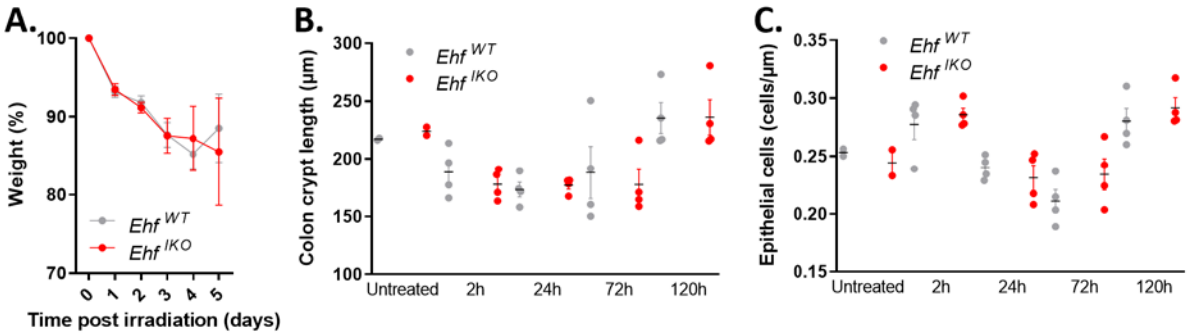

Figure 4.14. Effect of sub-lethal γ-irradiation (8Gy) on colonic epithelial cell damage and regeneration in 8-week-old *Ehf* ^{WT} and *Ehf* ^{IKO} mice. Colonic tissue was collected at 2, 24, 72 and 120 hours post irradiation to assess the impact of *Ehf* deletion on irradiation-induced DNA damage and epithelial regeneration. (A) Change in body weight of mice post irradiation. (B) Length of colonic crypts at all timepoints post irradiation. (C) Number of epithelial cells per micrometre crypt at all timepoints post irradiation. Values shown are mean ± SEM from n= 4 *Ehf* wildtype and *Ehf* knockout mice.

Next, to determine the extent of double-stranded DNA breaks induced by irradiation, colonic tissue from *Ehf* ^{WT} and *Ehf* ^{IKO} mice was stained with an anti-γH2AX antibody. While minimum staining was observed in non-irradiated control mice, at 2 hours post irradiation approximately 90% of epithelial cells stained positive for γH2AX in both *Ehf* ^{WT} and *Ehf* ^{IKO} mice. The number of γH2AX positive cells gradually decreased at subsequent timepoints, returning to baseline values after five days. However, no difference in the number γH2AX positive cells was observed between *Ehf* ^{WT} and *Ehf* ^{IKO} cells at any of the timepoints (Figure 4.15). Collectively, these results demonstrate that *Ehf* deletion does not impact on the extent of irradiation-induced DNA damage or epithelial regeneration.

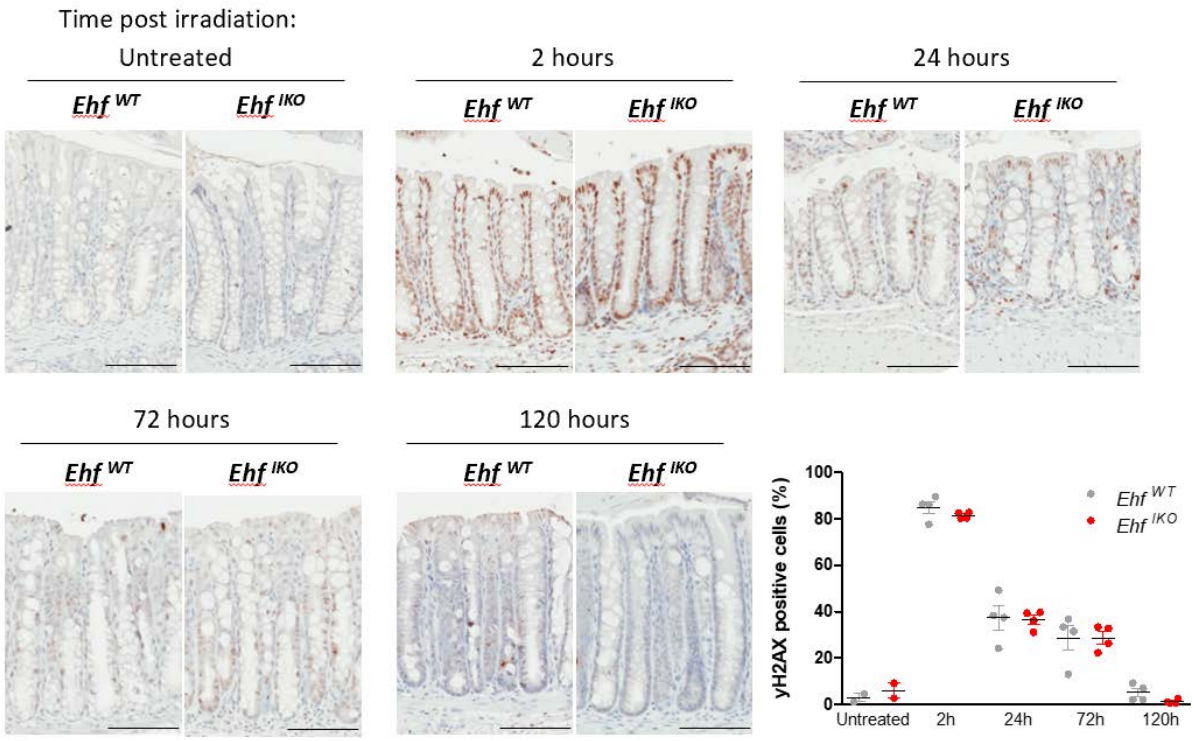

Figure 4.15. Extent of double-stranded DNA breaks following sub-lethal γ-irradiation (8Gy) of 8-week-old *Ehf* ^{WT} and *Ehf* ^{IKO} mice. Colonic tissue was collected at 2, 24, 72 and 120 hours post irradiation and stained with α-γH2AX, and the stain subsequently quantified. Values shown in the final panel are mean ± SEM from n= 4 *Ehf* wildtype and *Ehf* knockout mice.

4.3 Discussion

The EHF transcription factor is highly expressed in the colonic epithelium [4, 8], however its functional role in this tissue has not been extensively studied. To address this, we conditionally deleted *Ehf* in the intestinal epithelium by crossing *Ehf* $^{Lox/Lox}$ mice with *Villin* ^{CreERT2} deleter mice which revealed an essential role for EHF in the maintenance of intestinal epithelial cell homeostasis.

Specifically, *Ehf* deletion significantly increased colonic epithelial cell proliferation evidenced by increased Ki67 staining. Consistent with this finding, gene-expression profiling of colonic epithelial cells isolated from *Ehf* ^{WT} and *Ehf* ^{IKO} mice revealed a significant enrichment of G2/M checkpoint genes in *Ehf* ^{IKO} mice. Transcriptional profiling of these cells also revealed 4-fold increase in Reg4 expression in *Ehf* ^{IKO} mice. Reg4 is a marker of deep crypt secretory cells which contribute to the maintenance of the colonic stem cell niche [66], similar to the function of Paneth cells in the small intestine. High *Reg4* mRNA expression is associated with higher proliferation in colon cancer cells [244, 245] and is a predictor of poor prognosis in colorectal cancer patients [246]. Whether EHF impacts cell proliferation by directly regulating expression of cell cycle genes, or indirectly by altering the stem cell niche, or through other mechanisms, remains to be fully dissected.

Ehf deletion also significantly decreased goblet cell differentiation, evidenced by reduced PAS/AB staining. Notably, the gene expression profiling data revealed a significant reduction in Spdef and Creb3l1 expression in *Ehf* ^{IKO} mice. In addition to its expression in deep crypt secretory cells, Spdef is also important in maintaining the goblet cell lineage, as is Creb3l1, [50, 51] and may provide a possible mechanistic explanation for the reduction in goblet cell differentiation in these mice.

During the course of our studies, Zhu et al. reported that *Ehf* is a downstream target of the lncRNA lncGata6 (Zhu et al., 2018), and generated a mouse with whole-body deletion of *Ehf* using CRISPR-Cas9-mediated genome editing. They reported that EHF was required for the maintenance of small intestinal stem cells by driving expression of Lgr4 and Lgr5, and that *Ehf* deletion significantly decreased OLFM4-positive stem cells and reduced the number of all secretory cell lineages in the small intestine (Paneth, tuft, enteroendocrine and goblet cells). Although the focus of our study was the colonic epithelium where EHF is most highly expressed, examination of OLFM4-positive stem cells in the small intestine revealed no difference between *Ehf* $^{+/+}$ and *Ehf* $^{-/-}$ mice. One explanation for these discrepant findings may be that the *Ehf* knockout mice generated by Zhu et al. completely lacked all functional parts of the *Ehf* gene, as transcription was prematurely terminated in exon 2, whereas only the ETS DNA-binding domain was deleted in our model.

Interestingly, we observed a significant enrichment of the EMT gene signature in *Ehf* ^{IKO} mice, however we did not observe any increased susceptibility of *Ehf* ^{IKO} mice to spontaneously develop

intestinal tumours. Similarly, we did not observe increased epithelial cell mobility along the colonic crypt axis, a feature that we have observed following *EHF* deletion in colorectal cancer cells (submitted - unpublished), and has previously been reported to occur following *EHF* knockdown in pancreatic and prostate cancer cell lines [30, 36]. These findings suggest that EHF may have different effects in tumour cells, which have undergone additional genetic and epigenetic alterations. The impact of *Ehf* deletion during *Apc*-initiated tumour formation and growth will be examined in Chapter 5.

Given the relatively modest intestinal phenotype of *Ehf* deletion alone, we next subjected the mice to a series of challenges, focussing on the gene expression changes observed in the colonic epithelial cells of *Ehf* knockout mice. First, we examined the impact of reduced expression of the cholesterol transport genes Abcg5 and Abcg8 in the ability of these mice to gain weight and thrive when fed a diet high in cholesterol. These genes are required for efflux of excess diet-derived sterols (cholesterol) back into the gut lumen [247]. Contrary to our expectations, *Ehf* deletion did not impact weight gain in *Ehf* ^{IKO} mice fed this died. This implies that the downregulation of these genes is insufficient to impact body weight, or that the mice may be able to compensate for the loss of these genes by upregulating alternate pathways, which may be revealed by additional studies.

Finally, we challenged the intestinal epithelium of *Ehf* ^{WT} and *Ehf* ^{IKO} mice by subjecting the mice to whole-body γ-irradiation. Given that *Ehf* $^{-/-}$ mice have increased colonic epithelial cell proliferation compared to *Ehf* $^{+/+}$ mice we hypothesised that this may accelerate epithelial regeneration after exposure to damage. Furthermore, one of the most up-regulated gene in *Ehf* ^{IKO} mice compared to *Ehf* ^{WT} was *Reg4*. High expression of *Reg4* has been associated with resistance to radiotherapy in rectal cancer patients, by preventing the formation of double-stranded DNA breaks [248, 249]. However, contrary to our predictions, *Ehf* deletion did not impact on the response of the colonic epithelium to irradiation-induced DNA damage and epithelial regeneration following irradiation-induced apoptosis.

In summary, we have demonstrated that *Ehf* deletion increases colonic epithelial cell proliferation, decreases goblet cell differentiation and causes significant transcriptional changes in the colonic epithelium. However, this does not translate into any body weight or lifespan differences in mice. Furthermore, *Ehf* deletion does not impact on the response to the intestinal-specific challenges of a high fat/high cholesterol diet or to γ-irradiation.

Chapter 5: Impact of *Ehf* deletion on intestinal disease

5.1 Introduction

The first two chapters of this thesis focussed on defining a role of EHF in the maintenance of normal homeostasis of multiple epithelial tissues, in particular the colonic epithelium where Ehf is highly expressed [4, 8]. In this final chapter, we will turn our attention to the role of EHF in colitis and colonic tumorigenesis.

While the role of EHF in the progression of several tumour types has been relatively well studied in cultured cell lines, its role in colitis and colon tumour progression *in vivo* has not been previously investigated. The objective of this chapter was therefore to investigate the role of EHF in colonic disease using a mouse model of inflammatory bowel disease (IBD) and a mouse model of *Apc*-initiated colorectal tumorigenesis (CRC).

IBD is characterised by sustained inflammation of the intestine [118]. There are many factors that contribute to IBD, including genetic alterations [119], microbiota composition [122], weakening of tight junctions [123] and a reduction of the mucus layer [125]. To determine the role of EHF in this context we will study the impact of *Ehf* deletion in the intestine on DSS-induced acute colitis. DSS disrupts epithelial barrier integrity which increases colonic mucosal permeability causing inflammation. It is the most commonly used model of IBD and has been used to study a variety of factors which impact on the severity of IBD including pathogens, genetic predisposition, immune mechanisms and the role of the microbiota [250]. Furthermore, therapies used to treat human IBD have been found to be efficacious in the DSS mouse model, further demonstrating the relevance of this model for the translation of discoveries to human disease [251].

Colorectal cancer is a heterogenous disease and arises from genomic instability and/or epigenetic alterations. The *APC* gene is mutated in about 80-85% of sporadic CRCs [164] and is the event in the initiation of colorectal neoplasia [179]. Many mouse models of *Apc* loss have been generated in the past few decades [180-184], but without additional genetic modification *Apc*-initiated tumours rarely progress to invasive adenocarcinoma [185]. Unpublished data from our lab indicate that knockdown of *EHF* in well-differentiated colorectal cancer cell lines increase migration and invasion, while *EHF* re-expression in poorly differentiated colorectal cancer cell lines decrease migration and invasion (submitted – unpublished). Furthermore, EHF was found to co-operatively regulate differentiation of colorectal tumours with another transcription factor CDX1, and that combinatorial loss of these factors contributes to more aggressive disease.

To study the role of EHF in colorectal tumour formation we use a mouse model where exon 14 of the *Apc* gene is flanked by loxP sites (denoted *Apc* $^{580S/580S}$ in literature) [183]. We used this model in two contexts; (1) by deleting both alleles of Apc, which causes the rapid onset of colonic tumours and (2) by deleting one allele of Apc and allowing the second hit to spontaneously occur. To induce *Apc* deletion specifically in the colorectal epithelium we will cross these mice to *Cdx2* ^{CreERT2} deleter mice, which express Cre recombinase specifically in the colonic epithelium under the control of the Cdx2 promoter. Approximately 90% of the colorectal tumours which arise in these mice present as well-differentiated, epithelial-rich adenomas with tubular-type glands, however they rarely progress to carcinomas [235]. These mice will subsequently be crossed to *Ehf* floxed mice, in order to also delete *Ehf* specifically in the colon.

Based on our findings in the previous chapter that deletion of *Ehf* causes a loss of goblet cell differentiation, we hypothesised that *Ehf* knockout mice will be more sensitive to DSS-induced colitis. We also hypothesised that the increased rate of cell proliferation in the colon, and the impaired colonic differentiation observed in *Ehf* knockout mice, will make them more prone to colonic tumour formation.

5.2 Results

5.2.1 The impact of *Ehf* deletion on response to DSS-induced colitis.

To investigate the role of EHF in protection against inflammatory bowel disease (IBD), we studied the impact of *Ehf* deletion on disease severity to dextran sodium sulphate (DSS) induced acute colitis, a model used to assess the integrity of the intestinal epithelial barrier function and the role of the innate immune system in responding to this challenge. For this purpose, we provided *Ehf* $^{+/+}$ and *Ehf* $^{-/-}$ mice (n=8) with 2.5% dextran sodium sulphate (DSS) in the drinking water, *ad libitum* for five days. *Ehf* $^{+/+}$ and *Ehf* $^{-/-}$ mice given normal drinking water were used as controls. The mice were monitored daily, and disease severity scored according to a set of criteria that included general appearance, weight loss, stool consistency and presence of blood in the stool (Chapter 2.5 DSS-induced colitis, Table 2.3). To ensure that the observed response of these mice to DSS-induced acute colitis was due to genetic deletion of *Ehf* specifically in the colonic epithelium, we also repeated the study using the conditional mouse model of *Ehf* deletion described in Chapter 4 (*Ehf* ^{WT} and *Ehf* ^{IKO} mice).

5.2.1.1 Response of Ehf $^{+/+}$ and Ehf $^{-/-}$ mice to DSS-induced acute colitis.

Following DSS treatment, weight loss was significantly more pronounced in *Ehf* $^{-/-}$ compared with *Ehf* $^{+/+}$ mice over the 5-day treatment period (Figure 5.1A). Furthermore, the disease severity score was 2.5-fold higher in *Ehf* $^{-/-}$ compared with *Ehf* $^{+/+}$ mice, due to *Ehf* $^{-/-}$ mice experiencing a higher degree of weight loss, more frequent diarrhoea and appearance of blood in stool (Figure 5.1B). In addition, 25% of *Ehf* $^{-/-}$ mice displayed hunching behaviour, indicative of discomfort and/or pain at the end of the experimental period, whereas all *Ehf* $^{+/+}$ mice displayed normal behaviour.

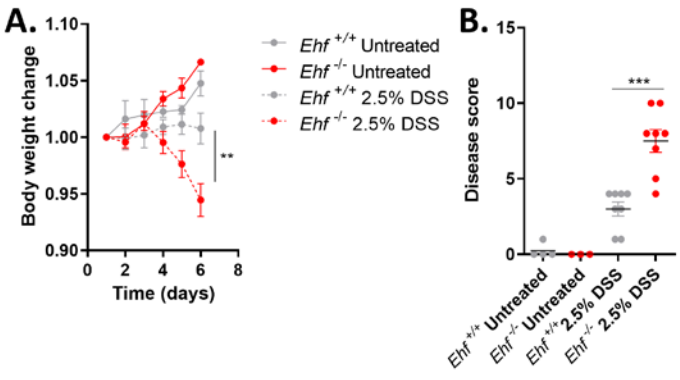

Figure 5.1. Assessment of body weight and disease severity of 8-week-old *Ehf* $^{+/+}$ and *Ehf* $^{-/-}$ mice subjected to DSS-induced acute colitis. (A) Body weight change. (B) Disease severity score at day 5. Values shown are mean ± SEM of n=4 mice per control group and n=8 mice per experimental group.

Consistent with these changes, the length of the colon was also significantly shortened in DSS-treated *Ehf* $^{-/-}$ mice compared to controls (Figure 5.2A). However, there was no difference in colon weights, spleen weights or total blood volume which was assessed by cardiac puncture at cull (Figure 5.2B-D).

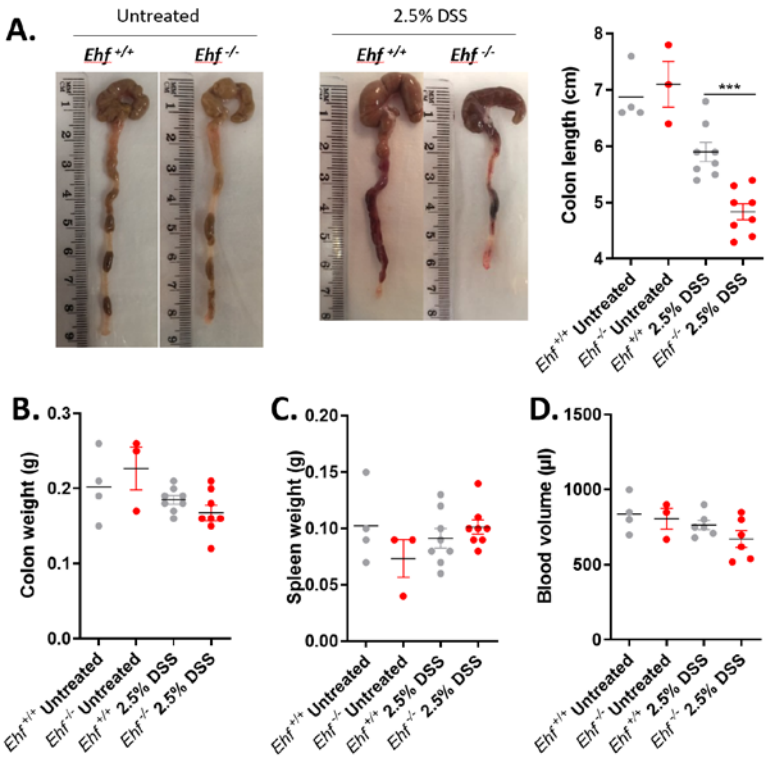

Figure 5.2. Physical readouts of DSS-induced acute colitis severity in 8-week-old *Ehf* $^{+/+}$ and *Ehf* $^{-/-}$ mice at cull. (A) Representative images and measurements of colon lengths at cull. (B) Colon weights, (C) spleen weights and (D) blood volume at cull. Values shown are mean ± SEM of n=4 mice per control group and n=8 mice per experimental group.

Next, histological analysis of the colonic epithelium of these mice was performed which revealed that *Ehf* deletion increased the extent and depth of immune cell infiltration, increased the area of crypt loss and ulceration, and led to more widespread oedema (Figure 5.3A-I). Collectively, these results suggest that *Ehf* deletion increases the extent and severity of DSS-induced acute colitis.

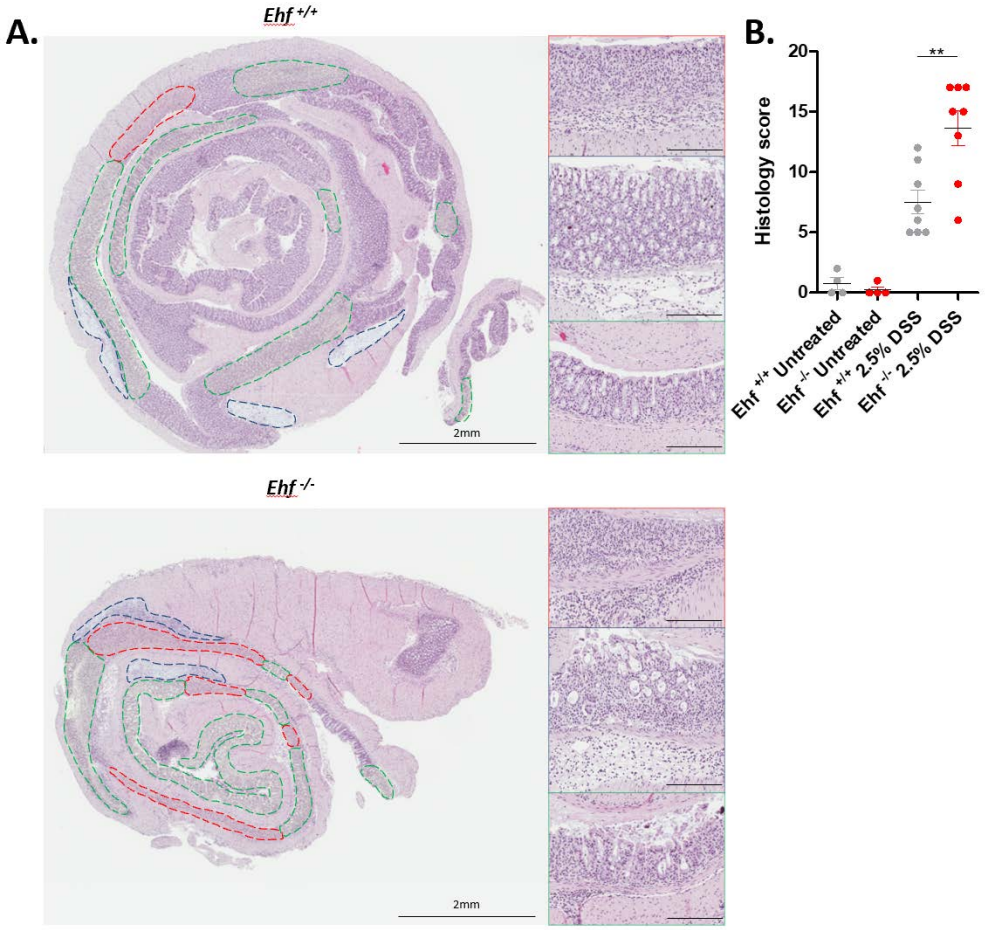

Figure 5.3. Histological impact of DSS-induced acute colitis in 8-week-old *Ehf* $^{+/+}$ and *Ehf* $^{-/-}$ mice. (A,E) Representative Haematoxylin and Eosin stained sections of the entire colon from *Ehf* $^{+/+}$ and *Ehf* $^{-/-}$ mice treated with 2.5% DSS for 5 days. Regions of ulceration are highlighted by a red border, areas of oedema with a blue border, and areas of epithelial erosion and/or crypt loss with a green border. (B-D,F-H) High-power fields of regions of (B,F) ulceration, (C,G) oedema, and (D,H) epithelial erosion and/or crypt loss. Scale bars: 200 µm. (I) Summary of the histology scores from *Ehf* $^{+/+}$ and *Ehf* $^{-/-}$ mice treated with or without 2.5% DSS. Values shown are mean ± SEM of n=4 mice per control group and n=8 mice per experimental group.

Finally, to determine what factors may have contributed to the observed increased severity of DSS-induced acute colitis in the *Ehf* $^{-/-}$ mice, we collected a piece of the whole colon for gene expression analyses of cytokine and chemokine constituents by q-RT-PCR. Consistent with the increased disease severity of *Ehf* $^{-/-}$ mice, the gene expression analyses revealed increased expression of the pro-inflammatory cytokines Il-6, Il-17, Il-33 and Tnf, and increased expression of the chemokine Cxcl in the colon of *Ehf* $^{-/-}$ mice compared to *Ehf* $^{+/+}$ mice (Figure 5.4A-E). However, the difference in gene expression between these mice was only significant for Il-17 and Cxcl.

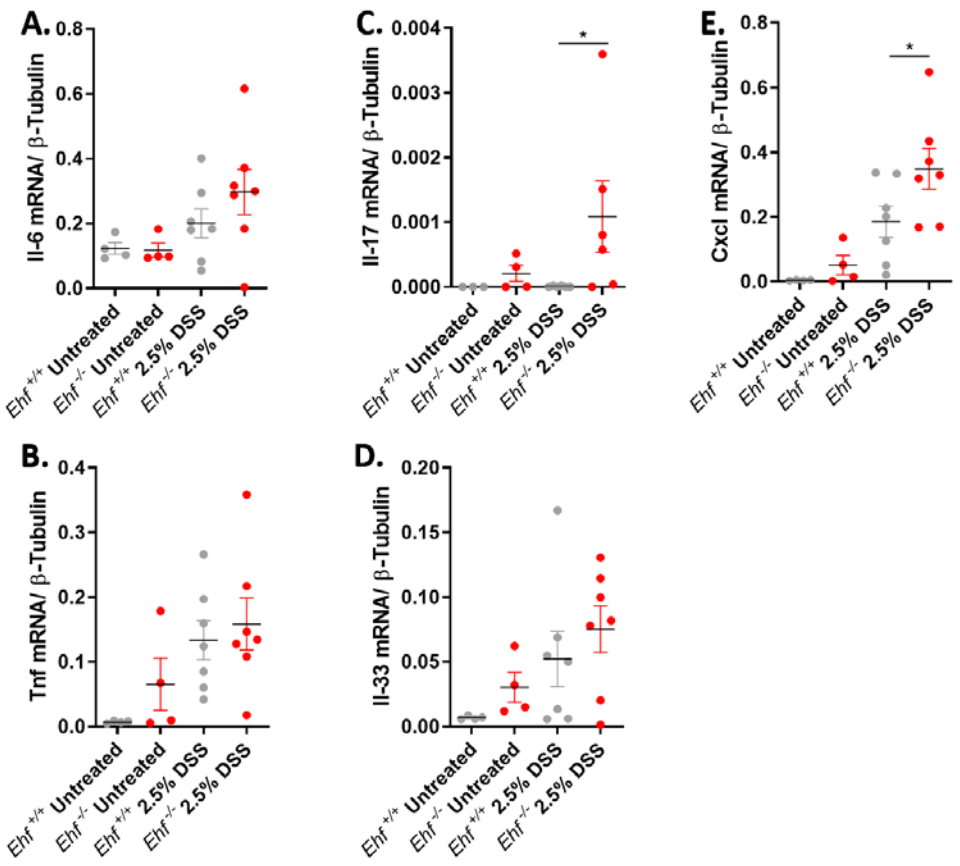

Figure 5.4. Changes in mRNA expression of immune gene markers following DSS-induced acute colitis of 8-week-old *Ehf* $^{+/+}$ and *Ehf* $^{-/-}$ mice. (A-D) Gene expression of the pro-inflammatory cytokines Il-6, Il-17, Tnf and Il-33; and (E) gene expression of the chemokine Cxcl. Values shown are mean ± SEM of n=4 mice per control group and n=8 mice per experimental group.

5.2.1.2 Response of Ehf ^{WT} *and Ehf* ^{IKO} *mice to DSS-induced acute colitis.*

To confirm that the increased sensitivity of whole body *Ehf* deleted mice to colitis was due to alterations in the colonic epithelium, we next assessed the susceptibility of *Ehf* ^{IKO} mice to DSS-induced acute colitis. As observed in whole-body *Ehf* $^{-/-}$ mice, the onset of acute colitis was markedly more severe in *Ehf* ^{IKO} mice compared with *Ehf* ^{WT} mice as assessed by the disease severity score (Figure 5.5B). Although the difference in body weight change in both DSS treated *Ehf* ^{WT} and *Ehf* ^{IKO} was minimal (Figure 5.5A), the *Ehf* ^{IKO} mice were more prone to the development of diarrhoea. Furthermore, the colon length of DSS-treated *Ehf* ^{IKO} mice was shorter compared to *Ehf* ^{WT} mice, however this was not statistically significant (Figure 5.5C).

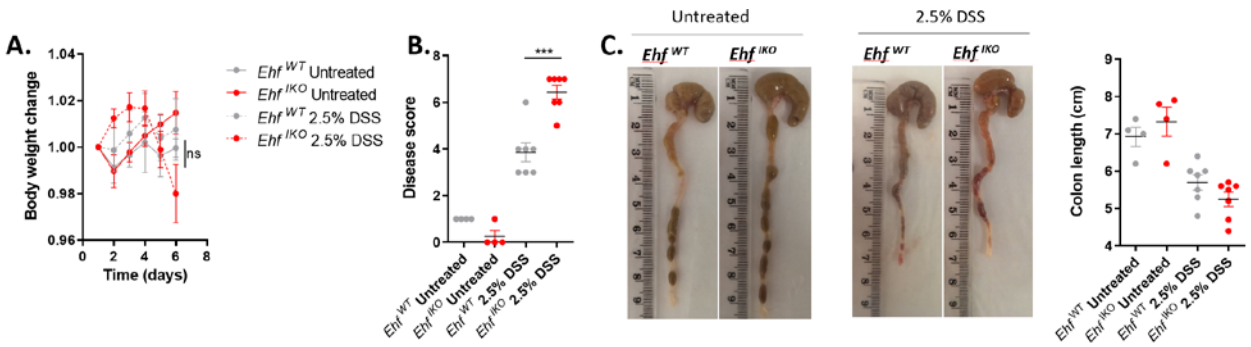

Figure 5.5. Sensitivity of 8-week-old *Ehf* ^{WT} and *Ehf* ^{IKO} mice to DSS-induced acute colitis. (A) Body weight; (B) Disease severity score at day 5; and (C) representative images and measurements of colon lengths at cull. Values shown are mean ± SEM of n=4 mice per control group and n=7 mice per experimental group.

As with the *Ehf* $^{-/-}$ mice, we also assessed the colonic histology of *Ehf* ^{WT} and *Ehf* ^{IKO} mice. Consistent with the result of the *Ehf* $^{-/-}$ mice, we observed that intestinal-specific *Ehf* deletion increased the extent and depth of immune cell infiltration, increased the area of crypt loss and ulceration, and led to more widespread oedema (Figure 5.6A-I).

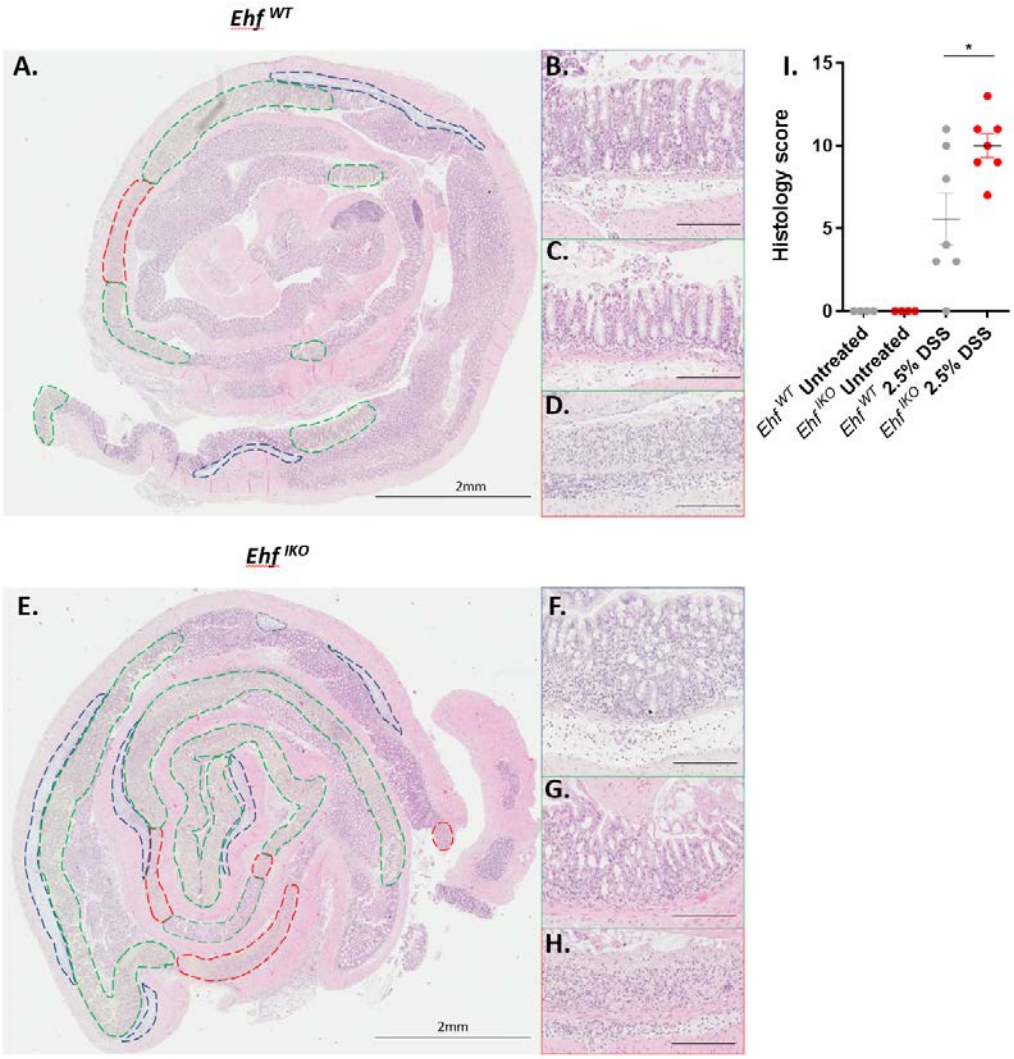

Figure 5.6. Histopathological assessment of the response of 8-week-old *Ehf* ^{WT} and *Ehf* ^{IKO} mice to DSS-induced acute colitis. (A,E) Representative Haematoxylin and Eosin stained sections of the entire colon from *Ehf* ^{WT} and *Ehf* ^{IKO} mice treated with 2.5% DSS for 5 days. Regions of ulceration are highlighted by a red border, areas of oedema with a blue border, and areas of epithelial erosion and/or crypt loss with a green border. (B-D,F-H) High-power fields of regions of (B,F) ulceration, (C,G) oedema, and (D,H) epithelial erosion and/or crypt loss. Scale bars: 200 µm. (I) Summary of the histology scores from *Ehf* ^{WT} and *Ehf* ^{IKO} mice treated with or without 2.5% DSS for 5 days. Values shown are mean ± SEM of n=4 mice per control group and n=7 mice per experimental group.

Finally, we analysed a piece of whole colon from *Ehf* ^{WT} and *Ehf* ^{IKO} mice for gene expression of the pro-inflammatory cytokines Il-6, Il-17, Il-33 and Tnf, and the chemokine Cxcl by q-RT-PCR. Similar to that observed in the colon of DSS-treated *Ehf* $^{-/-}$ mice, intestinal-specific deletion of *Ehf* significantly increased mRNA expression of the proinflammatory cytokines Il-6, Il-33 and Tnf, and

increased expression of the chemokine Cxcl (Figure 5.7A-E). Collectively, these results confirm that EHF-mediated disruption of colonic homeostasis in a mouse model of IBD is at least partly epithelial driven.

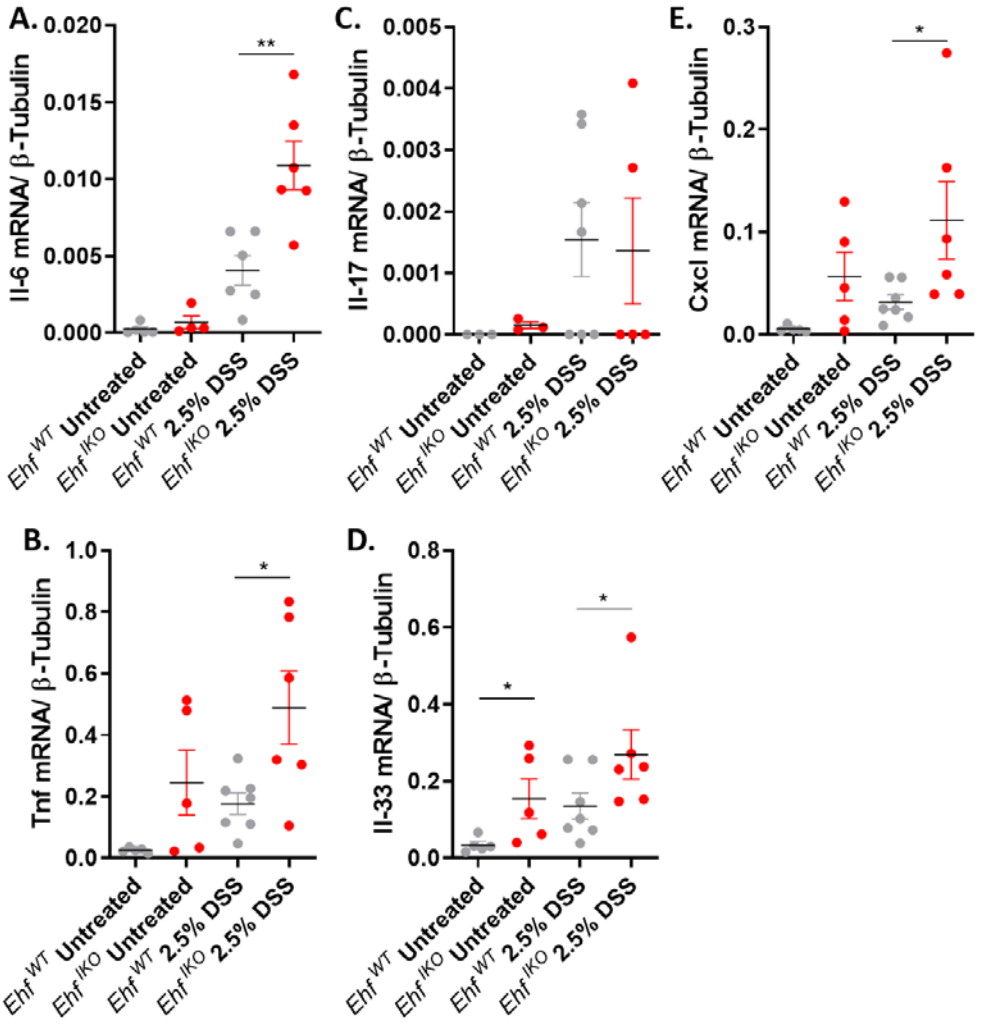

Figure 5.7. Changes in mRNA expression of immune gene markers following DSS-induced acute colitis in 8-week-old *Ehf* ^{WT} and *Ehf* ^{IKO} mice. (A-D) Gene expression of the pro-inflammatory cytokines Il-6, Il-17, Tnf and Il-33; and (E) of the chemokine Cxcl. Values shown are mean ± SEM of n=4 mice per control group and n=7 mice per experimental group.

5.2.2 The impact of colon-specific *Ehf* deletion in a rapid model of colorectal tumorigenesis initiated by bi-allelic loss of *Apc*

Next, to determine the role of EHF in colorectal tumourigenesis in mice, we examined the impact of *Ehf* deletion specifically in the colon on *Apc*-initiated tumour development. To achieve this, *Ehf* $^{Lox/Lox}$ mice were crossed to *Cdx2* ^{CreERT2} deleter mice (*Ehf* ^{CKO}), and in turn to *Apc* $^{Lox/Lox}$ mice. These

mice were treated with a low dose of tamoxifen to induce mosaic compound homozygous deletion of *Apc* (*Apc* ^{CKO}) and *Ehf* in the epithelium of the colon and caecum. *Ehf* ^{CKO};*Apc* ^{CKO} and *Ehf* ^{WT};*Apc* ^{CKO} controls were subsequently monitored for colon tumour development for 27 days post tamoxifen.

At the end of the 27 day experimental period, *Ehf* ^{WT};*Apc* ^{CKO} and *Ehf* ^{CKO};*Apc* ^{CKO} mice were culled, tumours counted and their sizes measured. As expected, all mice developed adenomas mainly in the colon and caecum, however only colonic adenomas were counted as this is where *Ehf* is most highly expressed (Figure 5.8A). No difference in the number, sizes or size distribution of adenomas was observed between *Ehf* ^{WT};*Apc* ^{CKO} and *Ehf* ^{CKO};*Apc* ^{CKO} mice (Figure 5.8B-D).

Surprisingly, 25% (2/8) *Ehf* ^{WT};*Apc* ^{CKO} mice and 75% (9/12) *Ehf* ^{CKO};*Apc* ^{CKO} mice developed small intestinal adenomas, primarily located in the duodenum. Interestingly, these adenomas appeared to coincide with the location of Peyer's patches. Two of the *Ehf* ^{CKO};*Apc* ^{CKO} mice that presented with small intestinal adenomas developed an intestinal intussusception (>2 cm length). This suggest that *Cdx2* ^{CreERT2} is likely expressed in a small subset of cells in the small intestine. While interesting, it was beyond the scope of this thesis to explore this further.

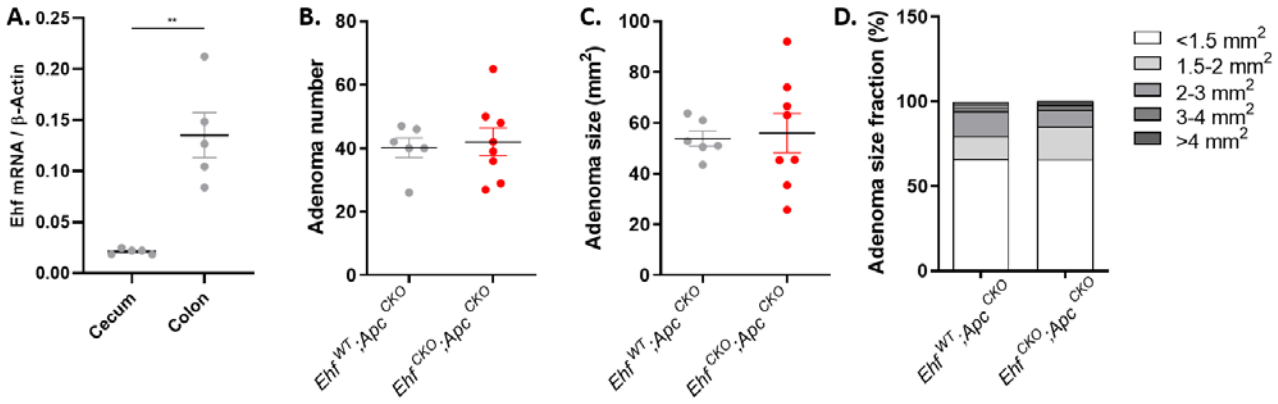

Figure 5.8. Impact of *Ehf* deletion on colonic adenoma formation in a mouse model of rapid *Apc*-initiated colorectal tumourigenesis. (A) Relative expression of Ehf in the colon and caecum in wild-type (*Ehf* $^{+/+}$) mice. Values shown are mean ± SEM or n=5 mice per group. (B) Number of adenomas in the colonic epithelium; (C) average adenoma size; and (D) size distribution of adenomas in the colonic epithelium of *Ehf* ^{WT};Apc ^{CKO} and *Ehf* ^{CKO};Apc ^{CKO} mice 27 days post tamoxifen-induced *Apc* deletion. Values shown are mean ± SEM of n=6 *Ehf* ^{WT};Apc ^{CKO} and n=8 *Ehf* ^{CKO};Apc ^{CKO} mice per group.

Next, because we only induced mosaic gene deletion of *Ehf* and *Apc*, we sought to confirm that the adenomas indeed contained compound *Ehf* and *Apc* deletion. To test this, we collected colonic adenomas (T) and adjacent normal colon (N) from *Ehf* ^{WT};*Apc* ^{CKO} and *Ehf* ^{CKO};*Apc* ^{CKO} mice, and assessed the gene expression levels of Ehf and the Wnt target genes Myc and Lgr5 by q-RT-PCR. Importantly, Ehf expression was reduced in adenomas of *Ehf* ^{CKO};*Apc* ^{CKO} mice demonstrating successful deletion of Ehf in these tumours (Figure 5.9A),. Likewise, expression of Myc and Lgr5 was increased in adenomas of both *Ehf* ^{WT};*Apc* ^{CKO} and *Ehf* ^{CKO};*Apc* ^{CKO} mice (Figure 5.9B,C), consistent with deletion of Apc and activation of the Wnt pathway in these adenomas. Notably, there was no decrease in Ehf expression in the adjacent normal colonic epithelial cells, and expression levels of Myc and Lgr5 were significantly lower compared to the adenomas. These findings suggest that *Ehf* and *Apc* are not deleted in these remaining normal epithelial cells, and that only those cells in which recombination occurred formed an adenoma.

Interestingly, there was no difference in Myc and Lgr5 gene expression levels between *Ehf* ^{WT};*Apc* ^{CKO} and *Ehf* ^{CKO};*Apc* ^{CKO} adenomas indicating that *Ehf* deletion does not further alter expression of the main constituents of the Wnt pathway.

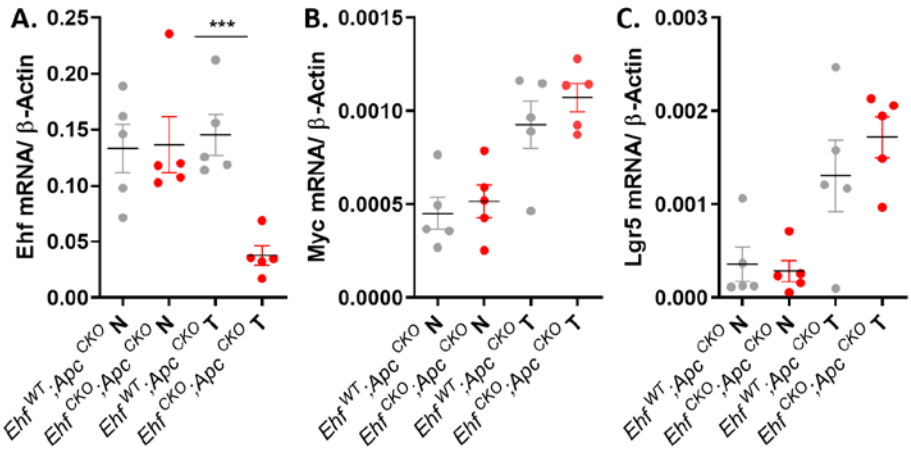

Figure 5.9. Validation of compound *Ehf* and *Apc* deletion in colonic tumours (T) and adjacent normal tissue (N) from *Ehf* ^{WT};*Apc* ^{CKO} and *Ehf* ^{CKO};*Apc* ^{CKO} mice 27 days post tamoxifen induction. Expression levels of the Wnt target genes Myc and Lgr5 were used as an indirect readout of *Apc* deletion. Gene expression of (A) Ehf and (B,C) the Wnt pathway target genes Myc and Lgr5. Values shown are mean ± SEM of n=5 mice per group.

To determine the impact of *Ehf* deletion on differentiation grade of *Apc*-initiated colonic adenomas, we collected colon sections and stained these with haematoxylin and eosin.

Histological analyses revealed no difference in differentiation grade of adenomas from *Ehf* ^{WT};*Apc* ^{CKO} and *Ehf* ^{CKO};*Apc* ^{CKO} mice (Figure 5.10A,B). Adenomas from both cohorts of mice were consistently low grade and well-differentiated, and none had progressed to carcinomas. Further to this, we assessed the gene expression levels of differentiation markers Villin (Vil1) and E-cadherin (Chd1) by q-RT-PCR. Consistent with the histological result, there was no difference in Vil1 and Cdh1 expression in adenomas of *Ehf* ^{WT};*Apc* ^{CKO} and *Ehf* ^{CKO};*Apc* ^{CKO} mice (Figure 5.10C,D). Collectively, this indicates that *Ehf* deletion does not impact on differentiation of *Apc*-initiated adenomas on mice.

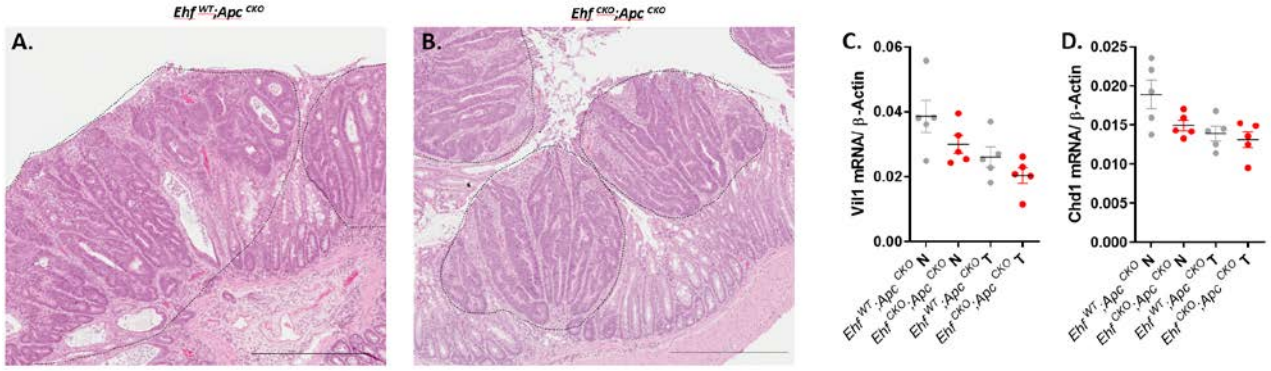

Figure 5.10. Impact of *Ehf* deletion on the differentiation status of *Apc*-initiated colonic tumours . (A,B) Representative haematoxylin and eosin stained images of colonic adenomas from *Ehf* ^{WT};*Apc* ^{CKO} and *Ehf* ^{CKO};*Apc* ^{CKO} mice. Scale bar = 500µm. (B,C) Gene expression levels of the differentiation markers Vil1 and Cdh1 from colonic tumours (T) and adjacent normal colon (N) from *Ehf* ^{WT};*Apc* ^{CKO} and *Ehf* ^{CKO};*Apc* ^{CKO} mice. Values shown are mean ± SEM of n=5 mice per group.

Having established that *Ehf* deletion does not alter the differentiation status of *Apc*-initiated adenomas, we sought to determine the impact of *Ehf* deletion on cell proliferation in these tumours. For this purpose, we measured the expression levels of cell proliferation markers by immunohistochemistry and q-RT-PCR. In contrast to the observed increase in cell proliferation observed in in the normal colonic epithelium of *Ehf* knockout mice, staining of adenomas with the epithelial cell proliferation marker BrdU revealed a modest decrease in proliferation in adenomas derived from *Ehf* ^{CKO};*Apc* ^{CKO} mice compared to adenomas from *Ehf* ^{WT};*Apc* ^{CKO} mice, although this was not statistically significant (Figure 5.11A,B). Furthermore, there was no difference in mRNA expression of the proliferation markers Mki67, Ccnd1 or Pcna in adenomas of *Ehf* ^{WT};*Apc* ^{CKO} and *Ehf* ^{CKO};*Apc* ^{CKO} mice (Figure 5.11C-E). However, as expected, levels of expression of these markers were generally higher in adenomas compared to normal colon. Collectively, these findings indicate that *Ehf* does not impact on the rate of cell proliferation in *Apc*-initiated adenomas.

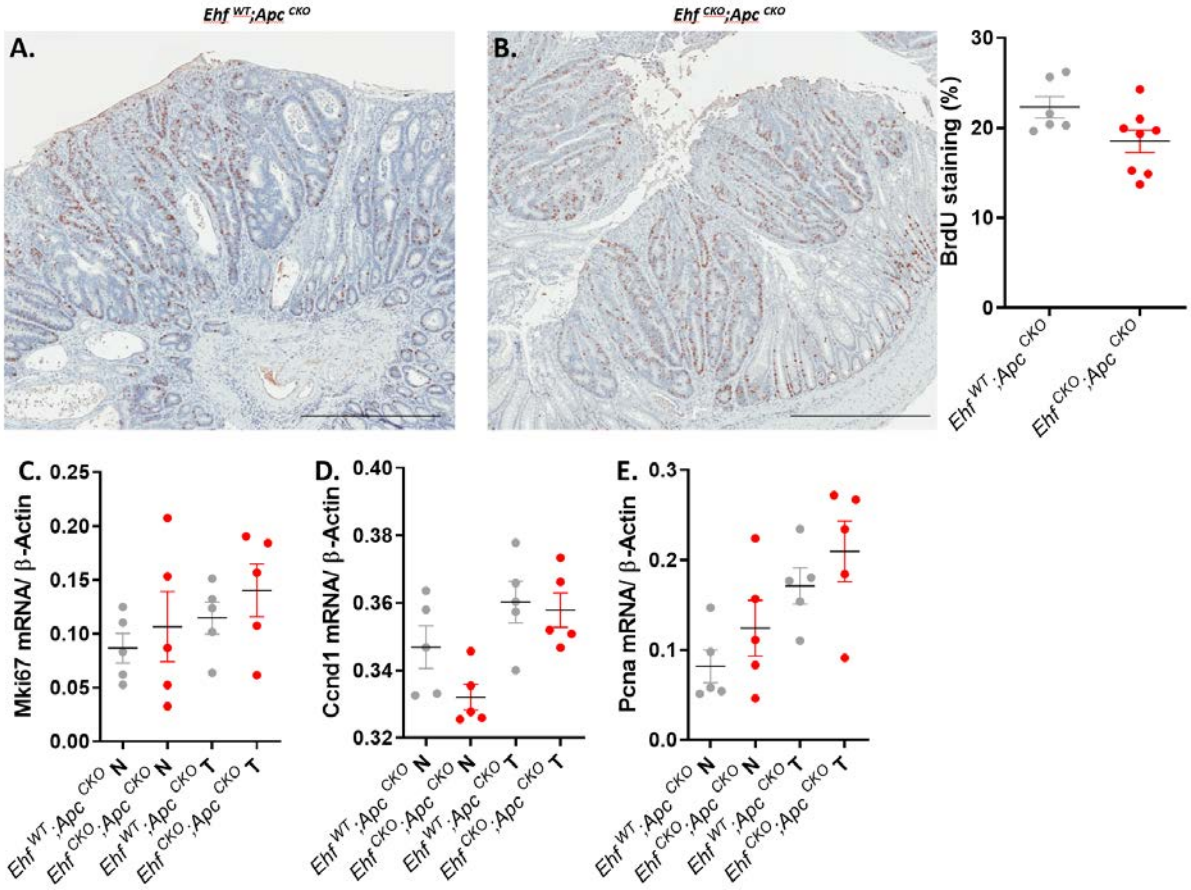

Figure 5.11. Impact of *Ehf* deletion on cell proliferation of colonic adenomas. (A,B) Representative BrdU-stained images of colonic adenomas from *Ehf* ^{WT};*Apc* ^{CKO} and *Ehf* ^{CKO};*Apc* ^{CKO} mice with corresponding quantification of percentage of BrdU-positive cells. Scale bar = 500µm. Values shown are mean ± SEM of n=6 *Ehf* ^{WT};Apc ^{CKO} and n=8 *Ehf* ^{CKO};Apc ^{CKO} mice per group (C-E) Gene expression of proliferation markers (C) Mki67, (D) Ccnd1 and (E) Pcna from colonic adenomas (T) and adjacent normal colon (N) from *Ehf* ^{WT};*Apc* ^{CKO} and *Ehf* ^{CKO};*Apc* ^{CKO} mice. Values shown are mean ± SEM of n=5 mice per group.

The contradictory results in cell proliferation between normal colonic epithelium and colonic adenomas were puzzling. Notably, upon re-examining the histology of the adenomas, we observed a larger stromal compartment containing non-proliferating cells in adenomas from *Ehf* ^{CKO};*Apc* ^{CKO} mice compared to adenomas from *Ehf* ^{WT};*Apc* ^{CKO} mice. To further investigate the amount of stroma in these mice we analysed gene expression levels of the stromal markers Tnc, Fap, Vim, Smad4 and Acta2 in colonic adenomas and adjacent normal colon from *Ehf* ^{WT};*Apc* ^{CKO} and *Ehf* ^{CKO};*Apc* ^{CKO} mice (Figure 5.12A-E). Expression of most of these stromal markers were similar in adenomas from mice of both cohorts, however Vim was significantly higher in *Ehf* ^{CKO};*Apc* ^{CKO} adenomas (Figure 5.12C). Vimentin (Vim) is both a marker of stromal cells as well as of epithelial-

to-mesenchymal transition (EMT). Increased expression of Vimentin may therefore indicate that *Ehf* deletion in *Apc*-initiated colorectal cancer is promoting EMT, however further studies are needed to fully establish a connection between *Ehf* deletion and EMT.

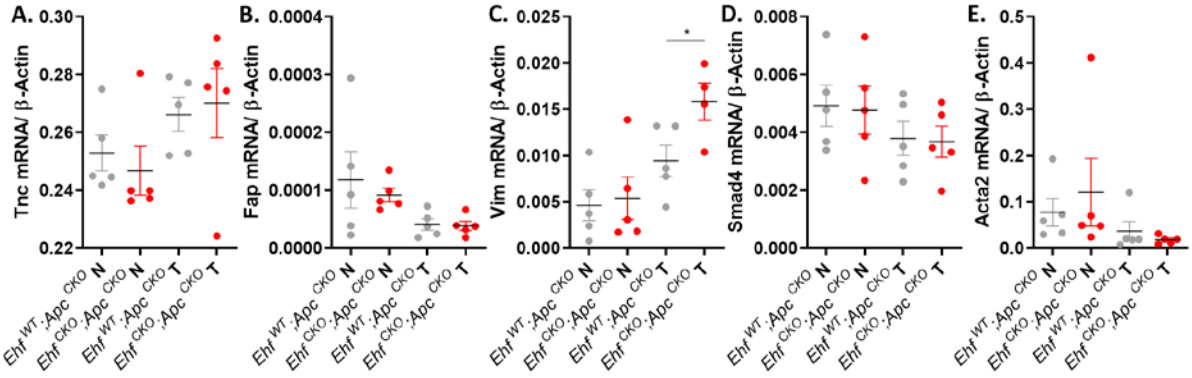

Figure 5.12. Impact of *Ehf* deletion on stromal gene expression in *Apc*-initiated colonic adenomas, assessed by qPCR. Gene expression of stromal markers (A) Tnc, (B) Fap, (C) Vim, (D) Smad4 and (E) Acta2 from colonic adenomas (T) and adjacent normal colon (N) from *Ehf* ^{WT};*Apc* ^{CKO} and *Ehf* ^{CKO};*Apc* ^{CKO} mice. Values shown are mean ± SEM of n=5 mice per group.

A second cohort of *Ehf* ^{WT};*Apc* ^{CKO} and *Ehf* ^{CKO};*Apc* ^{CKO} mice were aged and monitored multiple times per week for signs of ill health. A mouse recorded as being unwell according to the criteria stipulated by the approved ethics protocol was immediately culled (Chapter 2.2.1 Animal monitoring, Table 2.2). Most of the *Ehf* ^{WT};*Apc* ^{CKO} and *Ehf* ^{CKO};*Apc* ^{CKO} mice were culled due to weight loss (>20%), poor stool consistency or displaying hunching behaviour. Weight loss manifested significantly earlier in the *Ehf* ^{CKO};*Apc* ^{CKO} mice with a mean time of onset of 23 days post tamoxifen induction compared to 30 days for the *Ehf* ^{WT};*Apc* ^{CKO} mice (Figure 5.13A). The median ethically determined lifespan was also shorter for *Ehf* ^{CKO};*Apc* ^{CKO} mice compared to *Ehf* ^{WT};*Apc* ^{CKO} mice (24 days vs 36 days), however this was not statistically significant (p=0.1, Figure 5.13B). Taken together, these results indicate that *Ehf* deletion does not profoundly impact on the severity of *Apc*-initiated adenoma formation in a model of bi-allelic loss of *Apc*.

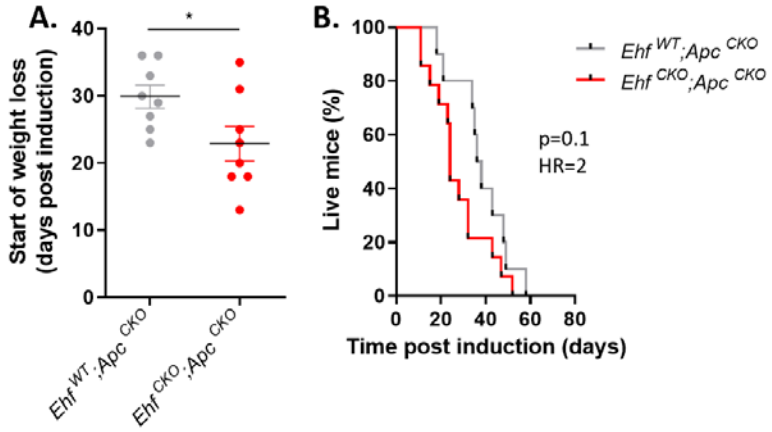

Figure 5.13. Impact of *Ehf* deletion on ethically determined lifespan of mice in a model of rapid *Apc*-initiated colorectal tumorigenesis. (A) Number of days post induction before weight loss was first observed. *P<0.05, t test. Values shown are mean ± SEM of n=8 mice per group. (B) Percentage of live *Ehf* ^{WT};*Apc* ^{CKO} and *Ehf* ^{CKO};*Apc* ^{CKO} mice at the given time point post tamoxifen induction. P=0.1, Mantel-Cox test, Hazard ratio (HR)=2. Values shown from n=10 *Ehf* ^{WT};*Apc* ^{CKO} and n=14 *Ehf* ^{CKO};*Apc* ^{CKO} mice.

5.2.3 The impact of colon-specific *Ehf* deletion on the severity of *Apc*-initiated colorectal cancer in a model of single-allelic loss of *Apc*

The model of colorectal tumorigenesis studied so far results in the very rapid initiation of colonic tumours due to the deletion of both *Apc* alleles. We postulated therefore that the speed of this model may not provide sufficient time for the role of EHF in tumour initiation or progression to manifest. We therefore next investigated the impact of *Ehf* deletion in a in the context of heterozygous deletion of *Apc* (*Apc* $^{CKO/+}$) in the epithelium of the colon and caecum. These mice develop adenomas only when the second allele of *Apc* is lost through a sporadic loss of heterozygosity event (mutation or deletion) that occurs spontaneously over time.

To study the impact of *Ehf* loss in tumour development in this context, we generated and monitored *Ehf* ^{WT};*Apc* $^{CKO/+}$ and *Ehf* ^{CKO};*Apc* $^{CKO/+}$ mice for colon tumour development over 52 weeks. At the study endpoint, 75% (9/12) *Ehf* ^{WT};*Apc* $^{CKO/+}$ and 63.6% (7/11) *Ehf* ^{CKO};*Apc* $^{CKO/+}$ mice were still alive (Figure 5.14A). The remainder were culled due to acute (>15%) and chronic (>20%) weight loss, rectal bleeding or displaying hunching behaviour. Although there was no difference in ethically determined survival, *Ehf* ^{CKO};*Apc* $^{CKO/+}$ male mice had significantly lower body weight compared with *Ehf* ^{WT};*Apc* $^{CKO/+}$ mice, although this difference was not observed in female mice (Figure 5.14B,C).

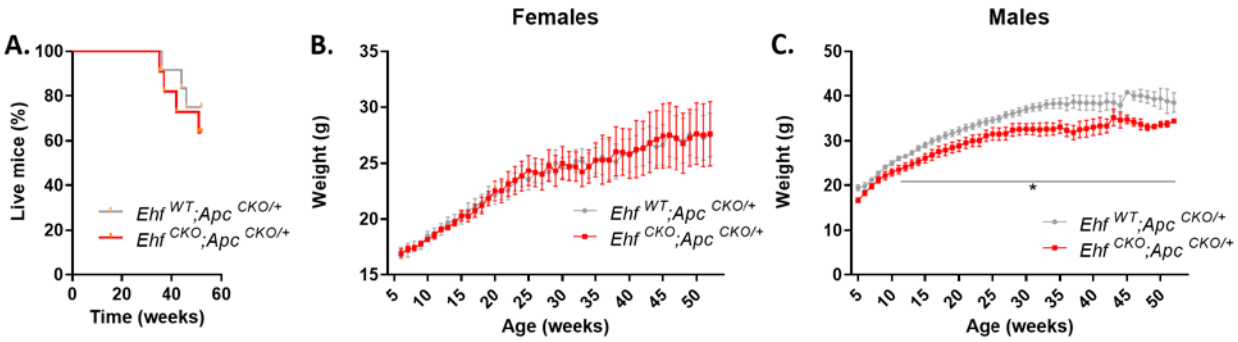

Figure 5.14. Impact of *Ehf* deletion on survival and body weight of mice in which colorectal tumorigenesis is initiated by single-allelic loss of *Apc*. (A) Percentage of live *Ehf* ^{WT};*Apc* $^{CKO/+}$ and *Ehf* ^{CKO};*Apc* $^{CKO/+}$ mice at the given time point. Values shown from n=12 *Ehf* ^{WT};*Apc* ^{CKO} and n=11 *Ehf* ^{CKO};*Apc* ^{CKO} mice. Body weight of (B) male and (C) female *Ehf* ^{WT};*Apc* $^{CKO/+}$ and *Ehf* ^{CKO};*Apc* $^{CKO/+}$ mice. Values shown are mean ± SEM of n=8 female and n=8 male mice per group.

At the end of the 52-week experimental period, mice were culled, and tumours quantified and histopathologically assessed. Notably, more *Ehf* ^{CKO};*Apc* $^{CKO/+}$ mice (6/11; 55%) developed adenomas compared to *Ehf* ^{WT};*Apc* $^{CKO/+}$ mice (4/12; 33%) and the number of colonic adenomas per mouse was higher in the *Ehf* ^{CKO};*Apc* $^{CKO/+}$ mice; however, this difference was not statistically significant (Figure 5.15A). Comparatively, colonic adenoma burden was significantly higher in *Ehf* ^{CKO};*Apc* $^{CKO/+}$ mice compared with *Ehf* ^{WT};*Apc* $^{CKO/+}$ mice, demonstrating that EHF suppresses the growth of *Apc*-initiated colonic adenomas (Figure 5.15B-D). No difference in tumour grade or evidence of metastases were observed in either genotype. Although adenomas arose predominantly in the caecum in *Ehf* ^{WT};*Apc* $^{CKO/+}$ mice, a higher proportion of tumours in the proximal, middle and distal colon were observed in *Ehf* ^{CKO};*Apc* $^{CKO/+}$ mice, demonstrating loss of EHF preferentially promotes tumour formation in these regions (Figure 5.15E). Notably, EHF expression was sixfold higher in the colon relative to the cecum (Figure 5.8A), which may explain the shift in location of tumour onset.

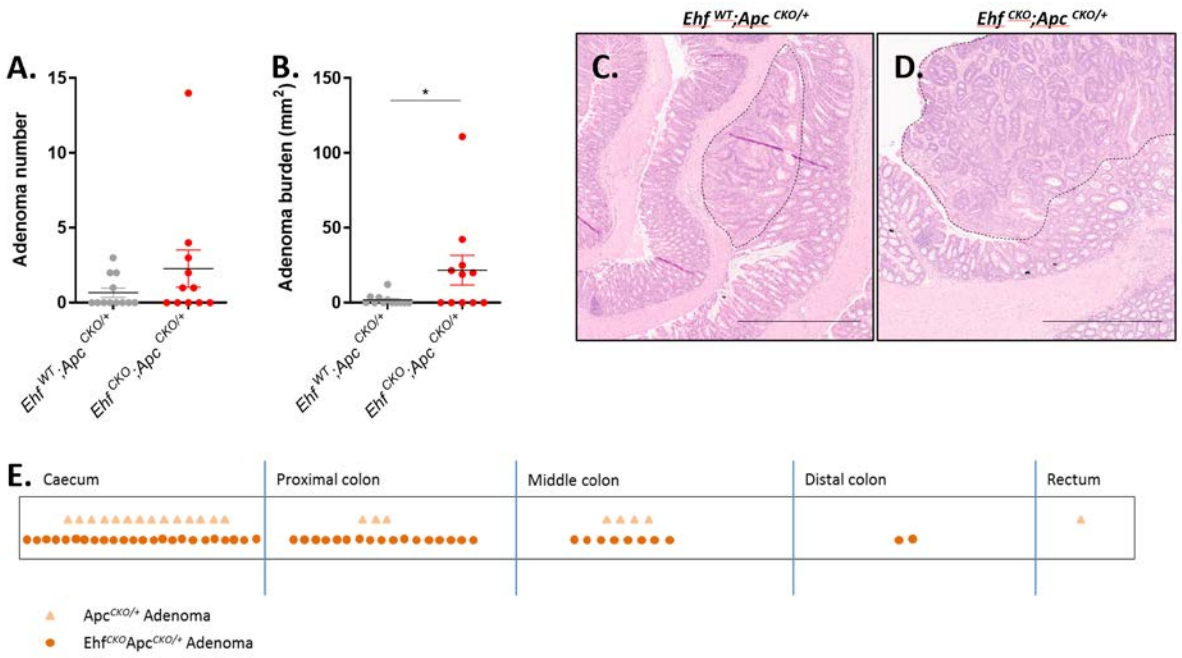

Figure 5.15. Impact of *Ehf* deletion on colorectal tumourigenesis initiated by single-allelic loss of *Apc*. (A,B) Effect of *Ehf* deletion on (A) adenoma number and (B) adenoma burden determined by macroscopic counting and measurement at the study endpoint. Values shown are mean ± SEM or n=12 *Ehf* ^{WT};*Apc* ^{CKO} and n=11 *Ehf* ^{CKO};*Apc* ^{CKO} mice. (C,D) Representative haematoxylin and eosin stained images of adenomas in the colon of *Ehf* ^{WT};*Apc* $^{CKO/+}$ and *Ehf* ^{CKO};*Apc* $^{CKO/+}$ mice. (E) Distribution of adenomas in the ceacum and colon of *Ehf* ^{WT};*Apc* $^{CKO/+}$ and *Ehf* ^{CKO};*Apc* $^{CKO/+}$ mice.

5.3 Discussion

In this chapter, by challenging the colonic epithelium of *Ehf* knockout mice we revealed an essential role for EHF in protecting this organ against DSS-induced acute colitis, and furthermore, from colon tumour development and growth.

First, we observed that mice with whole body deletion of *Ehf* (*Ehf* $^{-/-}$ mice) were more sensitive to DSS-induced acute colitis compared to *Ehf* $^{+/+}$ mice. Importantly, we subsequently demonstrated that this effect was mostly phenocopied in intestinal epithelial-specific *Ehf* knockout mice (*Ehf* ^{IKO}), demonstrating this effect was predominantly epithelial cell dependent. Notably however, the sensitivity to DSS-induced acute colitis was less severe in *Ehf* ^{IKO} mice. This may be due to incomplete *Ehf* deletion in the *Ehf* ^{IKO} model, although the possibility that it may be due to EHF also playing a role in other tissues cannot be fully eliminated. For example, EHF mRNA is highly expressed in mast cells stimulated with Tgf-β and its expression suppresses mast cell activation [22]. Mast cells are tissue-resident immune cells preferentially distributed throughout barrier tissues including the intestinal intraepithelial space [252]. Mast cells play multi-faceted roles in IBD through regulating epithelial permeability, immune signalling transmittance and maintenance and resolution of inflammatory responses [144, 253-258]. It is therefore possible that mast cell hyperactivation may contribute to the more severe disease observed in *Ehf* $^{-/-}$ mice compared to *Ehf* ^{IKO} mice.

Importantly, we noted a reduction in goblet cell differentiation in *Ehf* $^{-/-}$ mice in Chapter 4. Given the essential role of mucin in protecting the colonic epithelium from damage [70], it is possible that the reduced number of goblet cells may underpin the susceptibility of *Ehf* $^{-/-}$ mice to DSS-induced colitis. For example, *Muc2* $^{-/-}$ mice spontaneously develop colitis [69]. Further studies into the mechanism driving the increased susceptibility of *Ehf* knockout mice to DSS-induced acute colitis is needed.

Consistent with the increase in cell proliferation and evidence of possible EMT following *Ehf* deletion in the normal colonic epithelium (Chapter 4), we identified a potential tumour suppressive role for EHF in the colon, as loss of *Ehf* increased *Apc*-initiated colonic adenoma formation and burden.

In our model of heterozygous deletion of *Apc*, we observed mostly right-sided adenomas. Nearly all colonic right-sided tumours and adjacent normal tissue in humans are covered in invasive, polymicrobial biofilms, whereas left sided tumours are infrequently biofilm-positive [259]. In normal colonic homeostasis, the mucous layer creates a barrier between the colonic microbiota and epithelial cell layer [260]. Disrupted goblet cell differentiation in *Ehf* knockout mice, may therefore enable greater bacterial colonisation which could potentially lead to chronic

inflammation and ultimately higher levels of DNA damage in the colonic epithelium, to increase the risk of tumour development [260, 261]

Further to this, biofilms are associated with increased inflammation by increasing IL-6 and STAT3 signalling [259]. The IL-6 family of cytokines and their downstream effector STAT3 have been shown to promote colorectal cancer progression through increased epithelial cell proliferation and decreased apoptosis [262, 263]. Notably, EHF was demonstrated to be a negative regulator of IL-6 expression in prostate cancer cells which prevented STAT3 activation and subsequent expansion of the cancer stem-cell compartment [264]. Interestingly, we observed a significant increase in Il-6 mRNA expression in adenomas from *Ehf* ^{CKO};*Apc* ^{CKO} mice compared to adenomas from *Ehf* ^{WT};*Apc* ^{CKO} mice (data not shown). Furthermore, there was an increase in Il-6 mRNA in the colon of DSS-treated *Ehf* ^{IKO} and *Ehf* $^{-/-}$ mice suggesting that EHF may influence the IL-6/STAT3 axis in the colonic epithelium. Whether this reflects a change in immune cell infiltration, or de-repression of Il6 in colonic epithelial cells requires additional investigation.

In addition, EHF has been found to directly represses expression of the epigenetic regulators, EZH2 and BMI1, in prostate cancer cell lines [29, 30]. Whether expression of these genes is altered in *Ehf* deleted colon tumours and whether they contribute to the increased growth of these tumours therefore represents an interesting avenue to explore further. Gene expression profiling of *Apc*-mutant tumours with and without *Ehf* deletion would represent an ideal unbiased way in which to unveil the mechanisms by which *Ehf* loss contributes to tumour progression.

While our studies identify a novel tumour suppressor function for EHF in mice, it is important to extrapolate these findings to human colon cancers. In this regard, while our investigation of the cancer genome atlas (TCGA) database revealed EHF is rarely mutated in human CRCs [26], ongoing studies in our laboratory have recently shown that EHF expression is lost in a subset of poorly differentiated CRCs (submitted - unpublished), and that its loss may be due to epigenetic inactivation. Furthermore, re-expression of EHF in colon cancer cell lines decreased cell migration (submitted - unpublished), supporting the current finding that EHF has tumour suppressor activity.

In conclusion, in this chapter we identify a novel role for EHF in protecting against DSS-induced acute colitis, and furthermore in protecting against *Apc*-initiated colorectal tumour formation. The mechanisms driving these effects remain to be determined but may be related to the decrease in goblet cell differentiation in *Ehf* knockout mice, the increased rate of colonic cell proliferation, or to epithelial-to-mesenchymal transition, which transcriptional profiling revealed to be altered in *Ehf* ^{IKO} mice.

Chapter 6: General Discussion

6.1 Summary

ETS homologous factor (EHF) is a member of the ESE subfamily of ETS transcription factors and is highly expressed in multiple epithelial tissues including salivary gland, oesophagus, vagina, prostate, colon, skin, bladder and breast [26]. The *EHF* gene consists of a pointed domain (PNT) with potential for homodimerization, co-operative binding with other transcription factors and gene transactivation, and an evolutionarily conserved winged helix-turn-helix ETS DNA-binding domain which binds the A(T/C)(C/G)AGGAAGT consensus DNA sequence [6].

Few studies to-date have investigated the role of EHF in normal tissue homeostasis. In line with its high expression in the skin, a study using primary cell cultures suggested a key role for EHF in keratinocyte differentiation (Rubin et al., 2017). Profiling of enhancer regions in keratinocytes identified the GGAA Ets-binding motif as the most enriched transcription factor binding site, and *EHF* knockdown in organotypic human epidermal tissue revealed that EHF regulates ∼400 genes, including several associated with keratinocyte differentiation [21]. EHF is also highly expressed in the intestinal epithelium, and a role for EHF in maintaining the small intestinal stem cell compartment in mice was recently proposed [16].

In comparison, the role of EHF in tumour progression has been relatively well studied *in vitro*, with loss of expression and a potential tumour suppressive role suggested in prostate [30], pancreatic [36], colorectal [117] and oesophageal squamous cell carcinoma [39], where *EHF* loss has been shown to promote epithelial-to-mesenchymal transition and cell migration. Conversely, EHF has been shown to promote proliferation in cell line models of gastric [45], thyroid [49] and ovarian cancer [44].

To define the role of the EHF transcription factor in development, tissue homeostasis and intestinal disease we generated an *Ehf* floxed mouse which allows for conditional deletion of the ETS DNA binding domain of *Ehf*. In Chapter 3, we induced whole-body deletion of *Ehf* (*Ehf* $^{-/-}$) and investigated the phenotype of these mice. We found that these mice were viable but developed a range of pathologies over their lifespan, which revealed a key role for EHF in maintaining epidermal homeostasis, and in mammary gland differentiation during pregnancy. In Chapter 4, we undertook a detailed study of the role of EHF in the small intestinal and colonic epithelium by inducing intestinal-specific deletion of *Ehf* (*Ehf* ^{IKO}). These studies revealed that *Ehf* deletion caused major transcriptional changes, increased epithelial cell proliferation, and decreased goblet cell differentiation in the colon. Finally, in Chapter 5 we demonstrated that *Ehf* deletion increased

sensitivity of mice to DSS-induced acute colitis and promoted *Apc*-initiated adenoma development in the colon.

In this final discussion chapter, I will broadly discuss the future studies that are needed to complete our understanding of the role of EHF in tissue homeostasis and disease.

6.2 Assessment of the role of EHF on epidermal integrity and maintenance

Having established that EHF is essential for epidermal maintenance, it is now important to study the mechanism behind the observed phenotype. Although EHF was suggested to play a role in keratinocyte differentiation *in vitro* [21], we did not see evidence of this in our *Ehf* $^{-/-}$ mice. Based on our current findings, it is more likely that EHF is involved in wound healing processes or barrier integrity as we observed damage to the epidermis predominantly in areas exposed to grooming, fighting or other abrasions. Skin barrier experiments, wound healing assays and skin inflammation challenges could be useful approaches to definitively establish the role of EHF in the epidermis. Once we gain a clearer picture of the specific processes driving the observed phenotype we can isolate and profile the gene expression differences between *Ehf*-wildtype and *Ehf*-deleted cells to determine the genes involved, and elucidate the mechanism.

While expression of the EHF transcription factor is predominantly epithelial-restricted, expression has also been reported in mast cells and Langerhans cells of the skin [3, 22]. Langerhans cells are tissue-resident macrophages of the skin involved in innate immunity. Our findings in Chapter 3 were made using the *Ehf* whole body knockout mouse model. Performing experiments such as bone marrow transfers will therefore be required to define the role of the immune system in the observed phenotype. However, Langerhans cells are radio-resistant [265] and persists in mice following whole-body irradiation. Hence, to confirm whether the role of EHF in epidermal maintenance is purely epithelial driven, we will need to use a mouse model where *Ehf* is deleted specifically in keratinocytes which can be achieved, for example, by crossing our *Ehf* $^{Lox/Lox}$ mice with *K14* ^{Cre} or *K14* ^{CreERT2} deleter mice.

Finally, our histological analysis of the epidermis of *Ehf* $^{-/-}$ mice revealed features consistent with the potential onset of squamous cell carcinoma, including keratinous pearls, intercellular bridging and enlarged nuclei. Although the role of EHF in head and neck squamous cell carcinoma (HNSCC) has not been extensively investigated, a study by Sakamoto et al. found that EHF protein expression is lost in mesenchymal-like HNSCC cell lines compared with epithelial-like HNSCC cell lines and that re-expression of *EHF* in mesenchymal-like HNSCC cells decreased expression of vimentin, ZEB1 and N-cadherin, and consequently migration of these cells was suppressed [266]. In this context it was also demonstrated that *EHF* re-expression sensitised cells to the anti-cancer

effects of docetaxel. In contrast to this, Novoplansky et al. found that high EHF expression confers resistance to cetuximab treatment due to transcriptional activation of the HER2 and HER3 genes in HNSCC cell lines [267]. Further to these studies, EHF has been studied in other squamous cell carcinomas. Specifically, in oral squamous cell carcinoma (OSCC) depletion of EHF in OSCC cell lines decreased migration and invasion *in vitro* and reduced lung metastasis *in vivo* [268], while abnormal cellular localisation of EHF was shown to be associated with poorer patient outcome in oesophageal squamous cell carcinoma [39]. A logical follow-up study would therefore be the direct assessment of the impact of *Ehf* deletion on the development of squamous cell carcinoma, which can be assessed by challenging mice with topical application of the carcinogens DMBA/TPA (DMBA initiates tumour formation, and TPA promotes growth).

6.3 Assessment of the role of EHF in mammary gland development and differentiation

In Chapter 3 we established that *Ehf* $^{-/-}$ female mice were unable to support their pups and that the mammary developmental process of either alveologenesis or lactogenesis or both, which occur during pregnancy were impaired.

This exciting finding can be pursued in a number of ways. First, given that the impact of *Ehf* deletion on mammary gland differentiation was generated using *Ehf* whole body knockout mice, it is important to confirm that this effect is due to changes in mammary epithelial cells. This can be done by sorting epithelial from non-epithelial cells and performing gene expression profiling to determine the transcriptional changes occurring in the epithelial compartment. Sorting and quantifying the different cell types by either single-cell RNA-seq or single cell ChIP-seq could provide valuable insight into which specific cellular compartments are disrupted by *Ehf* deletion and whether the stem-progenitor-mature cell flux has been disrupted. Furthermore, confirmation that the phenotype of these mice is due to alterations in the mammary epithelial cell compartment could be achieved by generating mammary-specific *Ehf* knockout mouse models, which could be generated by crossing *Ehf* $^{Lox/Lox}$ mice with either *WAP* ^{Cre} or *MMTV* ^{Cre} deleter mice. Alternatively, we could transplant *Ehf* $^{-/-}$ epithelial cells into wildtype hosts and monitor mammary gland development and the ability of these mice to lactate.

Functionally, we observed a lactation deficiency of *Ehf* $^{-/-}$ female mice evidenced by milk-free stomach content of pups born to *Ehf* $^{-/-}$ female mice and reduced staining of milk protein in mammary glands of *Ehf* $^{-/-}$ mice. This was likely due to reduced alveolar area in the *Ehf* $^{-/-}$ mammary glands, however, we also notably observed a significant reduction in cytoplasmic lipid droplets in *Ehf* $^{-/-}$ mammary glands suggesting that the composition of milk may be altered. To quantify and

quantitively analyse these differences, lipidomic profiling of milk extracted from *Ehf*-wildtype and *Ehf*-knockout glands would be of considerable interest and provide important new knowledge.

As a number of signalling pathways and transcription factors and are known to regulate alveologenesis and lactogenesis including STAT5, ELF5, GATA3, NOTCH, BLIMP and FOXA1 [269, 270], it would be important to define the role of EHF in mammary development in these established contexts. In this regard, we observed that that expression of ELF5, a critical determinant of mammary development [209], was not significantly altered in expression in the mammary gland following *Ehf* deletion, suggesting EHF does not transcriptionally regulate ELF5. The relationship between EHF and ELF5 is not yet well defined in the mammary gland, however there is a study that suggest they are likely part of the same regulatory network in luminal progenitor cells [211]. However, single-cell RNA sequencing of mammary epithelial cells show that *Ehf* expression is turned on at an earlier timepoint during gestation compared with *Elf5* [232]. To define the relationship between *Ehf* and *Elf5* in the mammary gland we could breed the $Ehf^{-/-}$ mice with a mouse strain with forced inducible expression of *Elf5* (MMTV-rtTA; TetO-Elf5) to determine whether increased *Elf5* expression is able to rescue the phenotype of $Ehf^{-/-}$ female mice. However, other mechanisms of interaction may still be involved which need to be systematically addressed.

Finally, as key tissue-specific developmental regulators are often deregulated in the corresponding tumours which arise in these tissues, it would be of interest to investigate the role of EHF in breast cancer development and progression. Indeed, data recently generated in our laboratory show that EHF expression is downregulated in human breast cancers with poorly differentiated histology, and that its loss is associated with significantly poorer outcome in several breast cancer subtypes. Furthermore, loss of *EHF* expression is linked to promoter methylation, an established mechanism of tumour suppressor gene inactivation. Given these findings, EHF may represent a previously unrecognized tumour suppressor gene in this disease. It would therefore be of significant interest to study the role of EHF on the proliferation, differentiation and survival of human breast cancer cells and to define the transcriptional targets and biological processes regulated by EHF. And finally, determine the effect of targeted *Ehf* deletion in the mouse mammary gland on mammary tumour development.

6.4 Assessment of the role of EHF in inflammatory bowel disease (IBD) and colorectal tumourigenesis

In Chapter 4 and Chapter 5 we studied the role of EHF in intestinal epithelial homeostasis and disease and revealed an important role for EHF in preventing colitis and colorectal tumour

progression. However, additional studies are still needed to define the mechanism by which EHF impacts these processes.

6.4.1 IBD

We found that *Ehf* knockout mice are more sensitive to DSS-induced acute colitis compared to *Ehf* wildtype mice, although the mechanism underpinning this effect remains unknown. While disruption of the intestinal barrier integrity caused by the observed reduction in goblet cell differentiation of *Ehf* knockout mice may explain the increased sensitivity to colitis, there are other aspects of barrier integrity worth investigating such as expression of epithelial barrier genes and tight junction proteins.

Importantly, our findings show that the colonic epithelial compartment is a major contributor for the observed phenotype, however mice with whole-body deletion of *Ehf* did experience more severe colitis than mice with intestinal-specific deletion of *Ehf*. Given the published role of EHF in mast cells [22], it would be of interest to study colitis in a mast cell specific *Ehf* deleted mouse model (e.g., by using *CMA1* ^{Cre} which has active Cre recombinase in mast cells of the lung and colon [271]).

6.4.2 Colorectal tumourigenesis

We also studied the impact of *Ehf* deletion in two models of *Apc*-initiated colorectal tumourigenesis: bi-allelic and single-allelic deletion of the *Apc* gene. In the bi-allelic model of *Apc*-initiated tumourigenesis, we administered a low dose of tamoxifen to induce mosaic deletion of *Ehf* and/or *Apc*, however we still observed rapid onset of adenoma growth. While we considered this model to be too rapid to fully study the role of EHF in the context of *Apc*-initiated tumourigenesis, we did observe that *Ehf* deleted adenomas contained a larger stromal compartment compared to *Ehf* wildtype adenomas. Notably, *Ehf* deleted adenomas displayed significantly higher mRNA levels of Vimentin which is both a marker of stromal cells as well as epithelial-to-mesenchymal transition. This finding is consistent with the transcriptional changes that occur in the normal colonic epithelium where we discovered an enrichment of the EMT signature in *Ehf* ^{IKO} mice. It would be of significant interest to study this further by profiling the difference in gene expression in *Apc*-mutant tumours with and without *Ehf* deletion.

In the single-allelic model of *Apc*-initiated colorectal tumourigenesis we observed that *Ehf* deletion promoted tumour growth in the colonic epithelium. Interestingly, we observed that male *Ehf* ^{CKO};*Apc* $^{CKO/+}$ mice had worse overall health compared to male *Ehf* ^{WT};*Apc* $^{CKO/+}$ mice, which was not

reflected in female mice. This gender-bias has been reported previously in mice and humans [235, 272], and it has been demonstrated that oestrogen receptor α and β confer resistance to *Apc*-initiated colorectal tumourigenesis in mice [273]. It is therefore worth considering expanding the cohort so that the impact of *Ehf* deletion in male and female mice can be individually assessed. It may also be worth extending the experimental endpoint as 45% (5/11) *Ehf* ^{CKO};*Apc* $^{CKO/+}$ and 66% (8/12) *Ehf* ^{WT};*Apc* $^{CKO/+}$ mice did not present with colonic tumours at the study endpoint of 52 weeks. Expanding the cohort and extending the timeline would enable histopathological comparison of *Ehf*-deleted and *Ehf*-wildtype adenomas. Furthermore, this would allow for gene expression profiling of *Apc*-mutant tumours with and without *Ehf* deletion, which would represent an ideal unbiased way to gain insight into the mechanisms by which *Ehf* loss contributes to tumour progression.

To further cement *Ehf* as a novel tumour suppressor gene in the colon, it will be important to study *Ehf* deletion in other mouse models of colorectal tumourigenesis. First, using a model of colitis-associated cancer (DSS/AOM) would be of interest, and given our findings in Chapter 4 and Chapter 5, we would expect *Ehf* deletion to severely impact on tumour initiation and progression. Then, given the recent data generated in our laboratory which show that EHF expression is lost in a subset of poorly differentiated colorectal cancers, it would be interesting to study loss of *Ehf* in a *Braf* mutant mouse model, as loss of differentiation is more commonly observed in this subset of human colorectal cancers. Mouse models with *Braf* mutations have a long latency of adenoma formation [200] which can be accelerated upon loss of differentiation genes such as *Cdx2* and *Smad4* [201]. Using this model will therefore enable us to confirm or disprove the involvement of EHF in the differentiation grade of colorectal tumours.

6.5 Other tissues

The *Ehf* floxed mice provide a unique opportunity to study the EHF transcription factor in any cell type of interest. While our histological assessment of many epithelial tissues from *Ehf* $^{-/-}$ and *Ehf* $^{+/+}$ mice did not reveal and gross abnormalities following *Ehf* deletion, we have not assessed the impact of *Ehf* deletion in conditions of stress or in the context of tumourigenesis in these tissues. Most notable amongst these is that EHF has been proposed as a tumour suppressor gene in prostate cancer *in vitro* [30-32, 264], and it would be interesting to use the *Ehf* $^{Lox/Lox}$ mice to assess the impact of *Ehf* deletion on tumour development in this tissue (e.g. by studying *Ehf* $^{Lox/Lox}$;*Pten* $^{Lox/Lox}$;*PB* ^{Cre} mice). Similar studies could also be performed in the stomach, oesophagus, lung, pancreas and biliary tract where either tumour suppressive or oncogenic roles for EHF have been suggested from studies in cell lines [26].

6.6 Concluding remarks

In this thesis we have generated multiple novel mouse models which we have used to demonstrate a novel role for the EHF transcription factor in maintenance of epidermal, mammary and intestinal epithelial homeostasis and protection against DSS-induced colitis and colorectal tumour progression. These findings lay the groundwork for further investigation into the role of EHF in epidermal maintenance, mammary gland differentiation and colonic tumourigenesis, as well as multiple other epithelial tissues in which EHF is expressed. In summary, this body of work represent the first systematic study of the role of the EHF transcription factor in development, tissue homeostasis and intestinal disease *in vivo*.

Appendix A: Buffers for intestinal epithelial cell collection

Buffer 1

- PBS (93%)
- RNA secure (4%, Thermo Fisher Scientific, Australia)
- 0.5M EDTA (3%)

Buffer 2

- PBS (96%)
- RNA secure (4%)

Buffers for intestinal epithelial cell collection were prepared in advance and were stored at 4°C for up to two months.

Appendix B: Carmine alum solution

Carmine alum solution was prepared by dissolving 1g of Carmine (Sigma-Aldrich, USA) and 2.5g aluminium potassium sulfate (Sigma-Aldrich, USA) in 500ml of RO water in an Erlenmeyer flask using a magnetic stirrer. The solution was slowly brought to the boil, then boiled for 20 minutes, uncovered. After boiling, the solution was replenished to a total of 500mL with RO water and filtered through a Stericup Filter Unit (0.22µm, Merck Millipore, Australia). A few grains of thymol (Sigma-Aldrich, USA) were added to the solution as stabiliser, and the solution stored at 4°C.

Appendix C: Buffers for immunohistochemistry

Citrate buffer

- 10mM sodium citrate tribasic dihydrate (Sigma-Aldrich, USA)
- Adjusted to pH 6 using 33% HCl (Sigma-Aldrich, USA)
- 0.05% Tween20 (Croda International, UK)
- Stored at 4°C

Tris buffer

- 0.5M Trizma base (Sigma-Aldrich, USA)
- 9 % NaCl (9%, Sigma-Aldrich, USA)
- Adjusted to pH 9 using 33% HCl (Sigma-Aldrich, USA)
- 0.05% Tween20 (Croda International, UK)
- Stored at 4°C

EDTA buffer

- 1mM Ultrapure EDTA (Invitrogen, Australia)
- Adjusted to pH 8 using NaOH (25%, Sigma-Aldrich, USA)
- 0.05% Tween20 (Croda International, UK)
- Stored at 4°C

Tris-buffered saline with Tween20 (TBST)

- 0.5M Trizma base (Sigma-Aldrich, USA)
- 9% NaCl (Sigma-Aldrich, USA)
- Adjusted to pH 7.6 using 33% HCl (Sigma-Aldrich, USA)
- 0.05% Tween20 (Croda International, UK)
- Stored at room temperature

Appendix D: Differentially expressed genes

Table D. List of differentially expressed genes between *Ehf* ^{IKO} mice and the two control groups *Ehf* $^{Lox/Lox}$ and *Villin* $^{CreERT2-TMX}$ mice

Gene name	logFold Change (Ehf KO/WT)	CI.L	CI.R	AveExpr	t	P.Value	adj.P.Val	B
Gm13873	8.100514913	7.528405	8.672625	-1.19477	30.14865	5.83E-15	9.17E-11	13.19465
St6galnac6	-1.012469618	-1.19494	-0.83	8.541127	-11.8145	4.69E-09	3.69E-05	11.18586
Lpo	-4.274642912	-5.15198	-3.39731	3.036225	-10.3745	2.75E-08	0.000144	7.672268
Reg4	2.040397987	1.557653	2.523143	6.680342	8.999767	1.79E-07	0.000703	7.608086
Id4	1.66226896	1.250651	2.073887	1.908302	8.598873	3.21E-07	0.001009	6.759106
Gm13874	4.338942115	3.234666	5.443218	-1.35775	8.366442	4.54E-07	0.001191	5.087945
Hgfac	-0.664207867	-0.83765	-0.49077	7.223512	-8.15426	6.27E-07	0.001273	6.352987
Rab11fip5	1.202479179	0.882086	1.522872	2.774887	7.991509	8.06E-07	0.001273	6.10296
Syt8	1.962734966	1.438438	2.487032	1.885383	7.971113	8.32E-07	0.001273	5.928296
Chn2	-1.312916285	-1.66482	-0.96101	4.081638	-7.94411	8.68E-07	0.001273	6.070243
Ggh	-1.229458323	-1.56151	-0.8974	5.9354	-7.88385	9.53E-07	0.001273	5.958296
Cd177	-4.525948704	-5.75355	-3.29835	5.751033	-7.85031	1.01E-06	0.001273	5.908619
Klk15	2.94588541	2.143945	3.747826	-0.70934	7.82183	1.05E-06	0.001273	4.493605
Pla2g2a	1.998634722	1.417903	2.579366	2.483111	7.328119	2.33E-06	0.002615	5.097991
Plet1	-2.377488077	-3.07892	-1.67605	4.626962	-7.21713	2.79E-06	0.002931	4.952902
Cma1	3.608902058	2.535135	4.682669	0.217259	7.156483	3.09E-06	0.002958	4.246404
Ghr	0.86778759	0.608853	1.126722	4.11771	7.136052	3.19E-06	0.002958	4.800453
Mmp28	-0.844823769	-1.10267	-0.58698	4.049376	-6.97662	4.17E-06	0.00365	4.564976
Ace2	1.425778119	0.982406	1.86915	2.797923	6.847286	5.20E-06	0.004087	4.353456

Rph3al	-0.929548952	-1.2196	-0.6395	4.280304	-6.82396	5.41E-06	0.004087	4.306717
Fmo1	2.301315101	1.581605	3.021025	1.130417	6.808524	5.55E-06	0.004087	4.079587
Rap1gap	-0.746275108	-0.98023	-0.51232	7.042547	-6.79209	5.71E-06	0.004087	4.131871
Matn2	1.110769821	0.760307	1.461233	2.15318	6.748638	6.15E-06	0.004212	4.146679
Acss1	-0.75665081	-0.99952	-0.51378	6.209845	-6.63377	7.50E-06	0.004691	3.872641
Gsta3	1.349479047	0.914001	1.784957	3.795957	6.598335	7.98E-06	0.004691	3.911303
Pkib	2.302121668	1.558678	3.045566	0.554837	6.593479	8.05E-06	0.004691	3.594051
Trpv6	1.792371762	1.213127	2.371617	4.613251	6.588709	8.11E-06	0.004691	3.840998
Ambp	2.138823722	1.441285	2.836362	1.732652	6.528918	9.01E-06	0.004691	3.766594
Grk3	-1.305799184	-1.73181	-0.87979	3.777243	-6.52671	9.04E-06	0.004691	3.825295
Slc24a3	1.030077142	0.693465	1.366689	2.498019	6.515905	9.21E-06	0.004691	3.797931
Capg	0.602322903	0.405361	0.799285	4.645968	6.511503	9.29E-06	0.004691	3.710767
Mgst1	0.828193265	0.556738	1.099648	6.261144	6.496338	9.54E-06	0.004691	3.617865
Rab3b	2.050932374	1.367647	2.734218	1.301051	6.391219	1.15E-05	0.005474	3.476619
Acvr1c	0.795345573	0.527867	1.062824	4.500609	6.331424	1.28E-05	0.005906	3.401205
Col8a1	-2.433826473	-3.26112	-1.60653	4.076475	-6.26415	1.44E-05	0.006468	3.381189
Dab1	1.752146005	1.154354	2.349938	1.255921	6.241005	1.50E-05	0.006553	3.226969
Slc17a9	-0.855183288	-1.1494	-0.56096	6.023458	-6.18904	1.64E-05	0.006848	3.091328
Meg3	-1.848173144	-2.48514	-1.2112	5.257901	-6.17815	1.68E-05	0.006848	3.160591
Alpi	1.79953618	1.178694	2.420379	5.083034	6.171826	1.70E-05	0.006848	3.075071
H6pd	-0.661494361	-0.89111	-0.43188	4.679151	-6.13418	1.82E-05	0.007145	3.076349
Capn13	-1.1917253	-1.60713	-0.77632	5.445293	-6.1085	1.90E-05	0.007302	2.989878
Pglyrp1	-1.321378585	-1.78402	-0.85874	5.031631	-6.08161	2.00E-05	0.007466	2.981155

Zg16	0.79781314	0.517489	1.078137	9.795306	6.060039	2.08E-05	0.007466	2.851084
Dnah5	1.2766939	0.827887	1.7255	3.194888	6.057064	2.09E-05	0.007466	3.006615
Aldh3b2	0.994431616	0.644142	1.344721	3.047928	6.044809	2.13E-05	0.007466	2.995739
Cps1	1.498572928	0.958139	2.039007	4.567557	5.904321	2.76E-05	0.009394	2.620114
Mvb12b	-1.118865959	-1.52299	-0.71474	4.255178	-5.89516	2.80E-05	0.009394	2.701689
Gm10384	-2.868181524	-3.91073	-1.82563	1.249799	-5.85794	3.00E-05	0.009849	2.102194
Sipa1l2	-0.54514855	-0.74528	-0.34502	5.18563	-5.8001	3.34E-05	0.010735	2.419647
Ptp4a3	-0.912611994	-1.24912	-0.5761	3.439168	-5.77461	3.50E-05	0.011028	2.528837
Slc27a2	1.048745671	0.6607	1.436792	2.427372	5.754687	3.63E-05	0.011218	2.501136
Anxa13	0.932997513	0.586405	1.27959	3.015609	5.731862	3.79E-05	0.011479	2.44183
Slc34a2	1.88519226	1.182893	2.587492	5.405516	5.71568	3.91E-05	0.011606	2.221487
E130215H24Rik	-1.690926133	-2.32681	-1.05504	-0.2698	-5.66212	4.32E-05	0.012473	1.412223
Nccrp1	1.511596687	0.941715	2.081479	1.024932	5.647883	4.43E-05	0.012473	2.224538
Mrc1	1.211915502	0.754985	1.668846	1.893535	5.647512	4.44E-05	0.012473	2.30503
Alb	1.665840329	1.030503	2.301177	0.428231	5.582951	5.01E-05	0.01383	2.011008
Chrm1	-0.8548682	-1.18275	-0.52699	3.166221	-5.55165	5.31E-05	0.014238	2.13886
Gm44223	-1.907859043	-2.63993	-1.17579	2.592989	-5.54916	5.34E-05	0.014238	2.103149
Cbr3	0.665023265	0.409164	0.920883	4.495801	5.534391	5.49E-05	0.014395	1.946515
B4galt4	-0.793233422	-1.09978	-0.48669	4.892069	-5.50982	5.75E-05	0.014669	1.914474
Trim29	2.095533062	1.284134	2.906932	0.226329	5.499138	5.86E-05	0.014669	1.847005
A4gnt	-1.345794779	-1.86695	-0.82464	3.340752	-5.49853	5.87E-05	0.014669	2.044743
Capn2	0.439695753	0.268621	0.610771	5.962508	5.472686	6.16E-05	0.014806	1.742584
Spsb4	-3.423385034	-4.75622	-2.09055	0.051109	-5.46909	6.21E-05	0.014806	1.188395

Trpm6	0.698893874	0.426789	0.970999	7.832031	5.469013	6.21E-05	0.014806	1.719725
Itln1	2.639188161	1.608369	3.670007	0.348149	5.451582	6.42E-05	0.015057	1.807886
1810037I17Rik	0.509712752	0.310366	0.70906	4.823278	5.444403	6.50E-05	0.015057	1.750486
Ntan1	-0.529631171	-0.73922	-0.32004	4.809295	-5.38069	7.34E-05	0.016748	1.665916
Bach1	-0.438844319	-0.61403	-0.26365	6.273535	-5.33381	8.03E-05	0.018054	1.476946
Barx2	1.352603379	0.809565	1.895641	0.919763	5.30365	8.50E-05	0.018856	1.633392
Tm4sf1	1.196349048	0.714032	1.678666	1.211821	5.281531	8.87E-05	0.019399	1.625693
Pdxdc1	-0.5331018	-0.74868	-0.31752	8.697702	-5.26541	9.15E-05	0.019734	1.331267
Pdia5	-0.647188083	-0.91009	-0.38429	5.477736	-5.24168	9.58E-05	0.019886	1.345189
Pld2	1.08863127	0.646208	1.531055	1.291243	5.239345	9.62E-05	0.019886	1.557734
Rflnb	-0.633271131	-0.89079	-0.37575	6.436135	-5.23613	9.68E-05	0.019886	1.286596
Ace	-1.46265356	-2.05773	-0.86758	4.046296	-5.23365	9.73E-05	0.019886	1.518425
Sgsm3	-0.467986446	-0.65939	-0.27658	6.633826	-5.20611	0.000103	0.020233	1.221825
Mpp3	-0.678727993	-0.95635	-0.4011	3.976032	-5.20559	0.000103	0.020233	1.433413
Vipr2	-1.69069473	-2.38236	-0.99903	2.306595	-5.20482	0.000103	0.020233	1.495113
Kcnh6	0.973483245	0.573702	1.373264	3.136946	5.184908	0.000107	0.020765	1.423693
Ppif	-0.519077659	-0.73578	-0.30238	5.471849	-5.10045	0.000126	0.024152	1.067586
Gpc6	1.405510319	0.816471	1.99455	0.686381	5.080706	0.000131	0.024712	1.226937
Ces1g	1.666987212	0.967749	2.366226	5.399205	5.076234	0.000132	0.024712	0.996775
Fmo4	0.832937575	0.482173	1.183702	2.222507	5.056286	0.000137	0.02517	1.250093
Apol10a	-0.827760258	-1.17686	-0.47866	7.071074	-5.04875	0.000139	0.02517	0.911269
Aldob	0.661489523	0.382184	0.940795	6.503633	5.04288	0.000141	0.02517	0.899845
Crot	0.494663736	0.285641	0.703687	5.130779	5.039068	0.000142	0.02517	0.945916

Sgpl1	0.501335389	0.289284	0.713387	6.716165	5.034091	0.000143	0.02517	0.880661
Cp	1.104628256	0.637143	1.572113	1.278725	5.031335	0.000144	0.02517	1.194519
Npdc1	-0.540170552	-0.76977	-0.31057	5.039367	-5.00951	0.00015	0.025976	0.928596
Hykk	0.894458806	0.513251	1.275667	3.15915	4.996118	0.000154	0.026374	1.066258
Trim30d	0.644444846	0.36927	0.91962	4.597192	4.986685	0.000157	0.026575	0.886753
Aadac	0.794251883	0.454035	1.134469	4.921276	4.970926	0.000162	0.027115	0.823726
A1cf	0.528407483	0.301117	0.755698	4.993264	4.950189	0.000169	0.02794	0.781711
Syt2	1.097404873	0.623892	1.570917	1.889965	4.934806	0.000174	0.028236	1.033874
Prkrip1	-0.630441984	-0.90264	-0.35824	3.766469	-4.9316	0.000175	0.028236	0.932152
Stard8	-1.604887497	-2.29819	-0.91158	1.429097	-4.92895	0.000176	0.028236	0.925059
Spdef	-0.884332956	-1.26708	-0.50158	6.336688	-4.91968	0.000179	0.028464	0.676493
9430024E24Rik	-1.341697566	-1.92406	-0.75934	1.266335	-4.90565	0.000184	0.028509	0.877059
Cyp2w1	1.028221707	0.5816	1.474843	2.717929	4.902095	0.000185	0.028509	0.928934
Smim38	-1.491577374	-2.13974	-0.84342	2.101729	-4.90004	0.000186	0.028509	0.954623
Plcb4	-0.732819123	-1.05135	-0.41429	4.504835	-4.89868	0.000187	0.028509	0.783652
Wtip	-0.740710049	-1.06331	-0.41811	3.250566	-4.88893	0.00019	0.028633	0.90939
Spon2	1.239678021	0.69951	1.779846	1.368493	4.886686	0.000191	0.028633	0.943207
Sorcs2	-0.690339008	-0.99184	-0.38884	4.601103	-4.87534	0.000195	0.029002	0.723757
Ablim2	-0.761130361	-1.09427	-0.42799	4.299547	-4.86477	0.000199	0.029335	0.745639
Sgsm1	-0.506891497	-0.72992	-0.28386	5.012278	-4.83936	0.00021	0.030555	0.596241
Slc7a11	1.471541605	0.822825	2.120258	2.153663	4.830054	0.000213	0.030835	0.826768
Dock1	-0.34345241	-0.49508	-0.19183	7.144313	-4.82312	0.000216	0.030975	0.463373
Otc	1.028585705	0.573548	1.483623	3.653566	4.813135	0.000221	0.031307	0.650648

Creb3l1	-0.706383655	-1.01933	-0.39343	6.843028	-4.8062	0.000224	0.031382	0.435257
Scnn1b	-1.3443211	-1.94097	-0.74767	2.906716	-4.79752	0.000228	0.031382	0.775935
Plet1os	-2.442100142	-3.52613	-1.35807	0.539063	-4.79684	0.000228	0.031382	0.398352
Gfpt1	-0.414158282	-0.59811	-0.23021	9.699836	-4.794	0.000229	0.031382	0.422807
Rtl1	-1.573775562	-2.27466	-0.87289	1.615591	-4.78115	0.000235	0.031912	0.700038
Ifi27l2b	0.603597027	0.333908	0.873286	5.942218	4.765601	0.000242	0.032627	0.364141
Nnt	0.749361318	0.413588	1.085134	4.337665	4.75204	0.000249	0.033231	0.452366
Sptbn4	-1.768412526	-2.56216	-0.97466	1.843573	-4.7439	0.000253	0.033487	0.649789
Efcab14	-0.389215478	-0.56409	-0.21434	5.722798	-4.73917	0.000256	0.03349	0.336654
Plekhg1	0.477420031	0.262749	0.692091	4.985659	4.735458	0.000257	0.03349	0.359857
Itga1	0.543937026	0.297909	0.789965	4.459809	4.707591	0.000272	0.035103	0.355337
Clic4	0.81579435	0.446152	1.185437	5.527648	4.699303	0.000277	0.035289	0.247584
Kcnk10	1.560459577	0.852623	2.268297	0.287062	4.694116	0.000279	0.035289	0.522981
E2f3	0.469112432	0.256255	0.68197	4.628329	4.692693	0.00028	0.035289	0.309197
Shank2	-0.485111125	-0.70542	-0.2648	5.877259	-4.68854	0.000283	0.035299	0.22992
Acnat1	0.56218872	0.306201	0.818176	4.493264	4.676253	0.00029	0.035887	0.289072
Adamts17	-1.328246791	-1.93556	-0.72093	2.580321	-4.65694	0.000301	0.036924	0.525939
Slc52a3	-0.447672091	-0.65249	-0.24286	4.669334	-4.65408	0.000303	0.036924	0.266785
Soat2	1.041981334	0.564084	1.519879	1.209701	4.642583	0.00031	0.037489	0.498455
Rhbdf2	-0.509597282	-0.74539	-0.2738	4.640654	-4.60176	0.000336	0.040359	0.170365
Pla2g12b	1.482976558	0.794474	2.171479	0.505805	4.586309	0.000346	0.041308	0.360113
Scn2b	-3.190726351	-4.67503	-1.70643	1.012072	-4.57723	0.000353	0.041543	0.091305
Car12	-0.672538144	-0.98548	-0.35959	5.648179	-4.57595	0.000354	0.041543	0.02521

Zfp185	1.369498367	0.731066	2.007931	0.134335	4.567525	0.00036	0.041936	0.281362
Eci3	-0.957879421	-1.40631	-0.50945	2.023799	-4.54836	0.000374	0.043255	0.329641
Sobp	-1.597111222	-2.34766	-0.84657	1.032207	-4.53098	0.000387	0.04446	0.195014
Paqr7	1.138067721	0.602096	1.67404	1.074922	4.521271	0.000395	0.045005	0.276069
Papln	0.688806204	0.364088	1.013524	2.463143	4.51674	0.000398	0.045089	0.224669
Gas6	-0.574217274	-0.84563	-0.3028	8.17807	-4.50483	0.000408	0.045849	-0.17438
Oit1	-0.582057654	-0.8579	-0.30621	8.923935	-4.49299	0.000418	0.04635	-0.19264
Sybu	-1.3952935	-2.05664	-0.73395	2.624359	-4.49235	0.000418	0.04635	0.218964
Arel1	-0.401874458	-0.59267	-0.21108	5.72442	-4.48501	0.000424	0.046709	-0.17069
Inpp4b	0.519725792	0.271958	0.767494	4.60982	4.466457	0.00044	0.048071	-0.14066
Tfrc	0.573746185	0.300061	0.847431	7.640878	4.463791	0.000443	0.048071	-0.25778
Adcy9	-0.38193975	-0.56452	-0.19936	4.948663	-4.45417	0.000451	0.048674	-0.1673

Appendix E: 'Hallmark gene sets' G2M checkpoint genes

Table E. Genes enriched in the hallmark G2M checkpoint gene set in the MSigDB database in *Ehf* ^{IKO} mice.

Gene symbol	Rank in gene list	Rank metric score	Running ES
EFNA5	196	0.632	0.0151
MEIS1	374	0.464	0.0234
NDC80	446	0.417	0.0383
PBK	524	0.383	0.0509
CKS1B	528	0.38	0.0696
TTK	612	0.348	0.08
E2F2	619	0.344	0.0966
CDC45	621	0.343	0.1136
MEIS2	674	0.328	0.1256
POLQ	691	0.322	0.1403
STIL	751	0.303	0.1505
BARD1	821	0.286	0.159
CHEK1	881	0.271	0.1676
NUSAP1	898	0.266	0.1795
CKS2	947	0.256	0.1883
E2F3	974	0.25	0.1985
BUB1	976	0.249	0.2109
TGFB1	1017	0.24	0.2195
KNL1	1028	0.237	0.2304

HMMR	1122	0.221	0.2337
DMD	1126	0.22	0.2444
SUV39H1	1129	0.219	0.2551
KIF20B	1157	0.214	0.2636
CCNB2	1197	0.207	0.2706
PRIM2	1206	0.206	0.2802
NEK2	1212	0.206	0.29
SMC2	1260	0.199	0.296
GINS2	1261	0.199	0.306
BIRC5	1292	0.196	0.3132
UBE2C	1323	0.191	0.3202
KIF2C	1347	0.187	0.3276
MAD2L1	1417	0.176	0.3306
KIF15	1447	0.173	0.3368
CENPA	1450	0.172	0.3452
CCNA2	1475	0.169	0.3516
AURKA	1483	0.169	0.3595
KIF11	1499	0.167	0.3665
BRCA2	1507	0.165	0.3742
MNAT1	1517	0.164	0.3816
TPX2	1522	0.164	0.3895
CCNF	1535	0.162	0.3965
MACKS	1561	0.159	0.4024

PRC1	1562	0.159	0.4103
CDK1	1567	0.158	0.4179
KIF4A	1570	0.158	0.4256
CENPE	1589	0.156	0.4319
CENPF	1594	0.155	0.4393
EXO1	1614	0.154	0.4454
RAD54L	1770	0.14	0.4394
CDC25B	1823	0.134	0.4418
CDC6	1851	0.132	0.4461
PLK4	1874	0.129	0.4507
AURKB	1954	0.124	0.4502
KIF22	1960	0.123	0.4559
SMC4	1983	0.122	0.4602
RACGAP1	2015	0.119	0.4635
POLE	2148	0.11	0.4579
RAD21	2179	0.108	0.4608
TACC3	2185	0.108	0.4657
KPNA2	2191	0.107	0.4707
MKI67	2225	0.105	0.4731
ESPL1	2238	0.104	0.4773
RPS6KA5	2260	0.103	0.4807
STMN1	2293	0.101	0.4831
INCEP	2299	0.101	0.4877

POLA2	2386	0.096	0.4853
UBE2S	2409	0.094	0.4881
FBXO5	2460	0.092	0.4885
KIF23	2494	0.09	0.4903
HIF1A	2566	0.087	0.4887
CDKN3	2577	0.087	0.4922
PDS5B	2633	0.083	0.4917
SAP30	2651	0.082	0.4944
FOXN3	2656	0.082	0.4981

Appendix F: 'Hallmark gene sets' EMT checkpoint genes

Table F. Genes enriched in the hallmark epithelial to mesenchymal transition gene set in the MSigDB database in *Ehf* ^{IKO} mice.

Gene symbol	Rank in gene list	Rank metric score	Running ES
ATN2	41	1.102	0.0303
VCAM1	58	0.975	0.0589
ITGB3	93	0.856	0.0822
FAP	109	0.825	0.1062
FBN2	134	0.744	0.127
TFPI2	140	0.729	0.1489
ADAM12	149	0.717	0.1702
ELN	174	0.693	0.1894
WNT5A	182	0.664	0.2092
SPP1	191	0.643	0.2282
COL8A2	223	0.591	0.2437
BGN	258	0.558	0.258
SGCB	287	0.529	0.2718
CDH11	315	0.507	0.2851
SLIT3	329	0.497	0.2993
LUM	349	0.48	0.3124
THBS2	377	0.463	0.3243
SERPINH1	392	0.451	0.3369

DAB2	403	0.443	0.3497
FBLN2	431	0.428	0.3605
CALD1	481	0.399	0.3687
COL5A3	492	0.395	0.3799
PLAUR	517	0.384	0.3897
CAP2	533	0.376	0.4
TPM2	566	0.365	0.4085
FBLN1	601	0.353	0.4164
PLOD2	622	0.343	0.4253
COL5A2	624	0.343	0.4357
FERMT2	637	0.338	0.4451
COL4A1	650	0.334	0.4543
CAPG	705	0.318	0.4595
TNC	746	0.304	0.4655
SPARC	761	0.301	0.4735
LOXL1	769	0.299	0.4821
LOXL2	777	0.298	0.4906
COL5A1	782	0.297	0.4994
VCAN	789	0.294	0.5079
LOX	797	0.292	0.5162
GAS1	822	0.286	0.523
GPX7	840	0.284	0.5303
COL12A1	844	0.282	0.5387

COL1A1	868	0.275	0.5452
TIMP3	884	0.27	0.5522
MYL9	928	0.26	0.5566
COL6A3	939	0.258	0.5636
COL1A2	1012	0.241	0.565
COL4A2	1013	0.241	0.5724
TGFB1	1017	0.24	0.5795
IGFBP4	1052	0.232	0.5838
LAMC1	1061	0.231	0.5902
PMP22	1175	0.211	0.5872
FN1	1177	0.21	0.5936
COL6A2	1220	0.205	0.5963
COL3A1	1232	0.202	0.6016
FSTL1	1316	0.192	0.6006
NT5E	1393	0.18	0.5997
GEM	1448	0.172	0.6005
ITGA5	1460	0.171	0.6048
ITGB5	1462	0.171	0.61
PFN2	1476	0.169	0.6141
TNFRSF11B	1503	0.166	0.617
ACTA2	1520	0.164	0.6207

Appendix G: Gene set enrichment analysis by comparison to MSigDB curated gene sets

Table G. Gene set enrichment analysis by comparison to MSigDB CURATED GENE SETS; Up in *Ehf* ^{IKO} mice.

GS	SIZE	ES	NES	NOM p-val	FDR q-val	FWER p-val	RANK AT MAX	LEADING EDGE
REACTOME_ECM_PROTEOGLYCANS	52	0.77	2.2	0	0	0	1463	tags=60%, list=12%, signal=67%
FLORIO_NEOCORTEX_BASAL_RADIAL_GLIA_DN	164	0.65	2.17	0	0	0	2247	tags=66%, list=18%, signal=80%
KEGG_ECM_RECEPTOR_INTERACTION	67	0.71	2.08	0	0	0	1463	tags=52%, list=12%, signal=59%
ZHOU_CELL_CYCLE_GENES_IN_IR_RESPONSE_24HR	119	0.64	2.03	0	0.001	0.004	2596	tags=55%, list=21%, signal=70%
SCHUETZ_BREAST_CANCER_DUCTAL_INVASIVE_UP	233	0.59	2.02	0	0.001	0.005	1449	tags=43%, list=12%, signal=48%
MOLENAAR_TARGETS_OF_CCND1_AND_CDK4_DN	56	0.71	2.01	0	0.001	0.007	1883	tags=59%, list=15%, signal=69%
LEE_EARLY_T_LYMPHOCYTE_UP	88	0.65	2.01	0	0.001	0.007	2300	tags=64%, list=19%, signal=78%
ZHAN_MULTIPLE_MYELOMA_PR_UP	42	0.74	1.98	0	0.004	0.026	2247	tags=81%, list=18%, signal=99%
HOFFMANN_LARGE_TO_SMALL_PRE_BII_LYMPHOCYTE_UP	145	0.59	1.95	0	0.009	0.061	2607	tags=54%, list=21%, signal=68%
MEBARKI_HCC_PROGENITOR_FZD8CRD_UP	414	0.54	1.95	0	0.008	0.062	2311	tags=48%, list=19%, signal=58%
BURTON_ADIPOGENESIS_8	68	0.65	1.95	0	0.007	0.064	1522	tags=31%, list=12%, signal=35%
REACTOME_EXTRACELLULAR_MATRIX_ORGANIZATION	206	0.57	1.95	0	0.007	0.064	1463	tags=37%, list=12%, signal=42%
REACTOME_CROSSLINKING_OF_COLLAGEN_FIBRILS	16	0.85	1.94	0	0.008	0.076	1009	tags=69%, list=8%, signal=75%

KUNINGER_IGF1_VS_PDGFB_TARGETS_DN	37	0.72	1.93	0	0.008	0.084	1649	tags=59%, list=14%, signal=69%
WU_APOPTOSIS_BY_CDKN1A_VIA_TP53	48	0.69	1.92	0	0.009	0.101	2224	tags=60%, list=18%, signal=74%
FURUKAWA_DUSP6_TARGETS_PCI35_DN	65	0.66	1.92	0	0.008	0.101	2014	tags=49%, list=17%, signal=59%
REACTOME_BINDING_AND_UPTAKE_OF_LIGANDS_BY_SCAVENGER_RECEPTORS	29	0.75	1.92	0	0.008	0.105	1439	tags=55%, list=12%, signal=62%
ANASTASSIOU_MULTICANCER_INVASIVENESS_SIGNATURE	39	0.72	1.92	0	0.008	0.108	1758	tags=69%, list=14%, signal=81%
GOLDRATH_ANTIGEN_RESPONSE	306	0.54	1.91	0	0.009	0.128	2783	tags=48%, list=23%, signal=61%
REACTOME_ELASTIC_FIBRE_FORMATION	33	0.73	1.91	0	0.009	0.132	2007	tags=73%, list=16%, signal=87%
ISSAEVA_MLL2_TARGETS	41	0.7	1.9	0.004	0.01	0.154	1870	tags=51%, list=15%, signal=60%
BOQUEST_STEM_CELL_UP	159	0.57	1.89	0	0.01	0.165	1439	tags=36%, list=12%, signal=41%
PICCALUGA_ANGIOIMMUNOBLASTIC_LYMPHOMA_UP	158	0.57	1.89	0	0.01	0.179	2203	tags=47%, list=18%, signal=57%
WHITEFORD_PEDIATRIC_CANCER_MARKERS	106	0.6	1.89	0	0.011	0.198	2291	tags=53%, list=19%, signal=64%
MORI_IMMATURE_B_LYMPHOCYTE_DN	86	0.62	1.88	0	0.012	0.221	2440	tags=48%, list=20%, signal=59%
NABA_PROTEOGLYCANS	16	0.84	1.88	0	0.014	0.257	785	tags=56%, list=6%, signal=60%
KOBAYASHI_EGFR_SIGNALING_24HR_DN	234	0.54	1.88	0	0.013	0.259	2309	tags=46%, list=19%, signal=55%
FISCHER_G2_M_CELL_CYCLE	220	0.54	1.88	0	0.013	0.265	2408	tags=45%, list=20%, signal=56%
IGLESIAS_E2F_TARGETS_UP	134	0.58	1.87	0	0.014	0.28	2166	tags=39%, list=18%, signal=47%
MODY_HIPPOCAMPUS_NEONATAL	28	0.76	1.87	0.002	0.014	0.294	1173	tags=36%, list=10%, signal=39%

ROSTY_CERVICAL_CANCER_PROLIFERATION_CLUSTER	135	0.58	1.87	0	0.014	0.305	2247	tags=59%, list=18%, signal=71%
FARMER_BREAST_CANCER_CLUSTER_4	16	0.84	1.87	0	0.014	0.323	1226	tags=63%, list=10%, signal=69%
FARMER_BREAST_CANCER_CLUSTER_1	23	0.78	1.86	0	0.016	0.351	1227	tags=61%, list=10%, signal=68%
GAVIN_FOXP3_TARGETS_CLUSTER_P6	77	0.62	1.86	0	0.015	0.353	2299	tags=62%, list=19%, signal=76%
BLANCO_MELO_BRONCHIAL_EPITHELIAL_CELLS_INFLUENZA_A_DEL_NS1_INFECTION_DN	155	0.56	1.86	0	0.016	0.375	1895	tags=54%, list=16%, signal=63%
SOTIRIOU_BREAST_CANCER_GRADE_1_VS_3_UP	144	0.56	1.85	0	0.017	0.401	2309	tags=52%, list=19%, signal=63%
NABA_CORE_MATRISOME	159	0.56	1.85	0	0.017	0.408	1335	tags=43%, list=11%, signal=47%
CLASPER_LYMPHATIC_VESSELS_DURING_METASTASIS_DN	28	0.74	1.85	0	0.018	0.435	1393	tags=57%, list=11%, signal=64%
LEE_LIVER_CANCER_CIPROFIBRATE_UP	46	0.67	1.84	0	0.02	0.463	1475	tags=43%, list=12%, signal=49%
KANG_DOXORUBICIN_RESISTANCE_UP	53	0.64	1.84	0	0.021	0.5	2421	tags=66%, list=20%, signal=82%
HECKER_IFNB1_TARGETS	55	0.64	1.84	0	0.021	0.505	1945	tags=42%, list=16%, signal=50%
REACTOME_INTEGRIN_CELL_SURFACE_INTERACTIONS	65	0.63	1.84	0	0.021	0.509	1463	tags=52%, list=12%, signal=59%
REACTOME_RESOLUTION_OF_SISTER_CHROMATID_COHESION	111	0.58	1.83	0	0.021	0.529	2188	tags=40%, list=18%, signal=48%
REACTOME_ASSEMBLY_OF_COLLAGEN_FIBRILS_AND_OTHER_MULTIMERIC_STRUCTURES	48	0.66	1.83	0	0.021	0.533	1335	tags=54%, list=11%, signal=61%
TANG_SENESCENCE_TP53_TARGETS_DN	47	0.65	1.83	0	0.023	0.576	2493	tags=66%, list=20%, signal=83%
DORSEY_GAB2_TARGETS	17	0.79	1.81	0	0.029	0.673	934	tags=59%, list=8%, signal=64%

REACTOME_MET_PROMOTES_CELL_MOTILITY	37	0.68	1.81	0	0.03	0.685	1226	tags=35%, list=10%, signal=39%
PID_INTEGRIN1_PATHWAY	55	0.64	1.81	0	0.031	0.698	1461	tags=49%, list=12%, signal=56%
REACTOME_MOLECULES_ASSOCIATED_WITH_ELASTIC_FIBRES	26	0.73	1.81	0.002	0.031	0.705	2007	tags=73%, list=16%, signal=87%
REACTOME_MET_ACTIVATES_PTK2_SIGNALING	26	0.74	1.8	0	0.031	0.714	1226	tags=50%, list=10%, signal=55%
REACTOME_METABOLISM_OF_FAT_SOLUBLE_VITAMINS	35	0.69	1.8	0	0.031	0.716	1452	tags=40%, list=12%, signal=45%
CROMER_TUMORIGENESIS_UP	27	0.73	1.8	0	0.031	0.723	1478	tags=52%, list=12%, signal=59%
MORI_LARGE_PRE_BII_LYMPHOCYTE_UP	82	0.6	1.8	0.002	0.032	0.749	2577	tags=48%, list=21%, signal=60%
WANG_NEOPLASTIC_TRANSFORMATION_BY_CCND1_MYC	18	0.78	1.8	0.004	0.033	0.771	1086	tags=56%, list=9%, signal=61%
KONG_E2F3_TARGETS	88	0.59	1.79	0	0.036	0.794	2297	tags=57%, list=19%, signal=70%
SMID_BREAST_CANCER_LUMINAL_B_DN	321	0.5	1.79	0	0.038	0.82	1957	tags=36%, list=16%, signal=42%
KHETCHOUMIAN_TRIM24_TARGETS_UP	42	0.67	1.79	0	0.038	0.826	2148	tags=55%, list=18%, signal=66%
DUTERTRE_ESTRADIOL_RESPONSE_24HR_UP	290	0.51	1.78	0	0.039	0.841	2336	tags=49%, list=19%, signal=59%
GILDEA_METASTASIS	19	0.77	1.78	0	0.041	0.862	1251	tags=58%, list=10%, signal=64%
BENPORATH_PROLIFERATION	136	0.55	1.78	0	0.042	0.87	2591	tags=40%, list=21%, signal=51%
SILIGAN_BOUND_BY_EWS_FLT1_FUSION	28	0.71	1.78	0.002	0.042	0.87	1051	tags=25%, list=9%, signal=27%
WAMUNYOKOLI_OVARIAN_CANCER_GRADES_1_2_DN	55	0.63	1.77	0	0.043	0.884	1424	tags=33%, list=12%, signal=37%
KEGG_DRUG_METABOLISM_CYTOCHROME_P450	34	0.68	1.77	0	0.042	0.887	1123	tags=32%, list=9%, signal=36%

CHIBA_RESPONSE_TO_TSA_UP	38	0.67	1.77	0	0.043	0.897	1725	tags=42%, list=14%, signal=49%
POOLA_INVASIVE_BREAST_CANCER_UP	164	0.53	1.77	0	0.044	0.904	1758	tags=48%, list=14%, signal=56%
WESTON_VEGFA_TARGETS_6HR	32	0.69	1.77	0	0.043	0.907	2361	tags=66%, list=19%, signal=81%
REACTOME_SYNTHESIS_OF_BILE_ACIDS_AND_BILE_SALTS	21	0.74	1.77	0.002	0.043	0.908	391	tags=19%, list=3%, signal=20%
FARMER_BREAST_CANCER_CLUSTER_2	33	0.68	1.77	0.004	0.042	0.909	2312	tags=70%, list=19%, signal=86%
RODWELL_AGING_KIDNEY_NO_BLOOD_UP	161	0.53	1.76	0	0.044	0.92	1865	tags=35%, list=15%, signal=41%
MCBRYAN_PUBERTAL_TGFB1_TARGETS_DN	48	0.63	1.76	0	0.045	0.93	1176	tags=27%, list=10%, signal=30%
WINNEPENNINCKX_MELANOMA_METASTASIS_UP	153	0.54	1.76	0	0.045	0.93	2247	tags=40%, list=18%, signal=48%
SU_TESTIS	47	0.62	1.76	0	0.045	0.933	2003	tags=38%, list=16%, signal=46%
LI_WILMS_TUMOR_ANAPLASTIC_UP	16	0.79	1.76	0	0.045	0.935	2224	tags=81%, list=18%, signal=99%
REACTOME_DEPOSITION_OF_NEW_CENPA_CONTAINING_NUCLEOSOMES_AT_THE _CENTROMERE	27	0.7	1.76	0	0.046	0.94	1956	tags=59%, list=16%, signal=70%
MAGRANGEAS_MULTIPLE_MYELOMA_IGG_VS_IGA_DN	22	0.74	1.76	0	0.046	0.944	1045	tags=32%, list=9%, signal=35%
HOELZEL_NF1_TARGETS_DN	60	0.6	1.75	0.002	0.047	0.945	1330	tags=40%, list=11%, signal=45%
SCIBETTA_KDM5B_TARGETS_DN	72	0.6	1.75	0	0.046	0.946	2300	tags=43%, list=19%, signal=53%
REACTOME_RHO_GTPASES_ACTIVATE_FORMINS	125	0.54	1.75	0	0.046	0.947	3147	tags=51%, list=26%, signal=68%
CHICAS_RB1_TARGETS_GROWING	200	0.51	1.75	0	0.047	0.95	2185	tags=43%, list=18%, signal=51%

MEBARKI_HCC_PROGENITOR_WNT_DN_CTNNB1_DEPENDENT	17	0.77	1.75	0	0.047	0.95	861	tags=35%, list=7%, signal=38%
LINDVALL_IMMORTALIZED_BY_TERT_DN	56	0.6	1.75	0	0.047	0.952	1890	tags=48%, list=16%, signal=57%
HSIAO_LIVER_SPECIFIC_GENES	140	0.53	1.75	0	0.048	0.957	1286	tags=24%, list=11%, signal=26%
LEE_LIVER_CANCER_ACOX1_UP	54	0.61	1.75	0	0.048	0.959	1746	tags=39%, list=14%, signal=45%
REACTOME_DEFECTIVE_B4GALT7_CAUSES_EDS_PROGEROID_TYPE	16	0.78	1.75	0.006	0.048	0.96	785	tags=31%, list=6%, signal=33%
CHIANG_LIVER_CANCER_SUBCLASS_PROLIFERATION_UP	161	0.53	1.75	0	0.047	0.96	2577	tags=55%, list=21%, signal=69%
KIM_LIVER_CANCER_POOR_SURVIVAL_UP	20	0.77	1.74	0	0.048	0.966	618	tags=25%, list=5%, signal=26%
YAMASHITA_METHYLATED_IN_PROSTATE_CANCER	30	0.68	1.74	0	0.049	0.968	1462	tags=47%, list=12%, signal=53%
ZHOU_CELL_CYCLE_GENES_IN_IR_RESPONSE_6HR	80	0.58	1.74	0	0.049	0.968	2650	tags=51%, list=22%, signal=65%
NADLER_OBESITY_UP	53	0.61	1.74	0	0.048	0.968	2481	tags=43%, list=20%, signal=54%

References

1. Sizemore, G.M., et al., *The ETS family of oncogenic transcription factors in solid tumours.* Nature Reviews Cancer, 2017. **17**: p. 337.
2. Bochert, M.A., et al., *Molecular cloning and expression of Ehf, a new member of the ets transcription factor/oncoprotein gene family.* Biochem Biophys Res Commun, 1998. **246**(1): p. 176-81.
3. Sprater, F., A.-O. Hovden, and S. Appel, *Expression of ESE-3 Isoforms in Immunogenic and Tolerogenic Human Monocyte-Derived Dendritic Cells.* PLoS ONE, 2012. **7**(11): p. e49577.
4. Kas, K., et al., *ESE-3, a novel member of an epithelium-specific ets transcription factor subfamily, demonstrates different target gene specificity from ESE-1.* J Biol Chem, 2000. **275**(4): p. 2986-98.
5. Fujikawa, M., et al., *ESE-3, an Ets family transcription factor, is up-regulated in cellular senescence.* Cancer Science, 2007. **98**(9): p. 1468-1475.
6. Madison, B.J., et al., *Electrostatic repulsion causes anticooperative DNA binding between tumor suppressor ETS transcription factors and JUN-FOS at composite DNA sites.* J Biol Chem, 2018. **293**(48): p. 18624-18635.
7. Tugores, A., et al., *The Epithelium-specific ETS Protein EHF/ESE-3 Is a Context-dependent Transcriptional Repressor Downstream of MAPK Signaling Cascades.* Journal of Biological Chemistry, 2001. **276**(23): p. 20397-20406.
8. Kleinbaum, L.A., et al., *Human chromosomal localization, tissue/tumor expression, and regulatory function of the ets family gene EHF.* Biochem Biophys Res Commun, 1999. **264**(1): p. 119-26.
9. Stolzenburg, L.R., et al., *Regulatory dynamics of 11p13 suggest a role for EHF in modifying CF lung disease severity.* Nucleic Acids Res, 2017. **45**(15): p. 8773-8784.
10. Wright, F.A., et al., *Genome-wide association and linkage identify modifier loci of lung disease severity in cystic fibrosis at 11p13 and 20q13.2.* Nat Genet, 2011. **43**(6): p. 539-46.
11. Silverman, E.S., et al., *Constitutive and cytokine-induced expression of the ETS transcription factor ESE-3 in the lung.* Am J Respir Cell Mol Biol, 2002. **27**(6): p. 697-704.
12. Wu, J., et al., *Regulation of epithelium-specific Ets-like factors ESE-1 and ESE-3 in airway epithelial cells: potential roles in airway inflammation.* Cell research, 2008. **18**(6): p. 649-663.
13. Fossum, S.L., et al., *Ets Homologous Factor (EHF) has Critical Roles in Epithelial Dysfunction in Airway Disease.* Journal of Biological Chemistry, 2017.
14. Mutolo, M.J., et al., *A transcription factor network represses CFTR gene expression in airway epithelial cells.* Biochem J, 2018. **475**(7): p. 1323-1334.
15. Muñoz, J., et al., *The Lgr5 intestinal stem cell signature: robust expression of proposed quiescent '+4' cell markers.* Embo j, 2012. **31**(14): p. 3079-91.
16. Zhu, P., et al., *LncGata6 maintains stemness of intestinal stem cells and promotes intestinal tumorigenesis.* Nat Cell Biol, 2018. **20**(10): p. 1134-1144.
17. Terahara, K., et al., *Comprehensive gene expression profiling of Peyer's patch M cells, villous M-like cells, and intestinal epithelial cells.* J Immunol, 2008. **180**(12): p. 7840-6.
18. Asai, T. and S.L. Morrison, *The SRC family tyrosine kinase HCK and the ETS family transcription factors SPIB and EHF regulate transcytosis across a human follicle-associated epithelium model.* J Biol Chem, 2013. **288**(15): p. 10395-405.
19. Stephens, D.N., et al., *The Ets transcription factor EHF as a regulator of cornea epithelial cell identity.* J Biol Chem, 2013. **288**(48): p. 34304-24.
20. Appel, S., et al., *Epithelial-specific transcription factor ESE-3 is involved in the development of monocyte-derived DCs.* Blood, 2006. **107**(8): p. 3265-70.
21. Rubin, A.J., et al., *Lineage-specific dynamic and pre-established enhancer-promoter contacts cooperate in terminal differentiation.* Nat Genet, 2017. **49**(10): p. 1522-1528.

22. Yamazaki, S., et al., *The Transcription Factor Ehf Is Involved in TGF-beta-Induced Suppression of FcepsilonRI and c-Kit Expression and FcepsilonRI-Mediated Activation in Mast Cells.* J Immunol, 2015. **195**(7): p. 3427-35.
23. Kameyama, N., et al., *Involvement of ESE-3, epithelial-specific ETS factor family member 3, in transactivation of the ABCB1 gene via pregnane X receptor in intestine-derived LS180 cells but not in liver-derived HepG2 cells.* Drug Metab Pharmacokinet, 2016. **31**(5): p. 340-348.
24. Xu, M.Y., et al., *A 6 gene signature identifies the risk of developing cirrhosis in patients with chronic hepatitis B.* Front Biosci (Landmark Ed), 2016. **21**: p. 479-86.
25. Ramnath, D., et al., *Hepatic expression profiling identifies steatosis-independent and steatosis-driven advanced fibrosis genes.* JCI Insight, 2018. **3**(14).
26. Luk, I.Y., C.M. Reehorst, and J.M. Mariadason, *ELF3, ELF5, EHF and SPDEF Transcription Factors in Tissue Homeostasis and Cancer.* Molecules, 2018. **23**(9).
27. Park, C., I. Lee, and W.K. Kang, *Influence of small interfering RNA corresponding to ets homologous factor on senescence-associated modulation of prostate carcinogenesis.* Mol Cancer Ther, 2006. **5**(12): p. 3191-6.
28. Cangemi, R., et al., *Reduced expression and tumor suppressor function of the ETS transcription factor ESE-3 in prostate cancer.* Oncogene, 2007. **27**(20): p. 2877-2885.
29. Kunderfranco, P., et al., *ETS transcription factors control transcription of EZH2 and epigenetic silencing of the tumor suppressor gene Nkx3.1 in prostate cancer.* PLoS One, 2010. **5**(5): p. e10547.
30. Albino, D., et al., *ESE3/EHF Controls Epithelial Cell Differentiation and Its Loss Leads to Prostate Tumors with Mesenchymal and Stem-like Features.* Cancer Research, 2012. **72**(11): p. 2889.
31. Albino, D., et al., *Activation of the Lin28/let-7 Axis by Loss of ESE3/EHF Promotes a Tumorigenic and Stem-like Phenotype in Prostate Cancer.* Cancer Res, 2016. **76**(12): p. 3629-43.
32. Dallavalle, C., et al., *MicroRNA-424 impairs ubiquitination to activate STAT3 and promote prostate tumor progression.* J Clin Invest, 2016. **126**(12): p. 4585-4602.
33. Long, Z., et al., *Loss of EHF facilitates the development of treatment-induced neuroendocrine prostate cancer.* Cell Death Dis, 2021. **12**(1): p. 46.
34. Wang, L., et al., *EHF promotes colorectal carcinoma progression by activating TGF-β1 transcription and canonical TGF-β signaling.* Cancer Sci, 2020. **111**(7): p. 2310-2324.
35. Taniue, K., et al., *A member of the ETS family, EHF, and the ATPase RUVBL1 inhibit p53-mediated apoptosis.* EMBO Reports, 2011. **12**(7): p. 682-689.
36. Zhao, T., et al., *ESE3 Inhibits Pancreatic Cancer Metastasis by Upregulating E-Cadherin.* Cancer Research, 2017. **77**(4): p. 874.
37. Zhou, T., et al., *ESE3/EHF, a promising target of rosiglitazone, suppresses pancreatic cancer stemness by downregulating CXCR4.* Gut, 2021.
38. Liu, J., et al., *Tumoral EHF predicts the efficacy of anti-PD1 therapy in pancreatic ductal adenocarcinoma.* J Exp Med, 2019. **216**(3): p. 656-673.
39. Wang, L., et al., *Abnormal Localization and Tumor Suppressor Function of Epithelial Tissue-Specific Transcription Factor ESE3 in Esophageal Squamous Cell Carcinoma.* PLoS One, 2015. **10**(5): p. e0126319.
40. Galang, C.K., et al., *Changes in the Expression of Many Ets Family Transcription Factors and of Potential Target Genes in Normal Mammary Tissue and Tumors.* Journal of Biological Chemistry, 2004. **279**(12): p. 11281-11292.
41. He, J., et al., *Profile of Ets gene expression in human breast carcinoma.* Cancer Biol Ther, 2007. **6**(1): p. 76-82.
42. Bach, K., et al., *Differentiation dynamics of mammary epithelial cells revealed by single-cell RNA sequencing.* Nature Communications, 2017. **8**(1): p. 2128.
43. Watson, M.B., et al., *Expression microarray analysis reveals genes associated with in vitro resistance to cisplatin in a cell line model.* Acta Oncol, 2007. **46**(5): p. 651-8.

44. Cheng, Z., et al., *Knockdown of EHF inhibited the proliferation, invasion and tumorigenesis of ovarian cancer cells.* Mol Carcinog, 2016. **55**(6): p. 1048-59.
45. Shi, J., et al., *Increased expression of EHF via gene amplification contributes to the activation of HER family signaling and associates with poor survival in gastric cancer.* Cell Death Dis, 2016. **7**(10): p. e2442.
46. Xu, G., et al., *Screening Driving Transcription Factors in the Processing of Gastric Cancer.* Gastroenterol Res Pract, 2016. **2016**: p. 8431480.
47. Gu, M.L., et al., *Blockage of ETS homologous factor inhibits the proliferation and invasion of gastric cancer cells through the c-Met pathway.* World J Gastroenterol, 2020. **26**(47): p. 7497-7512.
48. Gong, Y.C., et al., *miR206 inhibits cancer initiating cells by targeting EHF in gastric cancer.* Oncol Rep, 2017. **38**(3): p. 1688-1694.
49. Lv, Y., et al., *Increased expression of EHF contributes to thyroid tumorigenesis through transcriptionally regulating HER2 and HER3.* Oncotarget, 2016. **7**(36): p. 57978-57990.
50. Gregorieff, A., et al., *The ets-domain transcription factor Spdef promotes maturation of goblet and paneth cells in the intestinal epithelium.* Gastroenterology, 2009. **137**(4): p. 1333-45.e1-3.
51. Noah, T.K., et al., *SAM pointed domain ETS factor (SPDEF) regulates terminal differentiation and maturation of intestinal goblet cells.* Exp Cell Res, 2010. **316**(3): p. 452-65.
52. Ng, A.Y., et al., *Inactivation of the transcription factor Elf3 in mice results in dysmorphogenesis and altered differentiation of intestinal epithelium.* Gastroenterology, 2002. **122**(5): p. 1455-66.
53. Van der Flier, L.G. and H. Clevers, *Stem cells, self-renewal, and differentiation in the intestinal epithelium.* Annual review of physiology, 2009. **71**: p. 241-260.
54. Cheng, H. and C.P. Leblond, *Origin, differentiation and renewal of the four main epithelial cell types in the mouse small intestine. V. Unitarian Theory of the origin of the four epithelial cell types.* Am J Anat, 1974. **141**(4): p. 537-61.
55. Barker, N., *Adult intestinal stem cells: critical drivers of epithelial homeostasis and regeneration.* Nat Rev Mol Cell Biol, 2014. **15**(1): p. 19-33.
56. Kozar, S., et al., *Continuous clonal labeling reveals small numbers of functional stem cells in intestinal crypts and adenomas.* Cell Stem Cell, 2013. **13**(5): p. 626-33.
57. Barker, N., et al., *Identification of stem cells in small intestine and colon by marker gene Lgr5.* Nature, 2007. **449**(7165): p. 1003-7.
58. Tian, H., et al., *A reserve stem cell population in small intestine renders Lgr5-positive cells dispensable.* Nature, 2011. **478**(7368): p. 255-9.
59. Li, N., et al., *Mouse Label-Retaining Cells Are Molecularly and Functionally Distinct From Reserve Intestinal Stem Cells.* Gastroenterology, 2016. **151**(2): p. 298-310.e7.
60. Yousefi, M., et al., *Msi RNA-binding proteins control reserve intestinal stem cell quiescence.* J Cell Biol, 2016. **215**(3): p. 401-413.
61. Ireland, H., et al., *Cellular inheritance of a Cre-activated reporter gene to determine Paneth cell longevity in the murine small intestine.* Dev Dyn, 2005. **233**(4): p. 1332-6.
62. Stappenbeck, T.S., *Paneth cell development, differentiation, and function: new molecular cues.* Gastroenterology, 2009. **137**(1): p. 30-3.
63. Geiser, J., et al., *A mouse model of acrodermatitis enteropathica: loss of intestine zinc transporter ZIP4 (Slc39a4) disrupts the stem cell niche and intestine integrity.* PLoS Genet, 2012. **8**(6): p. e1002766.
64. Sato, T., et al., *Paneth cells constitute the niche for Lgr5 stem cells in intestinal crypts.* Nature, 2011. **469**(7330): p. 415-8.
65. Kim, T.H., S. Escudero, and R.A. Shivdasani, *Intact function of Lgr5 receptor-expressing intestinal stem cells in the absence of Paneth cells.* Proc Natl Acad Sci U S A, 2012. **109**(10): p. 3932-7.

66. Sasaki, N., et al., *Reg4+ deep crypt secretory cells function as epithelial niche for Lgr5+ stem cells in colon.* Proceedings of the National Academy of Sciences of the United States of America, 2016. **113**(37): p. E5399-E5407.
67. Snoeck, V., B. Goddeeris, and E. Cox, *The role of enterocytes in the intestinal barrier function and antigen uptake.* Microbes and Infection, 2005. **7**(7): p. 997-1004.
68. Chang, W.W.L. and C.P. Leblond, *Renewal of the epithelium in the descending colon of the mouse. I. Presence of three cell populations: Vacuolated-columnar, mucous and argentaffin.* 1971. **131**(1): p. 73-99.
69. Van der Sluis, M., et al., *Muc2-deficient mice spontaneously develop colitis, indicating that MUC2 is critical for colonic protection.* Gastroenterology, 2006. **131**(1): p. 117-29.
70. Velcich, A., et al., *Colorectal Cancer in Mice Genetically Deficient in the Mucin Muc2.* 2002. **295**(5560): p. 1726-1729.
71. Sjolund, K., et al., *Endocrine cells in human intestine: an immunocytochemical study.* Gastroenterology, 1983. **85**(5): p. 1120-30.
72. Jenny, M., et al., *Neurogenin3 is differentially required for endocrine cell fate specification in the intestinal and gastric epithelium.* Embo j, 2002. **21**(23): p. 6338-47.
73. Gerbe, F., et al., *The intestinal epithelium tuft cells: specification and function.* 2012. **69**(17): p. 2907-2917.
74. Howitt, M.R., et al., *Tuft cells, taste-chemosensory cells, orchestrate parasite type 2 immunity in the gut.* Science (New York, N.Y.), 2016. **351**(6279): p. 1329-1333.
75. Middelhoff, M., et al., *Dclk1-expressing tuft cells: critical modulators of the intestinal niche?* Am J Physiol Gastrointest Liver Physiol, 2017. **313**(4): p. G285-g299.
76. Westphalen, C.B., et al., *Long-lived intestinal tuft cells serve as colon cancer-initiating cells.* The Journal of clinical investigation, 2014. **124**(3): p. 1283-1295.
77. May, R., et al., *Brief report: Dclk1 deletion in tuft cells results in impaired epithelial repair after radiation injury.* Stem cells (Dayton, Ohio), 2014. **32**(3): p. 822-827.
78. Mabbott, N.A., et al., *Microfold (M) cells: important immunosurveillance posts in the intestinal epithelium.* Mucosal Immunology, 2013. **6**: p. 666.
79. Jang, M.H., et al., *Intestinal villous M cells: An antigen entry site in the mucosal epithelium.* 2004. **101**(16): p. 6110-6115.
80. Madara, J.L., *Cup cells: structure and distribution of a unique class of epithelial cells in guinea pig, rabbit, and monkey small intestine.* Gastroenterology, 1982. **83**(5): p. 981-94.
81. Gerhart, J., *1998 Warkany lecture: signaling pathways in development.* Teratology, 1999. **60**(4): p. 226-39.
82. Bray, S.J., *Notch signalling: a simple pathway becomes complex.* Nat Rev Mol Cell Biol, 2006. **7**(9): p. 678-89.
83. Schröder, N. and A. Gossler, *Expression of Notch pathway components in fetal and adult mouse small intestine.* Gene Expression Patterns, 2002. **2**(3): p. 247-250.
84. VanDussen, K.L., et al., *Notch signaling modulates proliferation and differentiation of intestinal crypt base columnar stem cells.* Development (Cambridge, England), 2012. **139**(3): p. 488-497.
85. Milano, J., et al., *Modulation of notch processing by gamma-secretase inhibitors causes intestinal goblet cell metaplasia and induction of genes known to specify gut secretory lineage differentiation.* Toxicol Sci, 2004. **82**(1): p. 341-58.
86. Wong, G.T., et al., *Chronic treatment with the gamma-secretase inhibitor LY-411,575 inhibits beta-amyloid peptide production and alters lymphopoiesis and intestinal cell differentiation.* J Biol Chem, 2004. **279**(13): p. 12876-82.
87. van Es, J.H., et al., *Notch/gamma-secretase inhibition turns proliferative cells in intestinal crypts and adenomas into goblet cells.* Nature, 2005. **435**(7044): p. 959-63.
88. Pellegrinet, L., et al., *Dll1- and dll4-mediated notch signaling are required for homeostasis of intestinal stem cells.* Gastroenterology, 2011. **140**(4): p. 1230-1240.e1-7.
89. Stamataki, D., et al., *Delta1 expression, cell cycle exit, and commitment to a specific secretory fate coincide within a few hours in the mouse intestinal stem cell system.* PLoS One, 2011. **6**(9): p. e24484.

90. Ueo, T., et al., *The role of Hes genes in intestinal development, homeostasis and tumor formation.* Development, 2012. **139**(6): p. 1071-82.
91. Jensen, J., et al., *Control of endodermal endocrine development by Hes-1.* Nat Genet, 2000. **24**(1): p. 36-44.
92. Suzuki, K., et al., *Hes1-deficient mice show precocious differentiation of Paneth cells in the small intestine.* Biochem Biophys Res Commun, 2005. **328**(1): p. 348-52.
93. Shroyer, N.F., et al., *Intestine-specific ablation of mouse atonal homolog 1 (Math1) reveals a role in cellular homeostasis.* Gastroenterology, 2007. **132**(7): p. 2478-88.
94. Yang, Q., et al., *Requirement of Math1 for secretory cell lineage commitment in the mouse intestine.* Science, 2001. **294**(5549): p. 2155-8.
95. Kazanjian, A., et al., *Atonal homolog 1 is required for growth and differentiation effects of notch/gamma-secretase inhibitors on normal and cancerous intestinal epithelial cells.* Gastroenterology, 2010. **139**(3): p. 918-28, 928.e1-6.
96. Kim, T.H. and R.A. Shivdasani, *Genetic evidence that intestinal Notch functions vary regionally and operate through a common mechanism of Math1 repression.* J Biol Chem, 2011. **286**(13): p. 11427-33.
97. van Es, J.H., et al., *Intestinal stem cells lacking the Math1 tumour suppressor are refractory to Notch inhibitors.* Nat Commun, 2010. **1**: p. 18.
98. Shroyer, N.F., et al., *Gfi1 functions downstream of Math1 to control intestinal secretory cell subtype allocation and differentiation.* Genes Dev, 2005. **19**(20): p. 2412-7.
99. Katz, J.P., et al., *The zinc-finger transcription factor Klf4 is required for terminal differentiation of goblet cells in the colon.* Development, 2002. **129**(11): p. 2619-28.
100. Clevers, H., *Wnt/beta-catenin signaling in development and disease.* Cell, 2006. **127**(3): p. 469-80.
101. Mah, A.T., K.S. Yan, and C.J. Kuo, *Wnt pathway regulation of intestinal stem cells.* The Journal of physiology, 2016. **594**(17): p. 4837-4847.
102. Barker, N., et al., *Crypt stem cells as the cells-of-origin of intestinal cancer.* Nature, 2009. **457**(7229): p. 608-11.
103. Fevr, T., et al., *Wnt/beta-catenin is essential for intestinal homeostasis and maintenance of intestinal stem cells.* Mol Cell Biol, 2007. **27**(21): p. 7551-9.
104. van Es, J.H., et al., *A critical role for the Wnt effector Tcf4 in adult intestinal homeostatic self-renewal.* Molecular and cellular biology, 2012. **32**(10): p. 1918-1927.
105. Pinto, D., et al., *Canonical Wnt signals are essential for homeostasis of the intestinal epithelium.* Genes & development, 2003. **17**(14): p. 1709-1713.
106. Bastide, P., et al., *Sox9 regulates cell proliferation and is required for Paneth cell differentiation in the intestinal epithelium.* J Cell Biol, 2007. **178**(4): p. 635-48.
107. Mori-Akiyama, Y., et al., *SOX9 is required for the differentiation of paneth cells in the intestinal epithelium.* Gastroenterology, 2007. **133**(2): p. 539-46.
108. van den Brink, G.R., et al., *Sonic hedgehog expression correlates with fundic gland differentiation in the adult gastrointestinal tract.* Gut, 2002. **51**(5): p. 628-633.
109. Batts, L.E., et al., *Bmp signaling is required for intestinal growth and morphogenesis.* Dev Dyn, 2006. **235**(6): p. 1563-70.
110. van den Brink, G.R., et al., *Indian Hedgehog is an antagonist of Wnt signaling in colonic epithelial cell differentiation.* Nat Genet, 2004. **36**(3): p. 277-82.
111. Kosinski, C., et al., *Indian hedgehog regulates intestinal stem cell fate through epithelial-mesenchymal interactions during development.* Gastroenterology, 2010. **139**(3): p. 893-903.
112. Li, X., et al., *Deconvoluting the intestine: molecular evidence for a major role of the mesenchyme in the modulation of signaling cross talk.* Physiol Genomics, 2007. **29**(3): p. 290-301.
113. Haramis, A.P., et al., *De novo crypt formation and juvenile polyposis on BMP inhibition in mouse intestine.* Science, 2004. **303**(5664): p. 1684-6.

114. Auclair, B.A., et al., *Bone morphogenetic protein signaling is essential for terminal differentiation of the intestinal secretory cell lineage.* Gastroenterology, 2007. **133**(3): p. 887-96.
115. He, X.C., et al., *BMP signaling inhibits intestinal stem cell self-renewal through suppression of Wnt-beta-catenin signaling.* Nat Genet, 2004. **36**(10): p. 1117-21.
116. Beck, S.E., et al., *BMP-induced growth suppression in colon cancer cells is mediated by p21WAF1 stabilization and modulated by RAS/ERK.* Cell Signal, 2007. **19**(7): p. 1465-72.
117. Luk, I.Y.-N., *Investigating the role of the EHF transcription factor in the regulation of differentiation in colorectal cancer*. 2017.
118. Blumberg, R.S., L.J. Saubermann, and W. Strober, *Animal models of mucosal inflammation and their relation to human inflammatory bowel disease.* Curr Opin Immunol, 1999. **11**(6): p. 648-56.
119. Jostins, L., et al., *Host-microbe interactions have shaped the genetic architecture of inflammatory bowel disease.* Nature, 2012. **491**(7422): p. 119-24.
120. Ahn, S.H., et al., *Hepatocyte nuclear factor 4alpha in the intestinal epithelial cells protects against inflammatory bowel disease.* Inflamm Bowel Dis, 2008. **14**(7): p. 908-20.
121. Willson, T.A., et al., *Deletion of intestinal epithelial cell STAT3 promotes T-lymphocyte STAT3 activation and chronic colitis following acute dextran sodium sulfate injury in mice.* Inflamm Bowel Dis, 2013. **19**(3): p. 512-25.
122. Frank, D.N., et al., *Disease phenotype and genotype are associated with shifts in intestinal-associated microbiota in inflammatory bowel diseases.* Inflamm Bowel Dis, 2011. **17**(1): p. 179-84.
123. Wang, F., et al., *Interferon-gamma and tumor necrosis factor-alpha synergize to induce intestinal epithelial barrier dysfunction by up-regulating myosin light chain kinase expression.* Am J Pathol, 2005. **166**(2): p. 409-19.
124. Suenaert, P., et al., *Anti-tumor necrosis factor treatment restores the gut barrier in Crohn's disease.* Am J Gastroenterol, 2002. **97**(8): p. 2000-4.
125. Boltin, D., et al., *Mucin function in inflammatory bowel disease: an update.* J Clin Gastroenterol, 2013. **47**(2): p. 106-11.
126. Kiesler, P., I.J. Fuss, and W. Strober, *Experimental Models of Inflammatory Bowel Diseases.* Cellular and Molecular Gastroenterology and Hepatology, 2015. **1**(2): p. 154-170.
127. Panwala, C.M., J.C. Jones, and J.L. Viney, *A Novel Model of Inflammatory Bowel Disease: Mice Deficient for the Multiple Drug Resistance Gene, mdr1a, Spontaneously Develop Colitis.* The Journal of Immunology, 1998. **161**(10): p. 5733.
128. Larsson, J.M.H., et al., *Altered O-glycosylation profile of MUC2 mucin occurs in active ulcerative colitis and is associated with increased inflammation.* Inflammatory Bowel Diseases, 2011. **17**(11): p. 2299-2307.
129. Fu, J., et al., *Loss of intestinal core 1-derived O-glycans causes spontaneous colitis in mice.* The Journal of clinical investigation, 2011. **121**(4): p. 1657-1666.
130. Powrie, F., et al., *Phenotypically distinct subsets of CD4+ T cells induce or protect from chronic intestinal inflammation in C. B-17 scid mice.* Int Immunol, 1993. **5**(11): p. 1461-71.
131. Read, S., V. Malmström, and F.J.J.o.E.M. Powrie, *Cytotoxic T lymphocyte–associated antigen 4 plays an essential role in the function of CD25+ CD4+ regulatory cells that control intestinal inflammation.* 2000. **192**(2): p. 295-302.
132. Shevach, E.M.J.I., *Mechanisms of foxp3+ T regulatory cell-mediated suppression.* 2009. **30**(5): p. 636-645.
133. Aranda, R., et al., *Analysis of intestinal lymphocytes in mouse colitis mediated by transfer of CD4+, CD45RBhigh T cells to SCID recipients.* 1997. **158**(7): p. 3464-3473.
134. Franke, A., et al., *Sequence variants in IL10, ARPC2 and multiple other loci contribute to ulcerative colitis susceptibility.* 2008. **40**(11): p. 1319.
135. Franke, A., et al., *Genome-wide meta-analysis increases to 71 the number of confirmed Crohn's disease susceptibility loci.* Nat Genet, 2010. **42**(12): p. 1118-25.

136. Glocker, E.-O., et al., *Inflammatory bowel disease and mutations affecting the interleukin-10 receptor.* 2009. **361**(21): p. 2033-2045.
137. Kühn, R., et al., *Interleukin-10-deficient mice develop chronic enterocolitis.* 1993. **75**(2): p. 263-274.
138. Hoshi, N., et al., *MyD88 signalling in colonic mononuclear phagocytes drives colitis in IL-10-deficient mice.* 2012. **3**: p. 1120.
139. Shouval, D.S., et al., *Interleukin-10 receptor signaling in innate immune cells regulates mucosal immune tolerance and anti-inflammatory macrophage function.* 2014. **40**(5): p. 706-719.
140. Sellon, R.K., et al., *Resident enteric bacteria are necessary for development of spontaneous colitis and immune system activation in interleukin-10-deficient mice.* 1998. **66**(11): p. 5224-5231.
141. Okayasu, I., et al., *A novel method in the induction of reliable experimental acute and chronic ulcerative colitis in mice.* 1990. **98**(3): p. 694-702.
142. Chami, B., et al., *The role of CXCR3 in DSS-induced colitis.* 2014. **9**(7): p. e101622.
143. Fukata, M., et al., *Toll-like receptor-4 is required for intestinal response to epithelial injury and limiting bacterial translocation in a murine model of acute colitis.* 2005. **288**(5): p. G1055-G1065.
144. He, Z., et al., *Mast cells are essential intermediaries in regulating IL-33/ST2 signaling for an immune network favorable to mucosal healing in experimentally inflamed colons.* Cell Death Dis, 2018. **9**(12): p. 1173.
145. Pull, S.L., et al., *Activated macrophages are an adaptive element of the colonic epithelial progenitor niche necessary for regenerative responses to injury.* 2005. **102**(1): p. 99-104.
146. Krieglstein, C.F., et al., *Collagen-binding integrin α 1 β 1 regulates intestinal inflammation in experimental colitis.* 2002. **110**(12): p. 1773-1782.
147. Han, S.W., et al., *DICAM Attenuates Experimental Colitis via Stabilizing Junctional Complex in Mucosal Barrier.* Inflamm Bowel Dis, 2018.
148. Neurath, M., I. Fuss, and W.J.I.r.o.i. Strober, *TNBS-colitis.* 2000. **19**(1): p. 51-62.
149. Neurath, M.F., et al., *Antibodies to interleukin 12 abrogate established experimental colitis in mice.* 1995. **182**(5): p. 1281-1290.
150. Davidson, N.J., et al., *IL-12, but not IFN-gamma, plays a major role in sustaining the chronic phase of colitis in IL-10-deficient mice.* The journal of immunology, 1998. **161**(6): p. 3143-3149.
151. Simpson, S.J., et al., *T cell-mediated pathology in two models of experimental colitis depends predominantly on the interleukin 12/Signal transducer and activator of transcription (Stat)-4 pathway, but is not conditional on interferon gamma expression by T cells.* The Journal of Experimental Medicine, 1998. **187**(8): p. 1225-1234.
152. Mannon, et al., *Anti–Interleukin-12 Antibody for Active Crohn's Disease.* The New England Journal of Medicine, 2004. **351**(20): p. 2069-2079.
153. Sandborn, W.J., et al., *A randomized trial of Ustekinumab, a human interleukin-12/23 monoclonal antibody, in patients with moderate-to-severe Crohn's disease.* Gastroenterology, 2008. **135**(4): p. 1130-41.
154. Boirivant, M., et al., *Oxazolone colitis: A murine model of T helper cell type 2 colitis treatable with antibodies to interleukin 4.* The Journal of Experimental Medicine, 1998. **188**(10): p. 1929-1939.
155. Heller, et al., *Oxazolone Colitis, a Th2 Colitis Model Resembling Ulcerative Colitis, Is Mediated by IL-13-Producing NK-T Cells.* Immunity, 2002. **17**(5): p. 629-638.
156. Welfare, A.I.o.H.a. *Bowel Cancer Statistics*. 2018; Available from: https://bowel-cancer.canceraustralia.gov.au/statistics.
157. DeSantis, C.E., et al., *Cancer treatment and survivorship statistics, 2014.* CA Cancer J Clin, 2014. **64**(4): p. 252-71.
158. Jasperson, K.W., et al., *Hereditary and familial colon cancer.* Gastroenterology, 2010. **138**(6): p. 2044-2058.

159. Munkholm, P., *Review article: the incidence and prevalence of colorectal cancer in inflammatory bowel disease.* Aliment Pharmacol Ther, 2003. **18 Suppl 2**: p. 1-5.
160. Brenner, H., M. Kloor, and C.P. Pox, *Colorectal cancer.* Lancet, 2014. **383**(9927): p. 1490-502.
161. DeSantis, C.E., et al., *Cancer treatment and survivorship statistics, 2014.* 2014. **64**(4): p. 252-271.
162. Grady, W.M. and S. Markowitz, *Genomic instability and colorectal cancer.* Curr Opin Gastroenterol, 2000. **16**(1): p. 62-7.
163. Rajagopalan, H., et al., *The significance of unstable chromosomes in colorectal cancer.* Nature Reviews Cancer, 2003. **3**: p. 695.
164. Goss, K.H. and J. Groden, *Biology of the adenomatous polyposis coli tumor suppressor.* J Clin Oncol, 2000. **18**(9): p. 1967-79.
165. Markowitz, S.D. and M.M. Bertagnolli, *Molecular origins of cancer: Molecular basis of colorectal cancer.* The New England journal of medicine, 2009. **361**(25): p. 2449-2460.
166. Radtke, F., H. Clevers, and O. Riccio, *From Gut Homeostasis to Cancer*. Vol. 6. 2006. 275-89.
167. Ward, R., et al., *Microsatellite instability and the clinicopathological features of sporadic colorectal cancer.* Gut, 2001. **48**(6): p. 821.
168. Huang, J., et al., *APC mutations in colorectal tumors with mismatch repair deficiency.* Proc Natl Acad Sci U S A, 1996. **93**(17): p. 9049-54.
169. Losi, L., et al., *K-ras and p53 mutations in hereditary non-polyposis colorectal cancers.* Int J Cancer, 1997. **74**(1): p. 94-6.
170. Esteller, M., et al., *A gene hypermethylation profile of human cancer.* Cancer Res, 2001. **61**(8): p. 3225-9.
171. Kane, M.F., et al., *Methylation of the hMLH1 promoter correlates with lack of expression of hMLH1 in sporadic colon tumors and mismatch repair-defective human tumor cell lines.* Cancer Res, 1997. **57**(5): p. 808-11.
172. Yamane, L., et al., *Serrated pathway in colorectal carcinogenesis.* World journal of gastroenterology, 2014. **20**(10): p. 2634-2640.
173. Kambara, T., et al., *BRAF mutation is associated with DNA methylation in serrated polyps and cancers of the colorectum.* Gut, 2004. **53**(8): p. 1137-1144.
174. Leggett, B. and V. Whitehall, *Role of the Serrated Pathway in Colorectal Cancer Pathogenesis.* Gastroenterology, 2010. **138**(6): p. 2088-2100.
175. Ogino, S., et al., *CpG island methylator phenotype-low (CIMP-low) in colorectal cancer: possible associations with male sex and KRAS mutations.* The Journal of molecular diagnostics, 2006. **8**(5): p. 582-588.
176. Ogino, S., et al., *Molecular correlates with MGMT promoter methylation and silencing support CpG island methylator phenotype-low (CIMP-low) in colorectal cancer.* Gut, 2007. **56**(11): p. 1564-1571.
177. Kwong, L.N., et al., *Identification of Mom7, a Novel Modifier of Apc^{Min/+} on Mouse Chromosome 18.* Genetics, 2007. **176**(2): p. 1237.
178. Papanikolaou, A., et al., *Sequential and morphological analyses of aberrant crypt foci formation in mice of differing susceptibility to azoxymethane-induced colon carcinogenesis.* Carcinogenesis, 2000. **21**(8): p. 1567-72.
179. Powell, S.M., et al., *APC mutations occur early during colorectal tumorigenesis.* Nature, 1992. **359**: p. 235.
180. Moser, A.R., et al., *ApcMin: A mouse model for intestinal and mammary tumorigenesis.* European Journal of Cancer, 1995. **31**(7): p. 1061-1064.
181. Khazaie, K., et al., *Abating colon cancer polyposis by Lactobacillus acidophilus deficient in lipoteichoic acid.* Proceedings of the National Academy of Sciences, 2012. **109**(26): p. 10462.
182. Robanus-Maandag, E.C., et al., *A new conditional Apc -mutant mouse model for colorectal cancer.* Carcinogenesis, 2010. **31**(5): p. 946-952.

183. Shibata, H., et al., *Rapid Colorectal Adenoma Formation Initiated by Conditional Targeting of the Apc Gene.* Science, 1997. **278**(5335): p. 120.
184. Smits, R., et al., *Loss of Apc and the entire chromosome 18 but absence of mutations at the Ras and Tp53 genes in intestinal tumors from Apc1638N, a mouse model for Apc-driven carcinogenesis.* Carcinogenesis, 1997. **18**(2): p. 321-327.
185. Halberg, R.B., et al., *Long-lived Min Mice Develop Advanced Intestinal Cancers through a Genetically Conservative Pathway.* Cancer Research, 2009. **69**(14): p. 5768.
186. Hamamoto, T., et al., *Compound disruption of smad2 accelerates malignant progression of intestinal tumors in apc knockout mice.* Cancer Res, 2002. **62**(20): p. 5955-61.
187. Takaku, K., et al., *Intestinal Tumorigenesis in Compound Mutant Mice of both Dpc4(Smad4) and Apc Genes.* Cell, 1998. **92**(5): p. 645-656.
188. Haigis, K.M., et al., *Differential effects of oncogenic K-Ras and N-Ras on proliferation, differentiation and tumor progression in the colon.* Nature Genetics, 2008. **40**: p. 600.
189. Halberg, R.B., et al., *Tumorigenesis in the multiple intestinal neoplasia mouse: Redundancy of negative regulators and specificity of modifiers.* Proceedings of the National Academy of Sciences, 2000. **97**(7): p. 3461.
190. Hung, K.E., et al., *Development of a mouse model for sporadic and metastatic colon tumors and its use in assessing drug treatment.* Proceedings of the National Academy of Sciences, 2010. **107**(4): p. 1565.
191. Boutin, A.T., et al., *Oncogenic Kras drives invasion and maintains metastases in colorectal cancer.* 2017. **31**(4): p. 370-382.
192. Edelmann, W., et al., *Tumorigenesis in Mlh1 and Mlh1/Apc1638N mutant mice.* Cancer Res, 1999. **59**(6): p. 1301-7.
193. Reitmair, A.H., et al., *MSH2 deficient mice are viable and susceptible to lymphoid tumours.* Nat Genet, 1995. **11**(1): p. 64-70.
194. de Wind, N., et al., *Inactivation of the mouse Msh2 gene results in mismatch repair deficiency, methylation tolerance, hyperrecombination, and predisposition to cancer.* Cell, 1995. **82**(2): p. 321-30.
195. Edelmann, W., et al., *Mutation in the mismatch repair gene Msh6 causes cancer susceptibility.* Cell, 1997. **91**(4): p. 467-77.
196. Prolla, T.A., et al., *Tumour susceptibility and spontaneous mutation in mice deficient in Mlh1, Pms1 and Pms2 DNA mismatch repair.* Nat Genet, 1998. **18**(3): p. 276-9.
197. Baker, S.M., et al., *Involvement of mouse Mlh1 in DNA mismatch repair and meiotic crossing over.* Nat Genet, 1996. **13**(3): p. 336-42.
198. Yang, G., et al., *Dominant effects of an Msh6 missense mutation on DNA repair and cancer susceptibility.* Cancer Cell, 2004. **6**(2): p. 139-50.
199. Kucherlapati, M.H., et al., *An Msh2 conditional knockout mouse for studying intestinal cancer and testing anticancer agents.* Gastroenterology, 2010. **138**(3): p. 993-1002.e1.
200. Rad, R., et al., *A genetic progression model of Braf(V600E)-induced intestinal tumorigenesis reveals targets for therapeutic intervention.* Cancer cell, 2013. **24**(1): p. 15-29.
201. Tong, K., et al., *Degree of Tissue Differentiation Dictates Susceptibility to BRAF-Driven Colorectal Cancer.* Cell reports, 2017. **21**(13): p. 3833-3845.
202. Yu, M., et al., *Inactivation of TGF-β signaling and loss of PTEN cooperate to induce colon cancer in vivo.* Oncogene, 2013. **33**: p. 1538.
203. Trobridge, P., et al., *TGF-β Receptor Inactivation and Mutant Kras Induce Intestinal Neoplasms in Mice via a β-Catenin-Independent Pathway.* Gastroenterology, 2009. **136**(5): p. 1680-1688.e7.
204. Nambiar, P.R., et al., *Preliminary analysis of azoxymethane induced colon tumors in inbred mice commonly used as transgenic/knockout progenitors.* Int J Oncol, 2003. **22**(1): p. 145-50.
205. Neufert, C., C. Becker, and M.F. Neurath, *An inducible mouse model of colon carcinogenesis for the analysis of sporadic and inflammation-driven tumor progression.* Nat Protoc, 2007. **2**(8): p. 1998-2004.

206. Pan, Q., et al., *Genomic variants in mouse model induced by azoxymethane and dextran sodium sulfate improperly mimic human colorectal cancer.* Scientific Reports, 2017. **7**(1): p. 25.
207. Chakrabarti, R., et al., *Elf5 regulates mammary gland stem/progenitor cell fate by influencing notch signaling.* Stem cells (Dayton, Ohio), 2012. **30**(7): p. 1496-1508.
208. Choi, Y.S., et al., *Elf5 conditional knockout mice reveal its role as a master regulator in mammary alveolar development: failure of Stat5 activation and functional differentiation in the absence of Elf5.* Dev Biol, 2009. **329**(2): p. 227-41.
209. Oakes, S.R., et al., *The Ets transcription factor Elf5 specifies mammary alveolar cell fate.* Genes & development, 2008. **22**(5): p. 581-586.
210. Zhou, J., et al., *Elf5 is essential for early embryogenesis and mammary gland development during pregnancy and lactation.* Embo j, 2005. **24**(3): p. 635-44.
211. Pellacani, D., et al., *Analysis of Normal Human Mammary Epigenomes Reveals Cell-Specific Active Enhancer States and Associated Transcription Factor Networks.* Cell Reports, 2016. **17**(8): p. 2060-2074.
212. Pal, B., et al., *Construction of developmental lineage relationships in the mouse mammary gland by single-cell RNA profiling.* Nat Commun, 2017. **8**(1): p. 1627.
213. Robinson, G.W., et al., *Regulation of Mammary Gland Development by Tissue Interaction.* 1999. **4**(1): p. 9-19.
214. Inman, J.L., et al., *Mammary gland development: cell fate specification, stem cells and the microenvironment.* Development, 2015. **142**(6): p. 1028.
215. Lyons, W.R., *Hormonal Synergism in Mammary Growth.* Proceedings of the Royal Society of London. Series B, Biological Sciences, 1958. **149**(936): p. 303-325.
216. Bocchinfuso, W.P., et al., *Induction of Mammary Gland Development in Estrogen Receptor-α Knockout Mice.* Endocrinology, 2000. **141**(8): p. 2982-2994.
217. Lydon, J.P., et al., *Mice lacking progesterone receptor exhibit pleiotropic reproductive abnormalities.* 1995. **9**(18): p. 2266-2278.
218. Silberstein, G.B. and C.W. Daniel, *Glycosaminoglycans in the basal lamina and extracellular matrix of the developing mouse mammary duct.* Developmental Biology, 1982. **90**(1): p. 215-222.
219. Nelson, C.M., et al., *Tissue Geometry Determines Sites of Mammary Branching Morphogenesis in Organotypic Cultures.* Science, 2006. **314**(5797): p. 298.
220. Hennighausen, L. and G.W. Robinson, *Information networks in the mammary gland.* Nat Rev Mol Cell Biol, 2005. **6**(9): p. 715-25.
221. Fata, J.E., V. Chaudhary, and R. Khokha, *Cellular Turnover in the Mammary Gland Is Correlated with Systemic Levels of Progesterone and Not 17β-Estradiol During the Estrous Cycle1.* Biology of Reproduction, 2001. **65**(3): p. 680-688.
222. Brisken, C., et al., *A paracrine role for the epithelial progesterone receptor in mammary gland development.* Proceedings of the National Academy of Sciences, 1998. **95**(9): p. 5076.
223. Liu, X., et al., *Stat5a is mandatory for adult mammary gland development and lactogenesis.* 1997. **11**(2): p. 179-186.
224. Ormandy, C.J., et al., *Null mutation of the prolactin receptor gene produces multiple reproductive defects in the mouse.* 1997. **11**(2): p. 167-178.
225. Liu, X., et al., *Functional rescue of Stat5a-null mammary tissue through the activation of compensating signals including Stat5b.* 1998. **9**(9): p. 795-804.
226. Yamaji, D., et al., *Development of mammary luminal progenitor cells is controlled by the transcription factor STAT5A.* 2009. **23**(20): p. 2382-2387.
227. Talhouk, R.S., et al., *Proteinases of the mammary gland: developmental regulation in vivo and vectorial secretion in culture.* Development, 1991. **112**(2): p. 439.
228. Giraddi, R.R., et al., *Single-Cell Transcriptomes Distinguish Stem Cell State Changes and Lineage Specification Programs in Early Mammary Gland Development.* Cell Rep, 2018. **24**(6): p. 1653-1666.e7.

229. Spike, B.T., et al., *A mammary stem cell population identified and characterized in late embryogenesis reveals similarities to human breast cancer.* Cell Stem Cell, 2012. **10**(2): p. 183-97.
230. Wuidart, A., et al., *Early lineage segregation of multipotent embryonic mammary gland progenitors.* Nat Cell Biol, 2018. **20**(6): p. 666-676.
231. Rios, A.C., et al., *In situ identification of bipotent stem cells in the mammary gland.* Nature, 2014. **506**(7488): p. 322-7.
232. Bach, K., et al., *Differentiation dynamics of mammary epithelial cells revealed by single-cell RNA sequencing.* Nat Commun, 2017. **8**(1): p. 2128.
233. Nguyen, Q.H., et al., *Profiling human breast epithelial cells using single cell RNA sequencing identifies cell diversity.* Nat Commun, 2018. **9**(1): p. 2028.
234. el Marjou, F., et al., *Tissue-specific and inducible Cre-mediated recombination in the gut epithelium.* Genesis, 2004. **39**(3): p. 186-93.
235. Hinoi, T., et al., *Mouse Model of Colonic Adenoma-Carcinoma Progression Based on Somatic Apc Inactivation.* Cancer Research, 2007. **67**(20): p. 9721.
236. Bertrand, H.G.M.J., et al., *A surgical approach in the treatment of preputial gland abscesses in mice.* BMC veterinary research, 2016. **12**: p. 16-16.
237. Anderson, S.M., et al., *Key stages in mammary gland development. Secretory activation in the mammary gland: it's not just about milk protein synthesis!* Breast Cancer Research, 2007. **9**(1): p. 204.
238. Mackereth, C.D., et al., *Diversity in Structure and Function of the Ets Family PNT Domains.* Journal of Molecular Biology, 2004. **342**(4): p. 1249-1264.
239. Lo, Y.H., et al., *SPDEF Induces Quiescence of Colorectal Cancer Cells by Changing the Transcriptional Targets of beta-catenin.* Gastroenterology, 2017. **153**(1): p. 205-218.e8.
240. Brisken, C., et al., *Prolactin Controls Mammary Gland Development via Direct and Indirect Mechanisms.* Developmental Biology, 1999. **210**(1): p. 96-106.
241. Dos Santos, C.O., et al., *An epigenetic memory of pregnancy in the mouse mammary gland.* Cell Rep, 2015. **11**(7): p. 1102-9.
242. Van der Flier, L.G., et al., *OLFM4 is a robust marker for stem cells in human intestine and marks a subset of colorectal cancer cells.* Gastroenterology, 2009. **137**(1): p. 15-17.
243. Merritt, A.J., et al., *Apoptosis in small intestinal epithelia from p53-null mice: evidence for a delayed, p53-indepdendent G2/M-associated cell death after γ-irradiation.* Oncogene, 1997. **14**(23): p. 2759-2766.
244. Kawasaki, Y., et al., *REG4 is a transcriptional target of GATA6 and is essential for colorectal tumorigenesis.* Scientific reports, 2015. **5**: p. 14291-14291.
245. Rafa, L., et al., *REG4 acts as a mitogenic, motility and pro-invasive factor for colon cancer cells.* Int J Oncol, 2010. **36**(3): p. 689-98.
246. Zhu, X., et al., *Overexpression of Reg4, alone or combined with MMP-7 overexpression, is predictive of poor prognosis in colorectal cancer.* Oncology reports, 2015. **33**(1): p. 320-328.
247. Wang, J., et al., *Relative roles of ABCG5/ABCG8 in liver and intestine.* Journal of lipid research, 2015. **56**(2): p. 319-330.
248. He, H.L., et al., *Overexpression of REG4 confers an independent negative prognosticator in rectal cancers receiving concurrent chemoradiotherapy.* J Surg Oncol, 2014. **110**(8): p. 1002-10.
249. Kobunai, T., T. Watanabe, and T. Fukusato, *REG4, NEIL2, and BIRC5 gene expression correlates with gamma-radiation sensitivity in patients with rectal cancer receiving radiotherapy.* Anticancer Res, 2011. **31**(12): p. 4147-53.
250. Perše, M. and A. Cerar, *Dextran Sodium Sulphate Colitis Mouse Model: Traps and Tricks.* Journal of Biomedicine and Biotechnology, 2012. **2012**: p. 13.
251. Melgar, S., et al., *Validation of murine dextran sulfate sodium-induced colitis using four therapeutic agents for human inflammatory bowel disease.* International Immunopharmacology, 2008. **8**(6): p. 836-844.

252. Albert-Bayo, M., et al., *Intestinal Mucosal Mast Cells: Key Modulators of Barrier Function and Homeostasis.* Cells, 2019. **8**(2).
253. Boeckxstaens, G., *Mast cells and inflammatory bowel disease.* Curr Opin Pharmacol, 2015. **25**: p. 45-9.
254. De Winter, B.Y., R.M. van den Wijngaard, and W.J. de Jonge, *Intestinal mast cells in gut inflammation and motility disturbances.* Biochim Biophys Acta, 2012. **1822**(1): p. 66-73.
255. Hamilton, M.J., et al., *Essential role for mast cell tryptase in acute experimental colitis.* Proc Natl Acad Sci U S A, 2011. **108**(1): p. 290-5.
256. Ishida, K., et al., *Role of chymase-dependent matrix metalloproteinase-9 activation in mice with dextran sodium sulfate-induced colitis.* J Pharmacol Exp Ther, 2008. **324**(2): p. 422-6.
257. Iwanaga, K., et al., *Mast Cell–Derived Prostaglandin D₂ Inhibits Colitis and Colitis-Associated Colon Cancer in Mice.* Cancer Research, 2014. **74**(11): p. 3011-3019.
258. Raithel, M., et al., *Release of mast cell tryptase from human colorectal mucosa in inflammatory bowel disease.* Scand J Gastroenterol, 2001. **36**(2): p. 174-9.
259. Dejea, C.M., et al., *Microbiota organization is a distinct feature of proximal colorectal cancers.* Proc Natl Acad Sci U S A, 2014. **111**(51): p. 18321-6.
260. Dejea, C.M., et al., *Patients with familial adenomatous polyposis harbor colonic biofilms containing tumorigenic bacteria.* Science, 2018. **359**(6375): p. 592-597.
261. Goodwin, A.C., et al., *Polyamine catabolism contributes to enterotoxigenic Bacteroides fragilis-induced colon tumorigenesis.* Proc Natl Acad Sci U S A, 2011. **108**(37): p. 15354-9.
262. Bromberg, J. and T.C. Wang, *Inflammation and cancer: IL-6 and STAT3 complete the link.* Cancer cell, 2009. **15**(2): p. 79-80.
263. Wang, L., et al., *IL-17 can promote tumor growth through an IL-6-Stat3 signaling pathway*. J Exp Med, 2009. **206**(7): p. 1457-64.
264. Albino, D., et al., *The ETS factor ESE3/EHF represses IL-6 preventing STAT3 activation and expansion of the prostate cancer stem-like compartment.* Oncotarget, 2016. **7**(47): p. 76756-76768.
265. West, H.C. and C.L. Bennett, *Redefining the Role of Langerhans Cells As Immune Regulators within the Skin.* Frontiers in Immunology, 2018. **8**(1941).
266. Sakamoto, K., et al., *EHF suppresses cancer progression by inhibiting ETS1-mediated ZEB expression.* Oncogenesis, 2021. **10**(3): p. 26-26.
267. Novoplansky, O., et al., *MET activation confers resistance to cetuximab, and prevents HER2 and HER3 upregulation in head and neck cancer.* International journal of cancer, 2019. **145**(3): p. 748-762.
268. Huang, W.C., et al., *A novel miR-365-3p/EHF/keratin 16 axis promotes oral squamous cell carcinoma metastasis, cancer stemness and drug resistance via enhancing β5-integrin/c-met signaling pathway.* J Exp Clin Cancer Res, 2019. **38**(1): p. 89.
269. Oakes, S.R., H.N. Hilton, and C.J. Ormandy, *The alveolar switch: coordinating the proliferative cues and cell fate decisions that drive the formation of lobuloalveoli from ductal epithelium.* Breast Cancer Res, 2006. **8**(2): p. 207.
270. Fu, N.Y., et al., *Stem cells and the differentiation hierarchy in mammary gland development.* Physiological reviews, 2020. **100**(2): p. 489-523.
271. Müsch, W., et al., *Generation and characterization of alpha-chymase-Cre transgenic mice.* Genesis, 2008. **46**(3): p. 163-6.
272. Lieberman, D.A., et al., *Prevalence of Polyps Greater Than 9 mm in a Consortium of Diverse Clinical Practice Settings in the United States.* Clinical Gastroenterology and Hepatology, 2005. **3**(8): p. 798-805.
273. Cho, N.L., et al., *Estrogen Receptors α and β Are Inhibitory Modifiers of Apc-Dependent Tumorigenesis in the Proximal Colon of Min/+ Mice.* Cancer Research, 2007. **67**(5): p. 2366-2372.